AD-A187 672 THE PHYSICS OF VERY SMALL STRUCTURES(U) CALIFORNIA INST 1/1
OF TECH PASADENA DEPT OF APPLIED PHYSICS T C MCGILL
1987 N00014-K-82-0556

UNCLASSIFIED F/G 20/3 NL

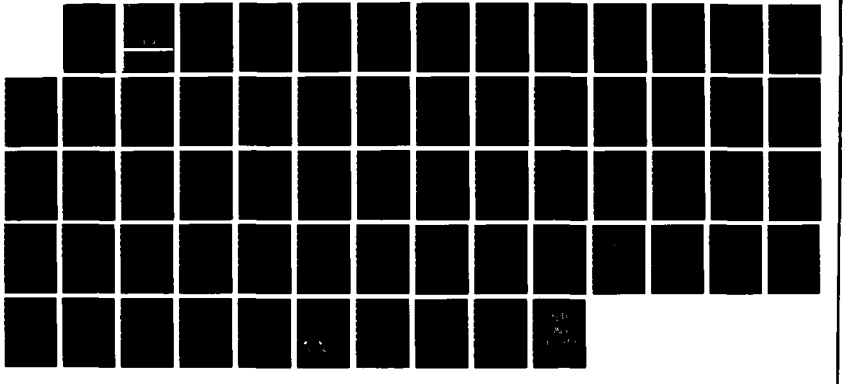

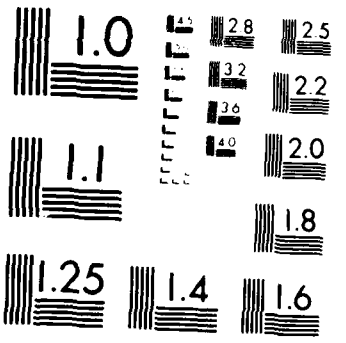

(12)

The Physics of Very Small Structures

Contract No. N00014-K-82-0556

From: September 30, 1982 To: September 30, 1985

PREPARED BY
T. C. McGill

CALIFORNIA INSTITUTE OF TECHNOLOGY

PASADENA, CALIFORNIA

(12)

FINAL TECHNICAL REPORT
TO
OFFICE OF NAVAL RESEARCH

The Physics of Very Small Structures

Contract No. N00014-K-82-0556

From: September 30, 1982 **To:** September 30, 1985

PREPARED BY
T. C. McGill

Department of Applied Physics
California Institute of Technology
Pasadena, California 91125
Tel. Number (818)356-4849

TABLE OF CONTENTS

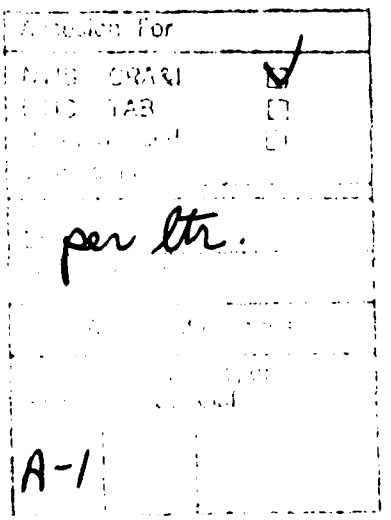

ABSTRACT

Studies of the basic properties of small structures that could be of major importance in the fabrication of new microdevices have been carried out. Some of the basic areas of major contribution include: transport over and through barrier structures, ohmic contacts and fluctuations, band offsets, and the search for lattice matches between silicides and silicon for application in microdevices. Seven graduate students received all or part of their support on this program. Four of them have obtained Ph. D.'s. The other three are still completing their programs.

I. Introduction

In recent years, it has become quite clear that the current trend in the development of modern electronics cannot continue. The strategy of continuing to shrink standard device structures to ever smaller dimensions to produce circuits of increasing density and complexity will begin to fail in a few more generations. Hence, it has become important to carry out major research programs looking for new device phenomena and exploring the physics and chemistry of the ultimate limitations in modern electronics. The research program, supported under this contract, is one such program trying to make major progress in understanding some of the key phenomena that could be important both in new device structures and also as an ultimate limiter of the current device technology.

Transport is a major issue in the limitations on current devices and possibilities for new devices. In this research program, we have explored transport through GaAs-GaAlAs heterostructures. Particular emphasis has been placed on tunnel barrier structures which have the possibililty for being important in new device structures. We have also explored the role of the discreteness of atoms in limiting the ultimate performance of such technically important aspects of devices as ohmic contacts. Transport over barriers of GaAlAs have been explored using photoresponse techniques. The precise nature of band offsets which critically determine the behavior of heterojunctions has also been explored. Finally, we have investigated the possibililty of new and novel lattice-matched structures involving silicon and silicides.

Major results of this study are contained in the next section. An appendix contains all of the publications that were supported under this program. One of the major outputs of a research program such as this one is graduate students. A list of the students supported and their current positions is contained in Section II. Overall conclusions are contained in Section IV.

II. Major Results

A. Tunneling

The primary research area was the study of transport, particularly tunneling through very narrow barrier structures with characteristic thicknesses of 50-100Å. One of the primary questions is the role of inelastic tunneling. In these processes phonons are admitted in the transport across the barrier. In a series of experiments carried out under this program, we made some of the first investigations of inelastic tunneling processes in these simple device structures. Major results of this study were presented in papers 1 and 2 in the Appendix.

We have had major success in studying what has become a very important device structure, the so-called double barrier resonant structure. We were the first group to observe resonant tunneling metal-organic-chemical-vapor deposited GaAs-AlAs-GaAs-AlAs-GaAs heterostructures. We were the third group to observe this phenomenon. We have also shown that the uniformity of such tunneling phenomenon can be very good, hence opening up the possibilities for actually fabricating meaningful devices with this technique. These very important results are contained in papers 3 and 4 in the Appendix.

We have also investigated the fundamental transport mechanisms in these double barrier structures. In particular, we have investigated the role of transport involving other parts of the band structure in addition to the Γ-point as well as the role of phonons in the transport. These results are contained in paper 5 in the Appendix.

While very exciting two-terminal devices have been fabricated based on the resonant tunneling through a double barrier structure, for these new device structures to be very useful a third-terminal is essential. Over the years, tunneling based transistors have been proposed but have had great difficulity in attaining performance levels which would make them interesting. Under this research project, we have proposed a novel three-terminal device based on tunneling. This device structure called the Stark transistor has the possibility of overcoming some of the historical problems of other tunneling transistor structures. While we have not had success in fabricating this device under this program, we believe that this proposed device structure opens up the possibility of making high-density, high-speed electronics based on tunnel structures. We report on these new device structures in paper 6 in the Appendix.

B. Transport Over Barriers

In addition to the transport through the barrier, reported in the above studies, we have also investigated the transport over barriers in GaAs-GaAlAs-GaAs heterostructure devices. In order to carry out these studies, we have used photons to excite the carriers over the barrier. While the initial plans for these experiments were to explore the details of resonances in the transfer of electrons across barriers, theoretical studies as well as the experiments indicated that these could not be observed due to the distribution in k of the electrons excited by the photons. However, a number of novel effects were observed and explained theoretically during this study. The results are contained in papers 7, 8 and 9 in the Appendix.

C. Ohmic Contacts and Fluctuation Phenomena

Ohmic contacts are one of the most important components of modern devices. As device dimensions that are shrunk to increase density and performance, ohmic contacts are likely to be a major limiter on device performance. Ohmic contacts are made using black art recipes which give little insight into exactly how they work. However, it is widely believed that the ohmic contact actually consists of a heavily doped region in the semiconductor in which tunneling dominates transport through a normally present Schottky barrier. There have been very few theoretical studies of ohmic contacts. The most popular theory is one that makes a number of simplifying assumptions which made comparision between specific contact resistance and theory impossible. Under this program, we have developed the first serious theoretical study of ohmic contact behavior. This study was specifically aimed at GaAs but is readily extendable to other systems. The results of this study are presented in paper 10 in the appendix.

One of the major issues in examining the properties of ohmic contacts is the discreteness of the dopant atoms. Most of the theories, including the one described in the preceeding paragraph, assume that the dopant atoms are uniformily distributed. However, in actual fact there are large fluctuations in potential due to the discreteness or the ionized dopants. During this program, we have initiated a study of this fundamental phenomenon to study the fluctuations that could occur in the ohmic contact behavior. This pioneering work is beginning to illustrate the ultimate limitations on shrinking devices due to the discreteness of the actual underlaying atomic structure. The preliminary results of this study are contained in paper 11 in the Appendix.

D. Band Offsets

One of the major unsolved problems in the study of heterojunctions is the determination of the band offset. The band offset measures the discontinuity between the valence bands or conduction bands of the two semiconductors on either side of the heterojunction. Within the last few years, it has been one of the primary sports of the theorists in this field to attempt to explain the values of band offsets. Under this program, we made an important contribution to this field indicating the kinds of effects that could result because of defects and dipole layers at these heterojunctions. Results of our study are included in the Appendix in paper 12.

E. Lattice Match Structure of Silicides and Silicon

Lattice match is thought to play a major role in growing device quality interfaces. One of the major areas of interest is the fabrication of device structures involving silicides and silicon. During this contract, we made a major search for lattice matches between silicide and silicon. Results of this study are contained in paper 13 in the Appendix.

III. Students Supported Under this Contract

One of the major outputs of any research program in a university environment is the graduate students. During this program the research of seven graduate students has been supported. A table of these graduate students and their current positions is given below.

Name	Degree	Year	Current Position
R. T. Collins	Ph.D	1984	Member Technical Staff, IBM T. J. Watson Research Center
A. Zur	Ph.D	1983	Member Technical Staff, Rafphael, Israel
A. R. Bonnefoi	Ph.D	1986	Prof. of Physics, Uruguay
T. E. Schlesinger	Ph.D	1985	Assistant Professor of Electrical Engineering, Carnegie Mellon Univ.
W. Boudville			Graduate Student at Caltech
T. K. Woodward			Graduate Student at Caltech
D. H. Chow			Graduate Student at Caltech

IV. Conclusions

During this research program, major results were obtained in the study of tunneling structures and the fabrication of two-terminal resonant tunneling devices. We also proposed a novel three-terminal tunneling device which has the possibility of giving both high-speed and high-density electronics. Additionally, we carried out extensive studies of the photovoltaic properties of GaAs-GaAlAs-GaAs barrier structures. These represented some of the first studies of the transport across these barriers. Ohmic contacts, which are likely to be a major limiter in III-V device technology, have been explored both in a continuum theory and one including the fluctuations due to dopants. The role of defects and dipole layers in producing band offsets has been studied in some very simple theoretical investigations. Lattice match between silicon and silicide structures has been studied in an attempt to identify new and potentially very interesting device structures. Under the program, seven graduates students have received support. Four of these graduate students have obtained degrees and are holding down positions in academic institutions or in industrial research laboratories. Three of the students are continuing to work towards degrees at Caltech.

APPENDIX

PUBLISHED PAPERS

Inelastic tunneling characteristics of AlAs/GaAs heterojunctions

R. T. Collins, J. Lambe, and T. C. McGill
California Institute of Technology, Pasadena, California 91125

R. D. Burnham
Xerox Corporation, Palto Alto, California 94304

(Received 7 November 1983; accepted for publication 12 December 1983)

We report the first observation of inelastic tunneling in electronic transport perpendicular to a thin AlAs layer sandwiched between two GaAs layers. Temperature dependent I–V, first derivative (dI/dV), and second derivative (d^2I/dV^2) measurements were made on AlAs/GaAs double heterojunctions for a range of AlAs layer thicknesses and dopings. For p-type AlAs barriers current transport at 4.2 K was due to tunneling, and reproducible structure was seen in the second derivative spectrum. This structure was associated with the inelastic excitation of AlAs optical phonons and with a density-of-states effect caused by optical phonon-electron coupling in the GaAs. A different second derivative spectrum which also exhibited reproducible structure was obtained for n-type AlAs layers. Several possible explanations for these differences are proposed.

PACS numbers: 73.40.Gk, 73.40.Lq, 73.60.Fw

Several studies of the electrical properties of the $Al_xGa_{1-x}As$/GaAs double heterojunctions have recently been reported.[1–3] In these papers the capacitance-voltage (C-V) and current-voltage (I-V) properties of thin $Al_xGa_{1-x}As$ barriers sandwiched between two GaAs layers were investigated. The currents obtained in the I-V measurements were attributed to thermionic emission over the offset barrier and tunneling through the barrier. Chang *et al.*[4] and Solner *et al.*[5] looked at the tunneling behavior of two $Al_xGa_{1-x}As$ barriers separated by a GaAs quantum well and Vojak *et al.*[6] observed tunneling behavior in multiple quantum well structures, but to our knowledge, no one has looked for structure in the tunneling I-V curve of a single $Al_xGa_{1-x}As$ barrier.

In this letter we report the first observation of inelastic tunneling in electronic transport perpendicular to a single AlAs barrier. Temperature-dependent I-V, first derivative (dI/dV), and second derivative (d^2I/dV^2) measurements were made on AlAs/GaAs double heterojunctions. Both the thickness and the doping of the AlAs layers were varied. When the AlAs layer was doped p type with Mg, transport at 4.2 K occurred mainly through electron tunneling. Reproducible structure was seen in the second derivative spectrum at the AlAs and GaAs optical phonon frequencies. These structures were attributed to the inelastic excitation of AlAs longitudinal optical phonons and to a density-of-states effect caused by coupling between electrons and optical phonons in the GaAs. In contrast, I-V curves and second derivative spectra for samples with n-type, Se-doped AlAs layers were considerably different. Possible explanations for these differences will be given.

The samples used in this study were grown by metalorganic chemical vapor deposition (MOCVD) using a technique described elsewhere.[7] The substrate used in making the structures was n-type GaAs doped with $2–3\times10^{18}$ cm^{-3} Si. An approximately 3-μm-thick epitaxial layer of GaAs doped with Se was grown on the substrate followed by a thin AlAs layer. The thicknesses of the AlAs layers varied from 60 to 250 Å from wafer to wafer. A second Se-doped GaAs layer was grown on top of the AlAs barrier. The epitaxial GaAs dopings varied but were typically $1–5\times10^{18}$ cm^{-3}. The AlAs was either doped n type at approximately 1×10^{18} cm^{-3} with Se or p type at about 1×10^{18} cm^{-3} with Mg. The

 0003-6951/84/050532-03$01.00

widths and dopings of the AlAs given above are extrapolations from measurements made on low aluminum content $Al_xGa_{1-x}As$ and could be in error since they have not actually been calibrated for AlAs.

Circular mesas 80–360 μm in diameter and more than 4 μm in height were defined on the epitaxial GaAs surface using photolithography and a 4:1:1 H_2SO_4:H_2O_2:H_2O GaAs etch. A (Au,Ge)-Ni ohmic contact was fabricated on the mesa surface and on the substrate. The samples were then mounted on standard transistor headers and wire bonded to provide contacts.

Temperature-dependent *I-V*, first derivative, and second derivative spectra were taken on the samples from room temperature to 4.2 K. The *I-V* measurements were made by applying a dc current source to the samples and measuring the resulting dc voltage. First and second derivatives were obtained using standard modulation techniques. First derivative spectra were taken by applying a 5-kHz current source to the samples and measuring the voltage across the sample at 5 kHz to obtain dV/dI. Second derivative spectra were taken using a second harmonic detection system as described by Lambe and Jaklevic.[8] It was operated at a fundamental frequency of 50 kHz with typical modulation voltages of 1–5 mV.

First, the results of measurements on samples with Mg-doped, *p*-type AlAs barriers will be presented. The *I-V* curves for *p*-type barriers exhibited increasing zero-bias resistance as temperature was decreased from room temperature to 77 K. From 77 to 4.2 K the curves maintained the same shape and resistance. As the thickness of the AlAs layer was increased from 60 to 120 Å, the zero-bias resistivity increased by about 2.5 orders of magnitude. The dependence of sample resistance on temperature and AlAs layer thickness strongly suggests that current flow at low temperatures was mainly due to electronic tunneling through the AlAs barrier. If this were true, the zero-bias resistivity should have an approximately exponential dependence on barrier width. Additional 60 Å increases in barrier width did result in greater zero-bias resistivity but by less than 2.5 orders of magnitude. It is likely that impurity states, edge effects, and other forms of leakage in the AlAs contribute to the low-temperature current. For small thicknesses the current would be dominated by tunneling through the barrier, while for larger thicknesses impurity conduction and other forms of leakage would be more important.

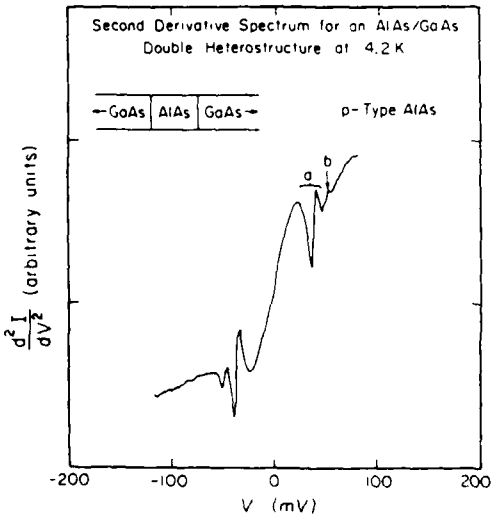

FIG. 1. Second derivative spectrum at 4.2 K for a *p*-type AlAs layer sandwiched between two *n*-type GaAs layers. The layer thickness was approximately 60 Å. The structure labeled (a) is attributed to an electronic density-of-states effect caused by electron-optical phonon coupling in the GaAs. The peak labeled (b) is caused by the inelastic excitation of longitudinal optical phonons in the AlAs barrier.

A second derivative spectrum taken at 4.2 K for a 60-Å-thick *p*-type AlAs barrier is given in Fig. 1. Two structures are present in both forward and reverse bias. The first, labeled (a), is at approximately the optical phonon frequencies of GaAs. It resembles similar structures previously observed in tunneling through GaAs Schottky barriers which were attributed to a density-of-states effect in the degenerate GaAs layers.[9] This self-energy effect is caused by coupling between electrons and longitudinal optical phonons in the GaAs. The structure labeled (a) is believed to arise from the same effect. The peak labeled (b) occurs at 50 meV which is the longitudinal optical phonon frequency of AlAs.[10] This peak is attributed to the inelastic excitation of longitudinal optical phonons in the AlAs by the electrons as they tunnel through the barrier. This is the first observation of these effects in the AlAs/GaAs system. The same results were obtained in two different wafers with approximately 60-Å-thick AlAs barriers. For barriers 120 Å thick or greater, this structure was not observed in the second derivative spectrum. This is probably due to the large decrease in tunneling current at these thicknesses which reduced the second derivative signal below the detectable limit of the measurement system.

When the measurements described above were made on samples with Se-doped, *n*-type AlAs layers, the results were not the same. *I-V* curves for the *n*-type AlAs layers also displayed increasing resistance with decreasing temperature. In contrast to the *p*-type layers, the resistance continued to increase until approximately 30 K. Furthermore, the zero-bias resistivity increased by less than an order of magnitude as the AlAs layer thicknesses increased from 60 to 250 Å, and the current flow was nearly an order of magnitude larger than in the 60-Å *p*-type barrier (Fig. 2). Changes in

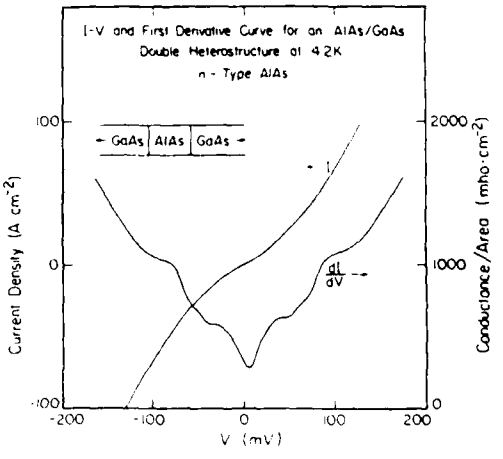

FIG. 2. *I-V* and dI/dV curves at 4.2 K for an *n*-type AlAs barrier sandwiched between two *n*-type GaAs layers. The AlAs layer thickness was approximately 80 Å.

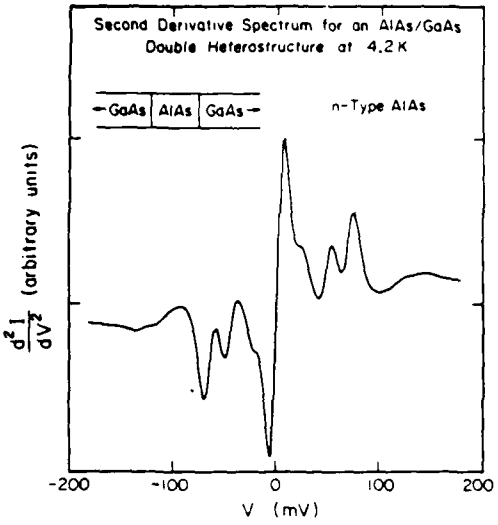

FIG. 3. Second derivative spectrum at 4.2 K for an approximately 80-Å-thick, *n*-type AlAs layer sandwiched between two *n*-type GaAs layers.

slope were visible in the *I-V* curves taken at 4.2 K. These changes in slope were as large as 60% as can be seen from the *dI/dV* curve given in Fig. 2. To study these, second derivative spectra were taken.

A second derivative spectrum at 4.2 K for an *n*-type barrier device is shown in Fig. 3. Five peaks representing increases in conductivity are evident in the positive bias direction. The two most prominent peaks occur at approximately 50 and 70 meV. Two peaks are also seen at about 125 and 145 meV. In addition, there is a 23-meV shoulder present on a strong zero-bias anomaly. The spectrum is fairly symmetric with respect to bias direction. Nearly identical second derivative spectra were observed for all AlAs thicknesses. The same peaks were seen, but there were differences in the measured voltages for the peaks and asymmetries between the voltages measured in both bias directions. These asymmetries and voltage differences were usually around 5–10 meV.

A definitive explanation for the differences between samples with *n*-type and *p*-type barriers has not been found, but some possible explanations can be proposed. If transport in the *n*-type AlAs samples is the result of tunneling, a model for these differences must describe why the actual tunneling barrier seen by the electrons is not increasing with the physical width of the AlAs layer in the *n*-type samples, as it is in the *p*-type samples. One possible explanation is that the doping in the *n*-type AlAs layer is actually larger than anticipated, and band bending in the AlAs results in the formation of two back-to-back AlAs/GaAs tunneling barriers with a connecting layer of AlAs. Increasing the AlAs layer thickness would only increase the width of the connecting AlAs layer. Then, the peaks in the second derivative spectrum may arise from the excitation of characteristic phonons in the AlAs/GaAs system by tunneling electrons (possibly wave vector-conserving phonons resulting from electrons moving from direct to indirect conduction-band minima). A voltage drop would occur across each barrier, causing the voltages at which the phonon associated peaks occur to differ from the phonon energies.

A second explanation includes the possibility that more impurities or defects are incorporated into the *n*-type layers than into the *p*-type layers, giving rise to impurity conduction in the barrier. This would not have an exponential dependence on barrier width. The peaks in the second derivative spectrum could indicate the onset of impurity-assisted tunneling or the excitation of vibrational modes of the impurities. Work is currently under way to test these models of current transport in the *n*-type barriers samples.

To summarize, we have observed current transport perpendicular to a thin AlAs layer sandwiched between two degenerately doped, *n*-type GaAs layers. Dependences of the associated *I-V* curves on temperature and thickness of the AlAs layer seem to indicate that for *p*-type AlAs barriers current flow at 4.2 K is largely due to tunneling through the AlAs barrier. Reproducible structure was observed in the second derivative spectrum for *p*-type AlAs barriers and associated with the inelastic excitation of longitudinal optical phonons in the AlAs and a density-of-states effect in GaAs caused by coupling between the electrons and optical phonons. Samples with *n*-type AlAs barriers did not have the same characteristics. The resistivity of the samples was nearly independent of AlAs layer thickness, and different peaks were observed in the second derivative spectrum. These peaks resulted from very large changes in the slope of the *I-V* curves and were very reproducible. A definitive explanation for the diffferences between *n*-type and *p*-type barriers has not been found, but some possibilites have been proposed.

The authors would like to acknowledge D. L. Smith, C. Mailhiot, R. S. Bauer, T. L. Paoli, and W. Streifer for valuable discussions and are grateful to H. Chung, R. D. Yingling, Jr., F. Endicott, M. Bernstein, M. Mosby, J. Tramontana, J. Walker, A. Alimonday, G. L. Harnagel, and R. Ritter for technical assistance with this work. This work was supported in part by the Office of Naval Research under contract No. N00014-82-K-0556.

[1] D. Delagebeaudeuf, P. Delescluse, P. Etienne, J. Massies, M. Laviron, J. Chaplart, and N. T. Linh, Electron. Lett. **18**, 85 (1982).
[2] A. C. Gossard, W. Brown, C. L. Allyn, and W. Wiegmann, J. Vac. Sci. Technol. **20**, 694 (1982).
[3] P. M. Solomon, T. W. Hickmott, H. Morkoç, and R. Fischer, Appl. Phys. Lett. **42**, 821 (1983).
[4] L. L. Chang, L. Esaki, and R. Tsu, Appl. Phys. Lett. **24**, 593 (1974).
[5] T. C. L. G. Solner, W. D. Goodhue, P. E. Tannenwald, C. D. Parker, and D. D. Peck, Appl. Phys. Lett. **43**, 588 (1983).
[6] B. A. Vojak, S. W. Kirchoefer, N. Holonyak, Jr., and R. Chin, J. Appl. Phys. **50**, 5830 (1979).
[7] R. D. Burnham, D. R. Scrifres, and W. Streifer, Electron. Lett. **18**, 1095 (1982).
[8] J. Lambe and R. C. Jaklevic, Phys. Rev. **165**, 821 (1968).
[9] J. W. Conley and G. D. Mahan, Phys. Rev. **161**, 681 (1967).
[10] M. Ilegems and G. L. Pearson, Phys. Rev. B **1**, 1576 (1970).

Summary Abstract: Elastic and inelastic tunneling characteristics of AlAs/GaAs heterojunctions

R. T. Collins, J. Lambe, and T. C. McGill

California Institute of Technology, Pasadena, California 91125

R. D. Burnham

Xerox Corporation, Palo Alto, California 94304

(Received 29 February 1984; accepted 24 April 1984)

PACS numbers: 73.40.Gk, 73.40.Lq

We report the observation, at low temperatures and bias voltages, of elastic and inelastic tunneling through AlAs barriers sandwiched between two GaAs layers. Previous studies of electronic transport perpendicular to $Al_xGa_{1-x}As$ barriers sandwiched between GaAs layers[1-4] have attributed currents passing through the barriers to thermionic emission at temperatures above 150 K or to tunneling through the $Al_xGa_{1-x}As$ barrier at low temperatures, but for bias voltages which were comparable to the barrier height. Two of these studies noted that at low temperatures and low biases more current passed through the barriers than could be accounted for by either of these processes, indicating that some form of leakage may be dominating current transport at low temperatures.[1,2] In all of these studies the barriers were 300 Å thick or thicker. The measurements reported here were made on samples with barriers thinner than 300 Å in an effort to enhance the tunneling current at low bias voltages relative to leakage. A more detailed account of most of these measurements is given in Ref. 5.

The samples used in this study were grown by metalorganic chemical vapor deposition (MOCVD) and by molecular beam epitaxy (MBE). In both cases an n-type epitaxial layer of GaAs was grown on a degenerately doped n-type GaAs substrate. A thin layer of AlAs was grown on top of this GaAs layer, followed by a final n-type layer of GaAs. In the MOCVD samples the epitaxial GaAs was doped with Se at $1-5\times10^{18}$ cm^{-3}, and the AlAs layer was either doped n type with Se or p type with Mg at approximately 1×10^{18} cm^{-3}. The AlAs layers were from 50–300 Å thick. The MBE samples came from two sources. In both cases the epitaxial GaAs layers were doped with Si at 1×10^{18} cm^{-3}, and the AlAs was unintentionally doped. The estimated AlAs layer thicknesses were from 50–150 Å. Devices were made on the wafers by defining mesas and fabricating (Au,Ge)–Ni contacts on the mesas. Temperature dependent current–voltage (I–V), first derivative (dI/dV), and second derivative (d^2I/dV^2) spectra were taken on the devices from room temperature to 4.2 K. Zero-bias resistances were obtained from the slope of the I–V curves at $\pm$ 3 mV.

Results of the measurements made on MOCVD grown samples will be discussed first. There was a large difference in the characteristics of the samples, depending upon whether the AlAs barrier was doped p type with Mg or n type with Se. The p-type barriers exhibited increasing resistance as temperature was decreased to 77 K, at which point the I–V curve maintained the same shape down to 4.2 K. The zero-bias resistances of p-type barrier samples increased rapidly with barrier width as is seen in Fig. 1. Figure 1 also includes the results of a WKB calculation of the zero-bias resistances expected for various barrier widths. This calculation was based on the technique of Kurtin *et al.*[6] Only contributions to the tunneling probability from the AlAs Γ points were included. The band offsets and effective masses were taken from Casey and Panish.[7] Although this model is only presented to give an idea of the orders of magnitude expected for tunneling resistances, the agreement is reasonable for small barrier widths. As the thickness of the barrier is increased, the measured zero-bias resistance does not increase at the rate predicted for tunneling, indicating that for thick AlAs layers, most of the low temperature current is due to some form of leakage. At smaller thicknesses the tunneling

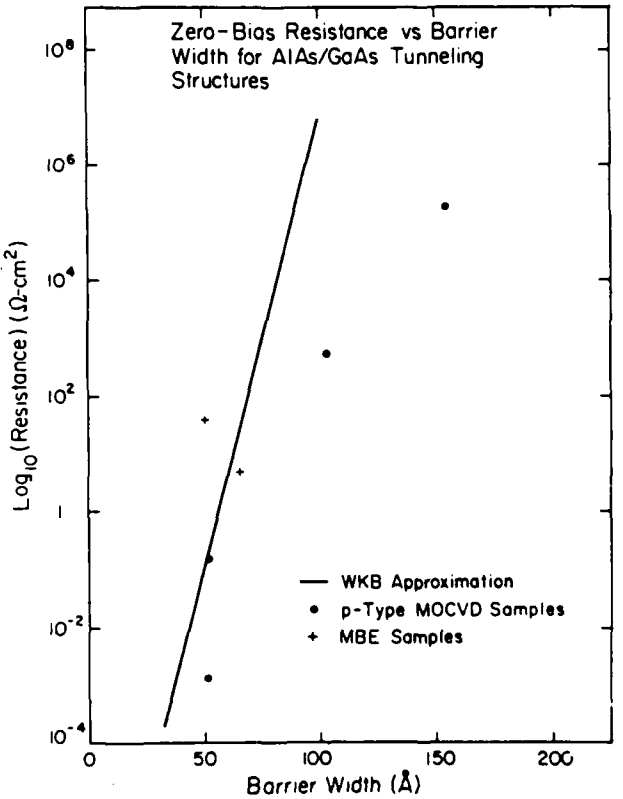

FIG. 1. Zero-bias resistivity at 4.2 K for MOCVD samples with p-type barriers and for MBE samples which had uniform resistivities between neighboring devices. The solid line is a theoretical calculation of zero-bias resistivity, using a WKB approximation to the tunneling probability.

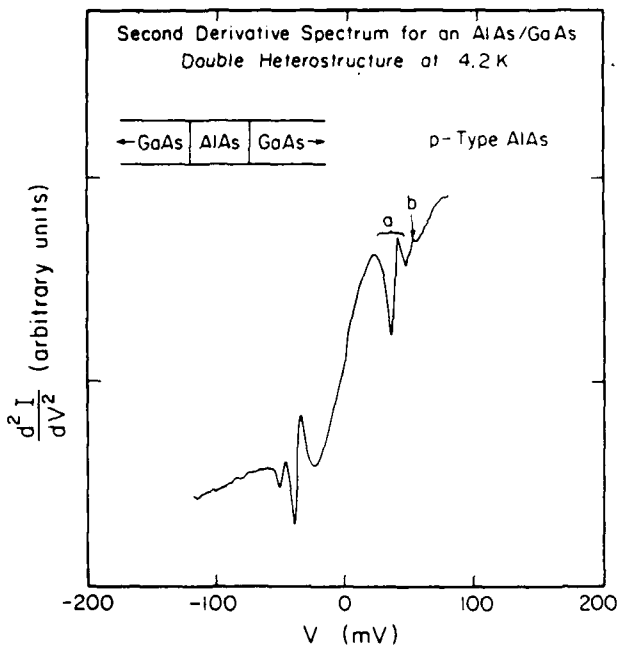

FIG. 2. Second derivative spectrum at 4.2 K for a *p*-type AlAs barrier sample grown by MOCVD. The layer thickness was approximately 50 Å. The structure labeled (a) is attributed to an electronic density-of-states effect caused by electron-optical phonon coupling in the GaAs. The peak labeled (b) is caused by the inelastic excitation of longitudinal optical phonons in the AlAs barrier.

current, which decreases exponentially with width, begins to dominate leakage.

When first and second derivatives were taken of the *I–V* curves of samples with 50 Å thick, *p*-type, AlAs layers, reproducible structure was evident (Fig. 2). Structure [labeled (a)] is present at the GaAs longitudinal optical (LO) phonon energy (36 meV) in both forward and reverse bias in Fig. 2 and is attributed to a density-of-states effect caused by electron–phonon coupling in the degenerate GaAs layers. Similar observations have been made in Schottky barrier tunneling in GaAs.[8] A peak, labeled (b), is also visible at approximately the AlAs LO phonon energy (50 meV) in the second derivative spectrum.[9] This peak is associated with the inelastic excitation of longitudinal optical phonons in the AlAs by the tunneling electrons. This is the first observation of these effects in the AlAs/GaAs system. These results were reproducible across a given wafer and were seen in two wafers with barriers of about the same thickness. When the AlAs barrier width increased to 100 Å or greater, no reproducible structure was observed.

When the MOCVD grown AlAs barriers were doped *n* type, the results were different. The zero-bias resistance changed by less than an order of magnitude as the AlAs layer width was increased from 60 to 250 Å. Five peaks were present in the second derivative spectra in both forward and reverse bias for all of the *n*-type barrier samples regardless of width. These peaks did not match those seen in the *p*-type barrier MOCVD samples. A definitive explanation for the results of measurements on *n*-type barriers has not been found. A more complete discussion of the differences between *n*- and *p*-type barrier MOCVD samples and the possible explanations for these differences is given in Ref. 5.

The zero-bias resistances for devices made from the two MBE grown samples with the thinnest AlAs layers (one from each source) are given in Fig. 1. These resistances are also consistent with the tunneling calculations, although from Fig. 1, it appears that either the MBE or MOCVD barrier widths may be in error by around 10 Å. The *I–V* curves for devices made from these wafers showed approximately the same behavior with temperature as the *p*-type MOCVD barrier samples. Devices made on the two wafers for which resistances are given in Fig. 1 showed some fluctuation from device to device in the zero-bias resistance. The remaining MBE samples studied had barrier widths of 100 Å or greater. The zero-bias resistances of neighboring devices made on these wafers fluctuated by many orders of magnitude. The largest resistances measured for the MBE samples were two or more orders of magnitude larger than the resistances of *p*-type MOCVD samples with the same barrier width. Much smaller fluctuations occurred in the resistivities of devices on the MOCVD grown wafers. The first and second derivative spectra for the MBE wafers did not show any reproducible structure, possibly because they had such large resistances that tunneling currents were beyond the detectable limits of our system. A reason for the large flunctuations in device resistance for the thicker barrier MBE samples has not been found.

Acknowledgments: The authors wish to acknowledge D. L. Smith, C. Mailhiot, R. S. Bauer, T. L. Paoli, and W. Streifer for valuable discussions and L. P. Erickson and G. W. Wicks for providing samples. We are also grateful to H. Chung, R. D. Yingling, Jr., F. Endicott, M. Bernstein, M. Mosby, J. Tramontana, J. Walker, A. Alimonday, G. L. Harnagel, and R. Ritter for technical assistance with this work. This work was supported in part by the Office of Naval Research under Contract No. N00014-82-K-0556.

[1] D. Delagebeaudeuf, P. Delescluse, P. Etienne, J. Massies, M. Laviron, J. Chaplart, and N. T. Linh, Electron Lett. **18**, 85 (1982).
[2] A. C. Gossard, W. Brown, C. L. Allyn, and W. Wiegmann, J. Vac. Sci. Technol. **20**, 694 (1982).
[3] P. M. Solomon, T. W. Hickmott, H. Morkoc, and R. Fischer, Appl. Phys. Lett. **42**, 821 (1983).
[4] T. W. Hickmott, P. M. Solomon, R. Fischer, and H. Morkoc, Appl. Phys. Lett. **44**, 90 (1984).
[5] R. T. Collins, J. Lambe, T. C. McGill, and R. D. Burnham, Appl. Phys. Lett. **44**, 532 (1984).
[6] S. L. Kurtin, T. C. McGill, and C. A. Mead, Phys. Rev. B **3**, 3368 (1971).
[7] H. C. Casey, Jr. and M. B. Panish, *Heterostructure Lasers Part A: Fundamental Principles* (Academic, New York, 1978), p. 192.
[8] J. W. Conley and G. D. Mahan, Phys. Rev. **161**, 681 (1967).
[9] M. Ilegems and G. L. Pearson, Phys. Rev. B **1**, 1576 (1970).

Resonant tunneling in GaAs/AlAs heterostructures grown by metalorganic chemical vapor deposition

A. R. Bonnefoi, R. T. Collins, and T. C. McGill
California Institute of Technology, Pasadena, California 91125

R. D. Burnham and F. A. Ponce
Xerox Corporation, Palo Alto, California 94304

(Received 25 October 1984; accepted for publication 13 November 1984)

We report the first observations of resonant tunneling in electronic transport perpendicular to two AlAs layers separated by a GaAs quantum well in GaAs/AlAs heterostructures grown by metalorganic chemical vapor deposition. Resonant tunneling can be observed as inflections in the *I-V* curves at room temperature. These inflections become more pronounced as the temperature is reduced, until negative differential resistance regions become visible for temperatures below 260 K. At low temperatures, the *I-V* curves not only reveal two large negative resistance regions corresponding to the first energy level in the GaAs quantum well but also a structure which shows evidence of resonant tunneling through the second and possibly the third energy states in the well. Second derivative (d^2I/dV^2) measurements confirm the existence of the resonances seen in the *I-V* curves.

Semiconductor heterostructures with small characteristic dimensions are now frequently fabricated from GaAs and $Al_xGa_{1-x}As$ using techniques such as molecular beam epitaxy (MBE) and metalorganic chemical vapor deposition (MOCVD). The conduction-band offset between the GaAs and the $Al_xGa_{1-x}As$ causes $Al_xGa_{1-x}As$ layers to act as potential energy barriers to electrons in the GaAs layers. This makes it possible to grow quantum well and quantum barrier structures, which are the object of considerable theoretical and experimental work. For these structures, a number of studies of electronic transport perpendicular to the layers have been reported.[1–6] Because an important current transport mechanism is tunneling, the associated tunneling effects yield novel electronic properties with very important theoretical and maybe practical applications. An interesting configuration is one in which two barriers are separated by a quantum well. There have been observations of resonant tunneling in MBE grown samples with a GaAs well adjacent to two $Al_xGa_{1-x}As$ barriers.[7,8] Following some preliminary work,[9,10] we report here observations of resonant tun-

 0003-6951/85/030285-03$01.00

neling in MOCVD grown structures with two AlAs barriers separated by a single GaAs quantum well. For the first time, resonant tunneling can be observed, not only through the lowest energy level in the GaAs well at room temperature, but also through higher energy states at lower temperatures, once the thermal current has been reduced.

The structure used in this study was grown by an MOCVD technique[11,12] on a GaAs substrate doped n type with Si at $2-3\times10^{18}$ cm^{-3}. The first layer grown on the substrate was one of GaAs, doped n type with Se at about 2×10^{18} cm^{-3} and with a thickness of 2–3 μm. Then, two thin layers of AlAs, doped p type with Mg[13,14] at approximately 1×10^{18} cm^{-3}, and separated by a thin layer of nominally undoped GaAs, were grown. Finally, a 1.8-μm top layer of GaAs, doped n type with Se at about 2×10^{18} cm^{-3}, was grown. The thicknesses of the AlAs barriers and the GaAs well were obtained from transmission electron microscopy measurements. The AlAs layer closer to the substrate was 52 Å thick, whereas the other one was only 42 A thick. The GaAs well between the two AlAs layers was 62 Å wide. Although the barriers were doped p type, they were fully depleted and still acted as potential energy barriers to the electrons in the GaAs electrodes. Devices were made by defining mesas on the epitaxial sample face using conventional photolithography as a GaAs etch (4:1:1, H_2SO_4:H_2O_2:H_2O). Ohmic contacts were made on the surface of the mesas and on the substrate by evaporating Au-Ge and Au, and annealing at 410 °C. The samples were then either mounted on transistor headers and wire bonded, or probed with a whisker. The mesas were circular and 15–80 μm in diameter.

Current-voltage curves (I-V), as well as first derivatives (dI/dV) and second derivatives (d^2I/dV^2) of the I-V curves, were measured from room temperature to 4.2 K. I-V curves were taken using a Tektronix 577 curve tracer. First and second derivatives were obtained using modulation techniques, with typical modulation voltages of 1–5 mV peak to peak.

Figures 1(a), 1(b), and 1(c) show experimental I-V curves at 300 K, 250 K, and 77 K, respectively. These curves were taken on 15-μm-diam devices, and were reproducible for devices of the same area across the whole wafer. Resonant tunneling is visible in the I-V curves at room temperature as inflections [Fig. 1(a)]. These become more pronounced as the temperature is reduced and yield negative differential resistance regions at temperatures as high as 260 K. In this sample, the I-V curves at 77 and 4.2 K were almost identical. The negative resistance regions exhibit features [Fig. 1(c)] which have not yet been identified but may be attributable to inelastic excitations of electronic states of impurities by the tunneling electrons.[15] Also note that the zero bias resistance varies very little with temperature, while the current at voltages greater than the resonance peaks decreases rapidly as the temperature is lowered. This is an indication that most of the current near zero bias is due to resonant tunneling, and that, at equilibrium, the Fermi level is close to the first resonance in the GaAs well.

In the low-temperature I-V curves [Fig. 1(c)], the ratio of the current at the peak to the current at the valley (I_p/I_v) is 3.8 in reverse bias and 3.4 in forward bias.

Whereas Fig. 1(a)–(c) show resonant tunneling effects associated with the lowest energy state in the GaAs well, an additional structure was observed at larger bias voltages in the low-temperature spectra. Although these features disappeared in the thermal current at room temperature, they could be identified without ambiguity at 77 K. Figure 2, which is a 4.2 K I-V curve, exhibits the structure at approximately -750 and 950 mV, in reverse bias and forward bias.

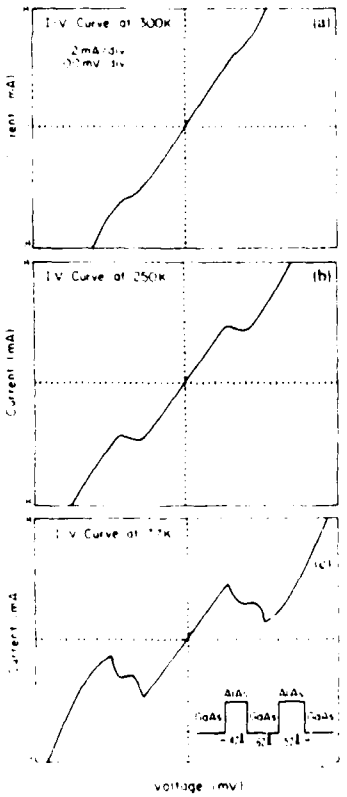

FIG. 1. Current-voltage curves at (a) 300 K, (b) 250 K, and (c) 77 K for circular devices 15 μm in diameter, in the voltage range $\pm$ 500 mV. The inflections and the negative resistance regions are due to resonant tunneling thorugh E_1, the lowest energy level in the GaAs quantum well

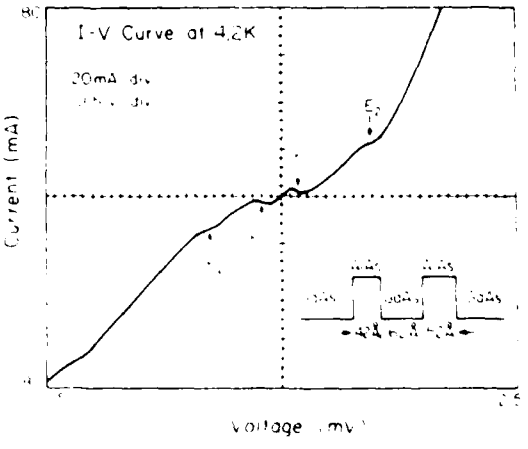

FIG. 2. Current-voltage curve at 4.2 K for circular devices 15 μm in diameter, in the voltage range $\pm$ 2.5 V. Besides the negative resistance regions due to resonant tunneling through E_1 ($\pm$ 200 mV), there are inflections due to resonant tunneling through E_2, the second energy level in the GaAs well ($-$ 750 mV and 950 mV), and maybe also through E_3, the third energy level ($-$ 2 V).

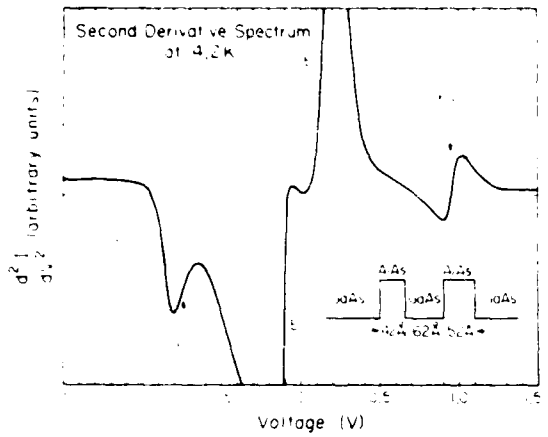

FIG. 3. Second derivative spectrum at 4.2 K for the same device as that of Fig. 2, in the voltage range ± 1.5 V. The very large peaks correspond to E_1, the first energy level in the GaAs well, and the small peaks to E_2, the second energy state in the well.

respectively. Although the amplitude of these effects with respect to the background current is much smaller than for the negative resistances discussed previously, they do correspond to tunneling through the first excited state in the GaAs well. These effects also appear in the derivative spectra. Figure 3 is a second derivative (d^2I/dV^2) at 4.2 K for the same device as that shown in Fig. 2. The peaks labeled E_2 match the structure identified in the I-V curve (Fig. 2) as the second resonance.

Calculations based on the Tsu and Esaki model,[16] and taking into account the fact that part of the voltage drop occurs in the GaAs, give reasonable agreement with the experimental data. These calculations give additional evidence that the structure observed in the I-V curves corresponds to the first and second resonances in the well. Furthermore, for a given GaAs well, the tunneling transmission probability associated with a resonance decreases rather quickly as the AlAs barriers become more asymmetric. This could explain the weakness of the second resonance with respect to the first one.

It should be mentioned that, although the structure corresponding to the first resonance is reproducible across the wafer both in position and amplitude, it is not quite so for the second resonance. This might be attributable to fluctuations in the quality of the contacts at the high currents imposed on the devices in this voltage range, and to gradual fluctuations in doping and/or layer thicknesses across the wafer.

Besides the two resonances discussed above, additional effects appear in the I-V curves in reverse bias at about -2 V (Fig. 2). This inflection is wide and its amplitude with respect to the background current is very small. Its position would be consistent with the location of the third resonance in the well. Technical limitations have prevented a more detailed study of this feature.

In summary, we have studied current transport perpendicular to two AlAs barriers separated by a GaAs quantum well in a GaAs/AlAs heterostructure grown by MOCVD. The I-V curves and their derivatives show evidence of resonant tunneling through the structure. Effects corresponding to the first resonance in the GaAs quantum well are visible in the I-V curves at room temperature, and negative resistance regions are observed at temperature as high as 260 K. The low-temperature I-V curves also display an additional structure corresponding to resonant tunneling through the second and perhaps the third energy levels in the well.

The authors wish to acknowledge R. S. Bauer, R. L. Thornton, D. L. Smith, T. L. Paoli, and W. Streifer for valuable discussions and are grateful to H. Chung, R. D. Yingling, Jr., F. Endicott, J. Tramontana, M. Bernstein, M. Mosby, J. Walker, A. Alimonda, G. L. Harnagel, and R. Ridder for technical assistance. This work was supported in part by the Office of Naval Research under contract No. N00014-82-K-0556.

[1] B. A. Vojak, S. W. Kirchoefer, H. Holonyak, Jr., R. D. Dupuis, P. D. Dapkus, and R. Chin, J. Appl. Phys. **50**, 5830 (1979).
[2] A. C. Gossard, W. Brown, C. L. Allyn, and W. Wiegmann, J. Vac. Sci. Technol. **20**, 694 (1982).
[3] D. Delagebeaudeuf, P. Delescluse, P. Etienne, J. Massies, M. Laviron, J. Chaplart, and N. T. Linh, Electron. Lett. **18**, 85 (1982).
[4] T. W. Hickmott, P. M. Solomon, R. Fisher, and H. Morkoç, Appl. Phys. Lett. **44**, 90 (1984).
[5] R. T. Collins, J. Lambe, T. C. McGill, and R. D. Burnham, Appl. Phys. Lett. **44**, 532 (1984).
[6] I. Hase, H. Kawai, K. Kaneko, N. Watanabe, Electron. Lett. **20**, 491 (1984).
[7] T. C. L. G. Sollner, W. D. Goodhue, P. E. Tannenwald, C. D. Parker, and D. D. Peck, Appl. Phys. Lett. **43**, 588 (1983).
[8] L. L. Chang, L. Esaki, and R. Tsu, Appl. Phys. Lett. **24**, 593 (1974).
[9] R. T. Collins, A. R. Bonnefoi, J. Lambe, T. C. McGill, and R. D. Burnham, Proceedings of the 17th ICPS Conference, San Francisco, August 6–10, 1984.
[10] R. T. Collins, A. R. Bonnefoi, J. Lambe, T. C. McGill, and R. D. Burnham, Proceedings of the International Conference on Superlattices, Illinois, August 13–16, 1984.
[11] H. M. Manasevit, Appl. Phys. Lett. **12**, 156 (1968).
[12] R. D. Dupuis and P. D. Dapkus, Appl. Phys. Lett. **31**, 466 (1977).
[13] C. R. Lewis, W. T. Dietze, and M. J. Ludowise, Electron. Lett. **18**, 569 (1982).
[14] R. D. Burnham, W. Streifer, D. R. Scifres, C. Lindstrom, T. L. Paoli, and N. Holonyak, Electron. Lett. **18**, 1095 (1982).
[15] N. Holonyak, Jr., D. L. Deune, R. D. Burnham, and C. B. Duke, Phys. Lett. **24**, 589 (1970).
[16] R. Tsu, and L. Esaki, Appl. Phys. Lett. **22**, 562 (1973).

Uniformity in the electrical characteristics of GaAs/AlAs tunnel structures grown by metalorganic chemical vapor deposition

A. R. Bonnefoi and T. C. McGill
California Institute of Technology, Pasadena, California 91125

R. D. Burnham
Xerox Corporation, Palo Alto, California 94304

(Received 17 December 1984; accepted for publication 20 May 1985)

Uniformity of current-voltage characteristics in GaAs/AlAs tunnel structures grown by metalorganic chemical vapor deposition has been investigated by studying electronic transport perpendicular to GaAs layers separated by one or two AlAs barriers. For each sample, measurements of the current-voltage curves and their first and second derivatives, for series of 10 to 80 identical devices taken randomly across the sample, gave reproducible and uniform results. These showed evidence that the doping concentrations and layer thicknesses were uniform across the wafers. In single barrier structures, they further suggested that the average fluctuations in the thicknesses of ultrathin layers should be within one atomic layer.

Semiconductor heterostructures with small characteristic dimensions are the object of considerable theoretical and experimental work. They are frequently fabricated from GaAs and $Al_xGa_{1-x}As$ using techniques such as molecular beam epitaxy (MBE) and metalorganic chemical vapor deposition (MOCVD). Since the conduction-band offset between the GaAs and the $Al_xGa_{1-x}As$ causes $Al_xGa_{1-x}As$ layers to act as potential energy barriers to electrons in the GaAs layers, it becomes possible to grow quantum well and quantum barrier structures. In these structures, an essential current transport mechanism is tunneling. The tunneling effects are associated with very important theoretical properties and are expected to yield novel electronic features of considerable interest. In the simplest configuration, where two GaAs layers are separated by a single $Al_xGa_{1-x}As$ barrier, elastic and inelastic tunneling take place.[1-4] In samples containing a GaAs quantum well adjacent to two $Al_xGa_{1-x}As$ barriers, resonant tunneling occurs.[5-10]

We report in this letter a systematic study of the reproducibility and the uniformity of these phenomena. We measured current-voltage (I-V) curves and their first (dI/dV) and second (d^2I/dV^2) derivatives for MOCVD grown structures with both one and two AlAs barriers. For each sample, several series of 10 to 80 identical devices of given sizes, taken at random across the sample, were systematically tested. The results of the measurements, which were strongly correlated to the parameters of the structures, showed evidence of the growth uniformity of the wafers.

The samples used in this study were grown by an MOCVD technique[11,12] on a GaAs substrate doped n type with Si at $(2-3)\times10^{18}$ cm^{-3}. The first layer grown on the substrate was one of GaAs, 2–3 μm thick, doped n type with Se at about 2×10^{18} cm^{-3}. Following this, either a single thin layer of AlAs, or two thin layers of AlAs separated by a thin layer of nominally undoped GaAs, were grown. Finally, a top layer of GaAs, doped n type with Se, was grown. The AlAs layers were doped p type with Mg (Refs. 13 and 14) at approximately 1×10^{18} cm^{-3}. In the single barrier samples, the AlAs layer was typically from 50 to 150 Å wide, whereas the top GaAs layer was approximately 3 μm thick and doped at about 5×10^{18} cm^{-3}. In the double barrier samples, the AlAs layers and the GaAs well were on the order of 50 Å wide, whereas the top GaAs layer was approximately 2 μm thick and doped at about 2×10^{18} cm^{-3}. Although the barriers were doped p type, they were fully depleted and still acted as potential energy barriers to the electrons in the GaAs electrodes. Devices were prepared on the samples by defining mesas on the epitaxial surface using conventional photolithography and a GaAs etch (4:1:1, H_2SO_4:H_2O_2:H_2O). Ohmic contacts were made on the surface of the mesas and on the substrate by evaporating Au-Ge and Au, and annealing at 400–420 °C for 15–20 s. Finally, the samples were either mounted on transistor headers and wire bonded, or probed with a whisker. The mesas were circular and 12–700 μm in diameter. For the purpose of this study, special care was taken to prepare all the samples and devices under similar conditions. In particular, since many electrical properties depend on the device area, the actual device diameters were carefully measured. Furthermore, in order to reduce the error introduced by undercutting during the etching process, the top GaAs layer was preliminary etched down to about 0.2 μm. The mesas were then obtained by etching only about 1 μm down from the surface. This procedure significantly reduced the uncertainty in the device areas and yielded well defined mesas.

Starting from wafers of about 2 cm^2, at least five small pieces of approximately 4 mm^2, chosen as far apart from each other as possible, were cleaved. A large number of mesas were then defined on each one of these pieces and, depending on their size, about 10 to 80 devices taken at random were systematically tested. Although this procedure was repeated for different device sizes ranging between 12 and 700 μm, a more thorough study was performed for devices close to 50 and 80 μm in diameter. Current-voltage curves, as well as their first and second derivatives, were measured at temperatures ranging from 4.2 to 300 K. The I-V curves gave information about current transport mechanisms. They revealed mainly elastic tunneling in the single barrier structures and resonant tunneling in the double barrier samples. Structure in the derivatives of the I-V curves indicated the presence of inelastic and resonant tunneling processes and allowed the identification of fundamental excitations creat-

 0003-6951/85/150307-03$01.00

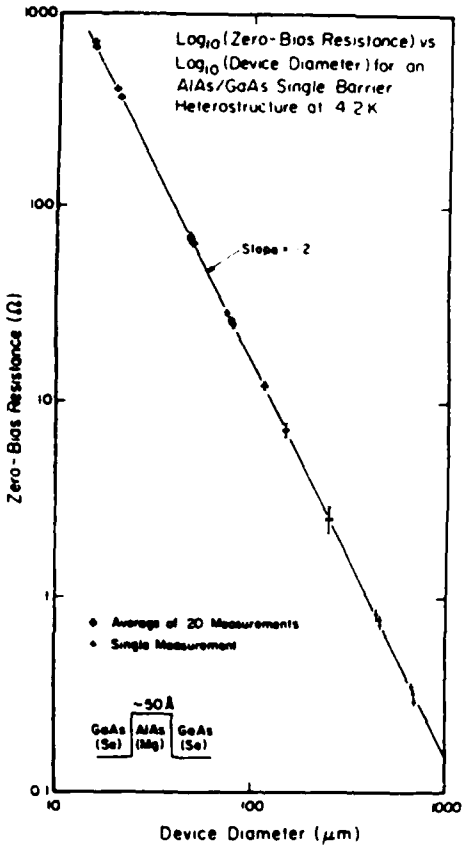

FIG. 1. Log_{10} (zero-bias resistance) vs log_{10} (device diameter) for a single-barrier sample.

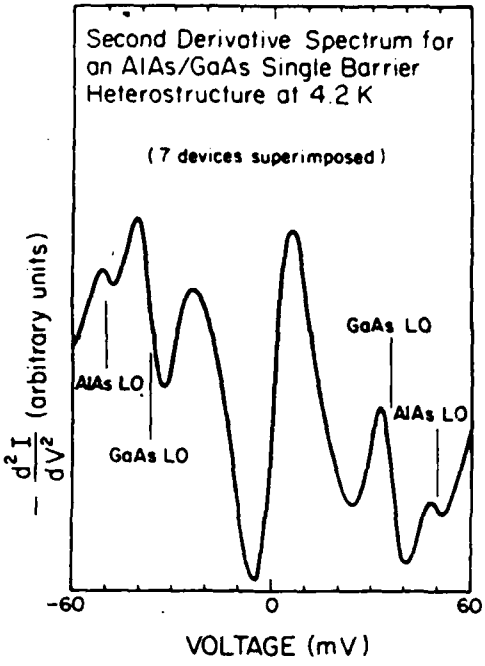

FIG. 2. Second derivative spectra at 4.2 K for seven devices, 78 μm in diameter, selected randomly among 100 of the same size, for a single barrier structure.

ed by the tunneling electrons. The *I-V* curves were taken using a Tektronix 577 curve tracer. Point-by-point measurements using a dc power supply were also made. First and second derivatives were obtained using modulation techniques, with typical modulation voltages of 1–5 mV peak to peak.[15]

Some of the properties which were found to be of interest are described below. For the one-barrier samples, in which elastic and inelastic tunneling occur, we studied (i) the zero-bias resistance at different temperatures and (ii) the uniformity and reproducibility of the *I-V* curves as well as their first and second derivatives. In the double-barrier structures, resonant tunneling takes place and the *I-V* curves feature regions of negative differential resistance. For these samples, we performed a careful study of (i) the zero-bias resistance at different temperatures, (ii) the voltages and currents at the peaks and valleys of the negative resistance regions, and (iii) the uniformity and reproducibility of the features displayed in the derivatives. Only a few of these properties are discussed in the present letter.

Figure 1 is a plot of the logarithm of the zero-bias resistance as a function of the logarithm of the device diameter for a single-barrier sample. The error bars correspond to averages of more than 20 measurements made on different devices of a given size and taken at random. The crosses correspond to single measurements. The curve passing through the experimental data is a straight line of slope almost exactly (− 2), indicating that the zero-bias resistance does scale with area. The zero-bias resistance, which depends on the transmission rate through the AlAs barrier for elastic tunneling, should decrease exponentially as the width of the barrier is increased. Therefore, it is expected to depend strongly on the thickness of the AlAs barrier through which the electrons actually tunnel. Since the tunneling electrons will always tend to pass through the thinnest part of a barrier, variations in the values of the zero-bias resistance are directly correlated to the fluctuations in the barrier width. Furthermore, keeping all the other parameters constant, a 7 Å change in the barrier thickness makes the zero-bias resistance vary by an order of magnitude.[15] Consequently, tunneling measurements provide a sensitive test of barrier thickness. In addition, the zero-bias resistance depends significantly on the doping concentrations, which define the actual position of the Fermi level in the GaAs electrodes. It should also depend on the contacts. However, these had resistances which were negligible compared to the tunneling resistances of the barriers. Therefore, they did not alter significantly the tunneling currents. In Fig. 1, it should be noted that the error bars, which represent the actual standard deviation of the results, are very small. This clearly indicates that the results of the measurements were reproducible across the whole wafer. This further shows that leakage and edge currents, as well as effects associated with the local fluctuations in the electrostatic potential due to the ionized dopants, were negligible compared to the tunneling currents. The above discussion about the dependence of the zero-bias resistance upon barrier thickness and doping concentrations allows us to conclude that both the doping profiles and the layer thicknesses were uniform across the entire sample. It further suggests that the average fluctuations in the thicknesses of ultrathin layers in single-barrier structures should be within one atomic layer.

Figure 2 is the superposition of seven second derivative (d^2I/dV^2) curves at 4.2 K for seven different devices, 78 μm

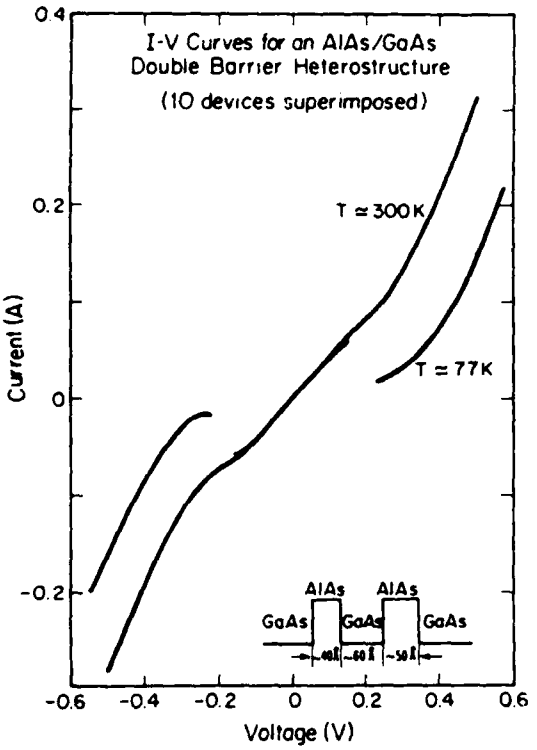

FIG. 3. *I-V* curves at 300 K and 77 K for ten devices, 78 μm in diameter, for a double-barrier sample.

in diameter, taken randomly among 100 of the same size. The sample is the same one as in Fig. 1. The fact that these spectra overlap exactly was a common feature of all the series of devices tested. Second derivative curves reveal inelastic tunneling through the AlAs barrier. Tunneling electrons can create fundamental excitations, provided the applied bias is increased above the excitation energy ($\hbar\omega_0$). Thus, there exists a threshold voltage $V_0 = \hbar\omega_0/e$, which corresponds to a change in the slope of the *I-V* curve. Since the structure is symmetric, the same changes should occur in forward and in reverse biases. Therefore, steps which are symmetric with respect to bias appear in the first derivative spectra at voltages $\pm V_0$, whereas the second derivative curves show peaks at the same voltages, but antisymmetric with respect to bias. In Fig. 2, a reproducible structure is observed at the GaAs and the AlAs longitudinal optical (LO) phonon energies, $\pm$ 36 meV and $\pm$ 50 meV, respectively.

For double-barrier samples, series of more than 60 devices were tested for devices close to 20, 50, and 80 μm in diameter. *I-V* curves as well as first and second derivatives were measured. In a given series, the curves would all coincide, except for an occasional one, which could be due to the preparation procedure, a bad contact, or an improper bond. Figure 3 shows experimental *I-V* curves at 300 and 77 K for 10 different devices, 78 μm in diameter, taken randomly across the wafer of a double-barrier sample. The breaks in the low-temperature *I-V* curves are due to the fact that the curve tracer used for these measurements could not reliably resolve regions of negative differential resistance. But a more detailed discussion of the negative resistance regions is not the subject of this letter and was reported elsewhere.[10] Resonant tunneling currents are critically dependent upon the layer thicknesses and the doping concentrations. Therefore, the reproducibility and uniformity of the experimental data are again a clear indication that the geometrical parameters and the doping profiles were uniform throughout the entire sample.

In summary, we have studied the reproducibility and uniformity of *I-V* characteristics and their derivatives in MOCVD grown GaAs/AlAs tunnel structures. We have investigated electronic transport, mainly elastic, inelastic,and resonant tunneling, perpendicular to GaAs electrodes separated by one or two AlAs layers. For each sample, systematic measurements were made on a large number of devices taken randomly across the wafer. The measured properties were critically dependent on the layer thicknesses and the doping concentrations. This study did not allow us to draw conclusions about the abruptness of the interfaces and the presence of defects and impurities. However, the reproducibility and uniformity of the experimental results showed evidence that the doping profiles and the geometrical parameters of the samples were uniform across the wafers. In the single barrier samples, they further suggested that the average fluctuations in the thicknesses of ultrathin layers should be within one atomic layer.

The authors wish to acknowledge R. S. Bauer, R. L. Thornton, D. L. Smith, T. L. Paoli, and W. Streifer for valuable discussions and are grateful to H. Chung, R. D. Yingling, Jr., F. Endicott, M. Bernstein, M. Mosby, J. Walker, A. Alimonda, and G. L. Harnagel for technical assistance. This work was supported in part by the Office of Naval Research under contract No. N00014-82-K-0556.

[1] A. C. Gossard, W. Brown, C. L. Allyn, and W. Wiegmann, J. Vac. Sci. Technol. **20**, 694 (1982).
[2] D. Delagebeaudeuf, P. Delescluse, P. Etienne, J. Massies, M. Laviron, J. Chaplart, and N. T. Linh, Electron. Lett. **18**, 85 (1982).
[3] R. T. Collins, J. Lambe, T. C. McGill, and R. D. Burnham, Appl. Phys. Lett. **44**, 532 (1984).
[4] I. Hase, H. Kawai, K. Kaneko, N. Watanabe, Electron. Lett. **20**, 491 (1984).
[5] R. Tsu and L. Esaki, Appl. Phys. Lett. **22**, 562 (1973).
[6] T. C. L. G. Sollner, W. D. Goodhue, P. E. Tannenwald, C. D. Parker, and D. D. Peck, Appl. Phys. Lett. **43**, 588 (1983).
[7] L. L. Chang, L. Esaki, and R. Tsu, Appl. Phys. Lett. **24**, 593 (1974).
[8] R. T. Collins, A. R. Bonnefoi, J. Lambe, T. C. McGill, and R. D. Burnham, Proceedings of the 17th ICPS Conference, San Francisco, August 6–10, 1984.
[9] R. T. Collins, A. R. Bonnefoi, J. Lambe, T. C. McGill, and R. D. Burnham, Proceedings of the International Conference on Superlattices, Illinois, August 13–16, 1984.
[10] A. R. Bonnefoi, R. T. Collins, T. C. McGill, R. D. Burnham, and F. A. Ponce, Appl. Phys. Lett. **46**, 285 (1985).
[11] H. M. Manasevit, Appl. Phys. Lett. **12**, 156 (1968).
[12] R. D. Dupuis and P. D. Dapkus, Appl. Phys. Lett. **31**, 466 (1977).
[13] C. R. Lewis, W. T. Dietze, and M. J. Ludowise, Electron. Lett. **18**, 569 (1982).
[14] R. D. Burnham, W. Streifer, D. R. Scifres, C. Lindstrom, T. L. Paoli, and N. Holonyak, Jr., Electron. Lett. **18**, 1095 (1982).
[15] R. T. Collins, Ph.D. thesis, California Institute of Technology, 1985.

Current transport mechanisms in GaAs/AlAs tunnel structures grown by metal–organic chemical vapor deposition

A. R. Bonnefoi, D. H. Chow, and T. C. McGill
T. J. Watson, Sr., Laboratory of Applied Physics, California Institute of Technology, Pasadena, California 91125

R. D. Burnham and F. A. Ponce
Xerox Corporation, Palo Alto, California 94304

(Received 5 March 1986; accepted 7 April 1986)

Elastic and inelastic tunneling processes are investigated in GaAs–AlAs–GaAs double heterojunctions grown in the [100] direction by metal–organic chemical vapor deposition (MOCVD). The AlAs quantum barriers in the heterostructures studied are doped *p*-type with Mg. Theoretical calculations of tunneling currents are performed and compared with experimental *I–V* data. It is found that for structures with thin AlAs barriers, the dominant current transport mechanism at low temperatures is tunneling through the AlAs band gap at both the Γ and *X* points. This is consistent with inelastic processes observable in first (dI/dV) and second (d^2I/dV^2) derivative spectra obtained with modulation techniques. A simple model, developed for calculating impurity-assisted tunneling currents, shows that the role of barrier impurities becomes more important as the barrier is grown thicker. Implications of some of these results for resonant tunneling heterostructures consisting of two AlAs quantum barriers separated by a GaAs quantum well are discussed. Experimental second derivative spectra showing reproducible features are also presented for these double barrier structures.

I. INTRODUCTION

Because of their numerous potential device applications, semiconductor quantum well and quantum barrier heterostructures are the object of considerable theoretical and experimental work. These structures are frequently fabricated from GaAs and $Al_xGa_{1-x}As$, using techniques such as molecular beam epitaxy (MBE) and metal–organic chemical vapor deposition (MOCVD) to achieve small characteristic dimensions. In structures with thin quantum barriers, an important current transport mechanism is electron tunneling. Several studies of electronic transport in single and double barrier tunnel structures have been reported.[1–10] The associated tunneling effects yield novel electronic properties, some of which remain to be fully understood. Most of the studies to date, both theoretical and experimental, have used $Al_xGa_{1-x}As$ quantum barriers in which the Al composition, *x*, was small enough that the alloy was still direct.[5–10] Furthermore, most of the experimental investigations have been performed on MBE grown wafers.[4–8] Only a few studies have been reported on MOCVD grown samples,[1–3] and/or structures in which the barriers consisted of indirect $Al_xGa_{1-x}As$,[3,4] or pure AlAs.[1,2]

In this paper, we concentrate primarily on current transport mechanisms at low temperatures in GaAs–AlAs–GaAs double heterojunctions grown by MOCVD in the [100] direction. In Sec. II, we briefly present the sample growth and preparation procedures. In Sec. III, we report both experimental and theoretical results for structures with thin *p*-type AlAs barriers. We first calculate current–voltage (*I–V*) characteristics at low temperatures due to elastic tunneling through the AlAs band gap at the Γ point, using the actual shape of the barrier obtained from band bending calculations. Upon comparing the calculated and experimental *I–V* curves, it is found that tunneling through the AlAs Γ-point barrier fails to explain the experimental data. This indicates that other transport mechanisms must contribute to the total current. Tunneling through the AlAs band gap at the *X* point is then discussed. Good theoretical fits of the experimental *I–V* data can be obtained by considering tunneling through both the Γ- and *X*-point barriers. In Sec. IV, we introduce a new element to the calculation of the theoretical *I–V* curves: the presence of trap levels in the AlAs band gap, due to defects or impurities. A simple model is developed to calculate the impurity-assisted tunneling current. This current becomes more important as the quantum barriers become thicker, and can actually become the dominant current transport mechanism through thick enough barriers. In Sec. V, implications of some of these results for resonant tunneling heterostructures made of two AlAs quantum barriers separated by a GaAs quantum well are discussed. For these structures, experimental derivative spectra showing reproducible and periodic features are also reported. Finally, the results of the present study are summarized in Sec. VI.

II. EXPERIMENTAL PROCEDURES

The samples used in this study were grown by an MOCVD technique[11,12] on a [100]-oriented GaAs substrate doped *n*-type with Si at $2–3\times10^{18}$ cm^{-3}. A first epitaxial layer of degenerate GaAs, doped *n*-type with Se, was grown 2–3 μm thick. In single barrier structures, this layer was followed first by an AlAs layer doped *p*-type with Mg,[13,14] and then by another GaAs layer, degenerately doped with Se. Samples were grown with GaAs dopings ranging between 1×10^{18} and 5×10^{18} cm^{-3}, AlAs barrier thicknesses between 40 and 250 Å, and barrier dopings estimated to vary between 1×10^{17} and 3×10^{18} cm^{-3}. In dou-

 0734-211X/86/040988-08$01.00

ble barrier structures, the first epitaxial GaAs layer was followed by two thin AlAs layers separated by a quantum well of nominally undoped GaAs. The AlAs barriers were doped *p*-type with Mg at approximately 1×10^{18} cm^{-3}. Finally, a GaAs top layer was grown, degenerately doped with Se. The thicknesses of the AlAs barriers and the GaAs wells were determined by transmission electron microscopy (TEM). Electrode dopings were obtained from Polaron doping profiles. Barrier dopings were estimated from the flow rates used during growth. They could thus be in error due to the difficulty of accurately calibrating dopings in such thin layers.

Devices were made by defining mesas on the epitaxial sample face using conventional photolithography and a GaAs etch (4:1:1, H_2SO_4:H_2O_2:H_2O). The mesas were circular and 50–700 μm in diameter. Ohmic contacts were made on the surface of the mesas and on the substrate by evaporating Au–Ge, or Au–Ge, Ni, Au, and then annealing at 380–410 °C for 20–30 s.

Measurements of current–voltage curves (I–V), as well as first (dI/dV) and second (d^2I/dV^2) derivatives of the I–V curves were performed at temperatures ranging from 300 to 4.2 K. The I–V curves were measured with an HP 4145 semiconductor parameter analyzer. The first and second derivative spectra were obtained using modulation techniques at 5 and 50 kHz, respectively.

III. RESULTS ON THIN SINGLE BARRIER STRUCTURES

In this section, we present both experimental and theoretical results for single barrier heterostructures having a thin AlAs barrier layer totally depleted of carriers. A number of studies have reported that the dominant current transport mechanism at low temperatures in $Al_xGa_{1-x}As$ quantum barrier structures is elastic tunneling through the $Al_xGa_{1-x}As$ direct band gap at the Γ point.[3,5,6] In these studies, theoretical I–V curves were calculated assuming a trapezoidal shape for the quantum barrier under applied bias, and compared to experimental data on logarithmic scales. Nevertheless, discrepancies were observed[5] which indicated that other current transport mechanisms can compete with elastic Γ-point tunneling. Theoretical studies have also reported that Γ-point electrons in the GaAs electrodes should tunnel through the $Al_xGa_{1-x}As$ band gap at the Γ point even in indirect alloys.[15,16] However, we show here that experimental data for structures with pure AlAs barriers cannot be explained by Γ-point tunneling alone. We propose that there is a small, but nonnegligible probability that the incident electrons tunnel through the AlAs X-point barrier.

Current densities are calculated using the following approach. First, the actual shape of the conduction band edge in the electrodes and the barrier is determined from band bending calculations. These calculations are found to be of critical importance, particularly in samples with heavily doped barriers. They are performed by solving Poisson's equation self-consistently throughout the entire heterostructure at each applied voltage. The transmission coefficient for tunneling electrons is then calculated using the WKB approximation. The attenuation constant in the barrier is determined from a two-band model, **k·p** theory formula[17] for electrons tunneling through the AlAs Γ point, and a simple "one-band model" formula for electrons tunneling through the AlAs X point. Finally, the current density, J, is calculated as a function of applied voltage, V, using the approach of Tsu and Esaki.[9]

Although our study was performed on a wide selection of samples and at temperatures ranging from 300 to 4.2 K, we only illustrate the most important results by discussing data obtained at low temperatures from a single barrier structure having a thin *p*-type AlAs barrier layer. A more detailed report, including results for heterostructures with *n*-type AlAs barriers, will be presented in a forthcoming publication.

In the structure of interest, the GaAs electrodes are doped *n*-type with Se at $4–5 \times 10^{18}$ cm^{-3}. The doping in the *p*-type AlAs barrier layer is estimated to be on the order of 10^{19} cm^{-3}. A barrier thickness of 48 Å was obtained from TEM measurements, accurate to within one monolayer. Figure 1 shows the calculated conduction band edge of the structure at the Γ and X points as a function of distance in the direction perpendicular to the plane of the layers. Figure 1(a) depicts thermal electronic equilibrium while Fig. 1(b) corresponds to an applied bias of 200 mV. In the band bending calculations, the dopings in the *n*-type GaAs electrodes and the *p*-type AlAs barrier are taken to be 4×10^{18} and 3×10^{18} cm^{-3}, respectively. The barrier thickness is 48 Å. The calculations are performed assuming a temperature of 0 K. The values of the band offsets are key parameters in determining the shape of the barriers seen by the tunneling electrons. These values are still a matter of debate. In a recent experimental study, Batey *et al.*[18] obtained a valence band discontinuity of 0.55 eV in GaAs–AlAs heterostructures. Using this result, values close to 190 meV and 1.04 eV can be calculated for the conduction band offsets at the X and Γ points, respectively. It should be noted that when such values are used, the X-point conduction band edge lies at higher energies in GaAs than in AlAs. This is illustrated in Fig. 1, with the solid line corresponding to the Γ-point conduction band edge and the dashed line to the X-point conduction band edge. Figure 1(a) shows that the barrier is totally depleted of carriers and that the effect of band bending is to increase the average barrier height seen by the tunneling electrons. This effect increases with barrier doping and thickness. In Fig. 1(b), a voltage of 200 mV is applied across the structure. This voltage alters the shape of the conduction band edge in the cladding layers as well as in the barrier. This is another essential factor in calculating tunneling currents. In Fig. 2, we show the experimental characteristic, $J_{exp}(V)$, at 4.2 K in the voltage range 0–200 mV and, on the same linear scale, the calculated current density, $J_{el}^{\Gamma}(V)$, for elastic Γ-point tunneling. Since the structure is symmetric, the J–V curves are symmetric with respect to the origin and we only show the forward bias direction. The two curves are in good agreement at very low biases ($\lesssim 20$ mV), but start to deviate significantly in magnitude and shape at higher voltages. While J_{el}^{Γ} varies almost linearly with voltage, the experimental cur-

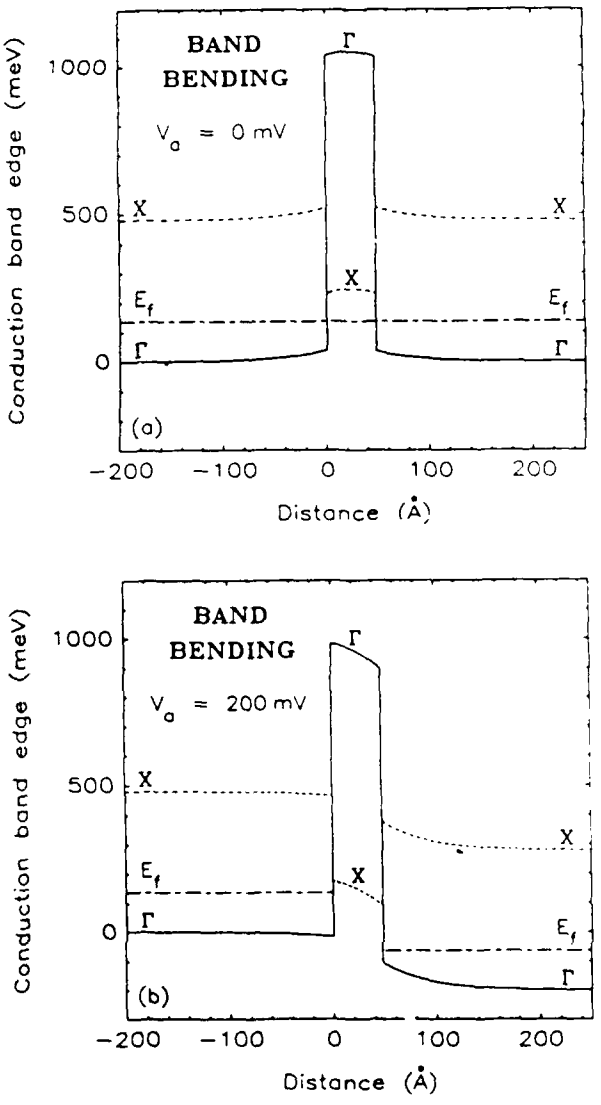

FIG. 1. Calculated conduction band edge at the Γ point (solid line) and at the *X* point (dashed line), as a function of distance in the direction perpendicular to the plane of the layers, for a GaAs–AlAs–GaAs single barrier heterostructure. The GaAs electrodes are doped *n*-type at 4×10^{18} cm^{-3}. The AlAs barrier is 48 Å thick and doped *p*-type at 3×10^{18} cm^{-3}. The conduction band discontinuities at the *X* and Γ points are 190 meV and 1.04 eV, respectively. (a) Corresponds to thermal electronic equilibrium, and (b) to an applied voltage of 200 mV. The solid–dashed lines correspond to the Fermi level, E_f, in the electrodes. The temperature is assumed to be 0 K.

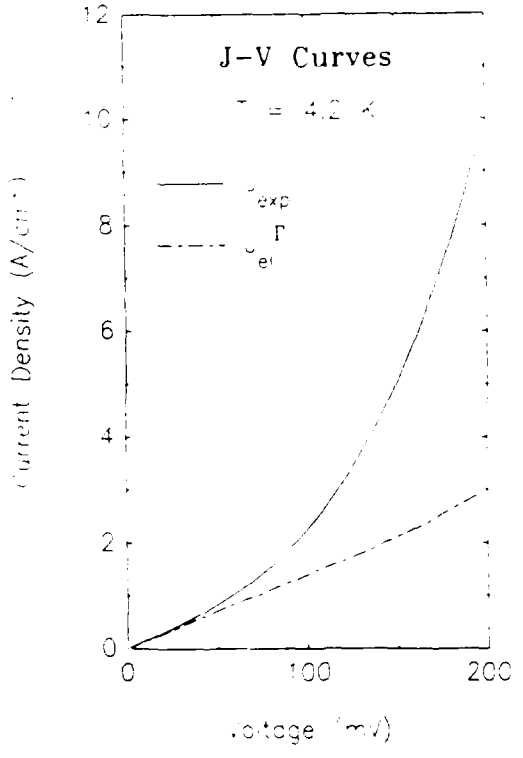

FIG. 2. Experimental and theoretical current–voltage characteristics for the single barrier structure shown in Fig. 1. The solid line corresponds to the experimental current density, J_{exp}. The dashed line is the calculated Γ-point elastic current density, J_{el}^{Γ}.

rent density, J_{exp}, displays a nearly exponential voltage dependence. Similar discrepancies between experimental and theoretical data are observed in all of our samples. This is a clear indication that elastic tunneling through the AlAs band gap at the Γ point does not account for all of the experimental current and that other transport mechanisms are present. These observations are further supported by derivative spectra which reveal threshold voltages for impurity-assisted and/or inelastic tunneling processes. This is illustrated in the second derivative curve, $(d^2I/dV^2)/I$, shown in Fig. 3. This spectrum displays two prominent and broad features, labeled (a) and (b), peaked at approximately 20 and 80 mV. It also reveals two narrower peaks at about 37 and 50 mV. These have been attributed previously to electron-optical phonon coupling in the GaAs electrodes, and the excitation of longitudinal optical (LO) phonons in the AlAs barrier, respectively.[1] Leakage has been eliminated as a possible source of current by verifying that the experimental *J–V* curves were reproducible and independent of device area. The behavior of the Γ-point elastic current can easily be understood in terms of the complex band structure of AlAs: In the band gap, the imaginary part of the complex wave vector at the Γ point varies very slowly with energy, except near the conduction and valence band edges. This is due to the small Γ-point effective mass. Therefore, because of the large conduction band offset ($\simeq 1$ eV), the Γ-point current remains slowly varying with voltage up to about 0.8 V.

In order to tentatively explain the discrepancies between experimental *J–V* data and calculated Γ-point elastic tunneling currents, a number of transport mechanisms can be suggested. The simplest is the emission of phonons or the excitation of collective modes by electrons tunneling through the AlAs Γ-point barrier. Although some of these inelastic processes may be resolved in derivative spectra, they yield currents which are typically at least two or three orders of magnitude smaller than elastic currents, and therefore too small to account for the observed discrepancies. Another possible current transport mechanism is tunneling via energy levels in the AlAs band gap or at the GaAs/AlAs interfaces. A simple model for impurity-assisted tunneling is developed in Sec. IV. Assuming that no impurity bands or clusters are

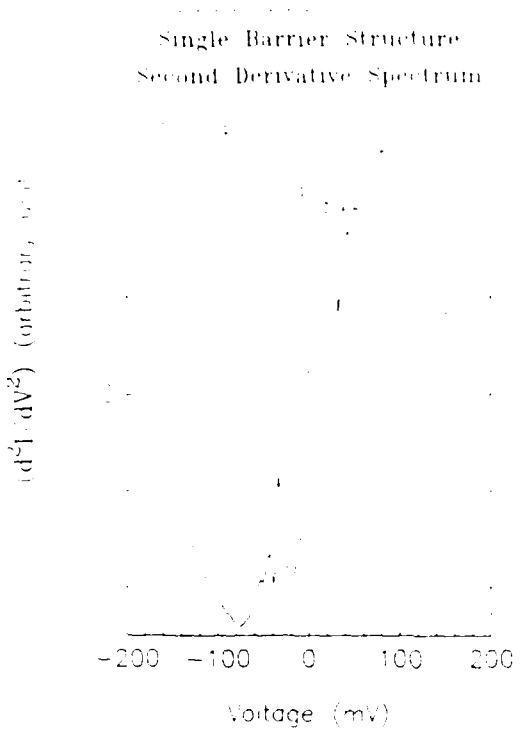

FIG. 3. Experimental second derivative spectrum $(d^2I/dV^2)(V)$, at 4.2 K for the single barrier heterostructure illustrated in Fig. 1. The two most prominent peaks labeled (a) and (b) may correspond to inelastic processes by which GaAs Γ-point electrons scatter into AlAs X-point states. The two narrower peaks at 37 and 50 mV have been attributed previously to electron-optical phonon coupling in the GaAs electrodes, and the excitation of longitudinal optical (LO) phonons in the AlAs barrier, respectively (Ref. 1).

formed, this mechanism gives negligible current densities for the 48 Å barrier structure considered here. Another possibility is to take into account tunneling through the AlAs band gap at symmetry points other than the Γ point. In the case of epitaxial growth in the [100] direction, an important contribution could come from the AlAs X-point valleys. For electrons tunneling from left to right, new channels open when the Fermi level in the left electrode and the X-point conduction band edge in the right electrode align. However, such processes can only occur at voltages >350 meV in the structure discussed here. This is again in disagreement with experimental data. Other mechanisms can allow electrons occupying Γ-point states in both GaAs electrodes to tunnel through the AlAs X-point barrier. Two such processes are discussed below.

First, Γ-point electrons near the GaAs–AlAs interface may scatter inelastically into virtual states beneath the four AlAs X valleys lying along the k_y and k_z directions, parallel to the plane of the layers. They may then tunnel through the AlAs band gap at the X point, and scatter again, near the AlAs–GaAs interface, into the Γ valley in the right electrode. Since electrons travel along the x axis, perpendicular to the plane of the layers, the effective mass in the barrier is the small transverse effective mass $m_t^* = 0.19m_e$, where m_e is the free electron mass. Such inelastic processes, which require two scattering events, can occur through a number of mechanisms such as phonon scattering, for example. Calculations of scattering matrix elements and current densities are being performed to determine which of these processes may explain the experimental data. The matrix elements can be complicated functions of the scattering mechanism, applied voltage, structure characteristics, electron energy, and temperature. In the present study, we simply assume that there is a small probability that incident electrons tunnel through the AlAs band gap at the X point and that the scattering matrix element for a given process is constant. The calculated current density for any such mechanism thus contains an empirical factor, B_{in}. Threshold voltages for these inelastic processes are chosen to coincide with some of the most prominent peaks observed in experimental second derivative spectra $(d^2I/dV^2)(V)$. The total theoretical current density, $J_{th}(V)$, is then calculated by summing the contributions from Γ-point elastic tunneling and X-point inelastic tunneling. Figure 4 is a plot of J_{th} as a function of applied voltage for the structure discussed here. Only two inelastic processes are used to calculate the X-point inelastic tunneling current. These two processes are assigned threshold voltages of 20 and 80 mV, and empirical B_{in}'s of 0.6×10^{-4} and 1.3×10^{-4}, respectively. The threshold voltages correspond to the two most prominent peaks labeled (a) and (b) in the second derivative curve illustrated in Fig. 3. Since two scattering events are required to allow electrons to tunnel through the AlAs X-point barrier, peaks should be observed

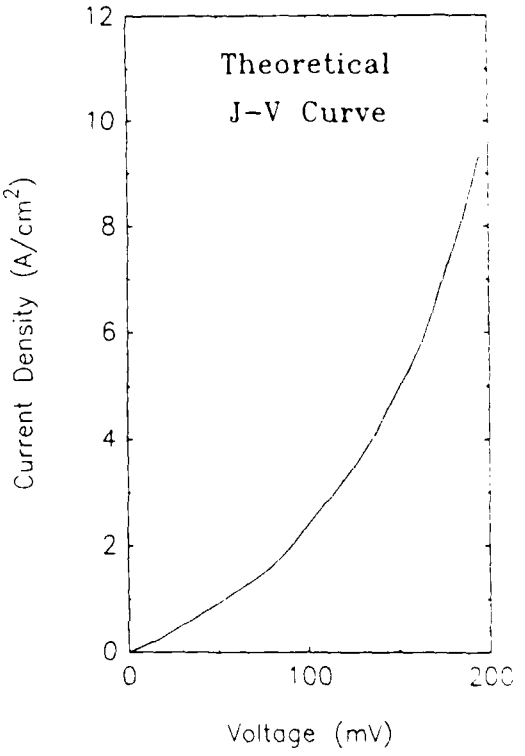

FIG. 4. Total theoretical current density, J_{th}, obtained by summing the contributions of Γ-point elastic tunneling and two X-point inelastic tunneling mechanisms, for the same single barrier structure as in Fig. 2. For the inelastic processes, threshold voltages of 20 and 80 mV are taken in agreement with experimental second derivative (d^2I/dV^2) data. The corresponding empirical B_{in}'s are 0.6×10^{-4} and 1.3×10^{-4}, respectively.

in the $(d^2I/dV^2)(V)$ spectra at voltages corresponding to the sum of the two scattering energies. Peak (a) would thus be consistent with the inelastic excitation of two X-point transverse acoustic (TA) phonons. On the other hand, the broad peak (b) may result from a number of scattering mechanisms which are not individually resolved in the spectrum shown in Fig. 3. Such inelastic processes could be the excitation of X-point longitudinal acoustic (LA), transverse optical (TO), and longitudinal optical (LO) phonons, for example. The experimental and theoretical J–V curves presented in Figs. 2 and 4 are in good agreement.

Another possible way for electrons to tunnel through the AlAs band gap at the X point arises from the coupling of AlAs X-point states to GaAs Γ-point states due to the breaking of translational symmetry in the direction perpendicular to the layers. This makes it possible for Γ-point electrons in one GaAs electrode to tunnel elastically through the AlAs X-point barrier into Γ-point states in the other GaAs electrode. In this process, the virtual X-point states to consider are those below the two X valleys lying along the k_x direction, perpendicular to the plane of the layers. Since electrons travel along the x axis, the effective mass of importance in the barrier is the large longitudinal effective mass $m_l^* = 1.1m_e$. Preliminary calculations indicate that the coupling of states having different symmetries in GaAs and AlAs may be significant in the heterostuctures studied and could yield current densities large enough to account for the discrepancies observed between experimental and Γ-point elastic tunneling currents.

We have proposed two separate mechanisms by which Γ-point electrons in the GaAs electrodes may tunnel through the AlAs X-point barrier. In fact, both processes may occur simultaneously, and the empirical factors used to calculate theoretical current densities can be modified accordingly. More detailed calculations of scattering matrix elements and the mixing of states of different symmetry are under way to obtain a quantitative picture of electron transport in these structures. Nevertheless, the preliminary results presented here suggest that (i) elastic tunneling through the AlAs Γ-point barrier is insufficient to account for experimental current densities; (ii) elastic and inelastic tunneling through the AlAs band gap at the X point could account for the observed discrepancies; and (iii) theoretical current densities in good agreement with experimental data can be obtained provided both Γ- and X-point tunneling contributions are taken into account.

Although these concepts have only been illustrated in terms of the experimental data related to one structure, it was found that samples having different doping concentrations and barrier thicknesses display the same general behavior. Nevertheless, further investigations are necessary to gain a better understanding of the specific mechanisms occurring in each sample and to build a unifying model for all of them. This work will be discussed more thoroughly in a forthcoming publication.

IV. IMPURITY-ASSISTED TUNNELING

In this section, a new element is added to the current density calculations, namely the effect of impurity energy levels in the AlAs band gap. Impurity atoms and crystal defects can create localized energy levels (traps) in the AlAs barrier.[19,20] If these "impurity states" lie in the AlAs band gap, they can affect tunneling currents through the structure. In this paper, we view traps as intermediate states through which two-step tunneling processes may occur: an electron first tunnels from one GaAs electrode to an intermediate state, and then from the intermediate state to the other electrode. This approach is similar to that used by Parker and Mead in their treatment of traps in Schottky barriers.[21]

A simple expression for the two-step tunneling current can be derived by assuming that there are N localized trap states per unit volume of AlAs, with each trap energy level, E_t, being a fixed energy, E_o, below the AlAs conduction band edge, E_c. For an arbitrary voltage applied to the structure, the AlAs conduction band edge and thus the trap energy level vary with position, x:

$$E_t(x) = E_c(x) - E_o . \tag{1}$$

In Fig. 5, this concept is illustrated by plotting the Γ-point conduction band edge and a trap energy level for a single p-type barrier heterostructure under applied bias. This figure is the result of a band bending calculation, in which the electrode and barrier dopings are taken to be 3×10^{18} and 1×10^{18} cm^{-3}, respectively. The barrier thickness is 100 Å and the applied voltage is 150 mV. The impurity level is

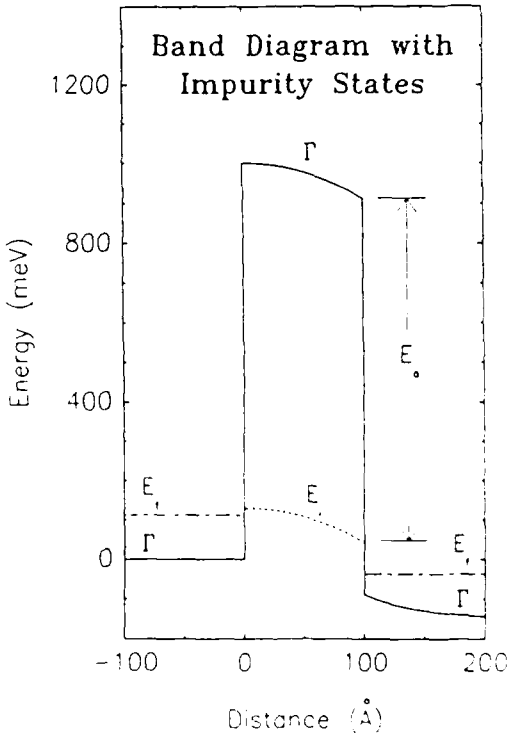

FIG. 5. Calculated Γ-point conduction band edge (solid line) as a function of distance in the direction perpendicular to the layers for a GaAs–AlAs–GaAs single barrier structure having an impurity level in the AlAs barrier layer. The impurity state (dashed line) lies 870 meV below the Γ-point conduction band edge in the barrier. The GaAs electrodes are doped n-type at 3×10^{18} cm^{-3}. The AlAs barrier layer is 100 Å thick, and doped p-type at 1×10^{18} cm^{-3}. A voltage of 150 mV is applied to the structure.

taken to be 870 meV below the AlAs Γ-point conduction band edge.

The elastic tunneling current density, J_1, between a trap state at position x_o and the left GaAs electrode is of the form

$$J_1 \propto T_1[E_t(x_o),x_o]\{f_l[E_t(x_o)] - F[E_t(x_o)]\}, \quad (2)$$

where T_1 is the WKB transmission probability for an electron with energy $E_t(x_o)$ tunneling from the left electrode to x_o, f_l is the occupation probability of the left electrode state with energy $E_t(x_o)$, and F is the occupation probability of the trap state. Similarly, the elastic tunneling current density, J_2, between the trap state at position x_o and the right electrode is given by:

$$J_2 \propto T_2[E_t(x_o),x_o]\{F[E_t(x_o)] - f_r[E_t(x_o)]\}, \quad (3)$$

where T_2 is the transmission probability for an electron with energy $E_t(x_o)$ tunneling from x_o to the right electrode, and f_r, is the occupation probability of the right electrode state with energy $E_t(x_o)$.

Under steady-state conditions, the trap level occupation probability, F, will adjust itself to make the two current densities equal. It follows that the impurity-assisted tunneling current, J_{imp}, takes the form:

$$J_{imp} = J_1 = J_2 \propto \frac{T_1 T_2}{T_1 + T_2}\{f_l[E_t(x_o)]\}. \quad (4)$$

A comparison of Eq. (4) with the usual expression for the one-step elastic tunneling current,[9] J_{el}, reveals that:

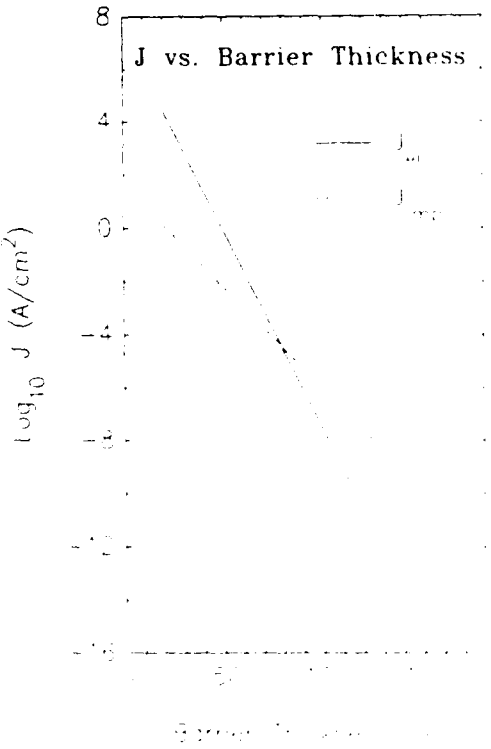

FIG. 6. Calculated current densities vs barrier thickness for one-step elastic tunneling (solid line) and impurity-assisted tunneling (dashed line). The dopings in the GaAs electrodes and the AlAs barrier are 3×10^{18} cm^{-3} and 1×10^{17} cm^{-3}, respectively. The applied voltage is 100 mV. The trap level is taken to be 950 meV below the Γ-point conduction band edge in the barrier.

$$J_{el} = C J_o \frac{1}{T_1(E)} \frac{T_1 T_2}{T_1 + T_2}, \quad (5)$$

where $T_1(E)$ is the transmission coefficient for electrons with energy E tunneling from the left electrode to the right electrode, and C is a constant which is proportional to the number of trap levels per unit volume, N, and the effective cross-sectional area of the traps, σ.

Figure 6 is a calculated plot of J_{imp} as a function of AlAs barrier thickness. The calculations are performed using a p-type barrier doping of 1×10^{18} cm^{-3}, and an n-type electrode doping of 3×10^{18} cm^{-3}. The applied voltage is 100 mV and the impurity energy level is taken to be 950 meV below the AlAs Γ-point conduction band edge. N is chosen to be 1×10^{17} cm^{-3}, and σ is assigned a value of ten times the cross-sectional area of the AlAs primitive cell. Changes in N and σ alter only the multiplicative constant, C, in Eq. (5), and therefore, do not change the qualitative behavior of J_{imp}. J_{el} is also calculated and plotted in Fig. 6 for comparison with J_{imp}. This reveals that the contribution to the total current density of one-step elastic tunneling is larger than that of impurity-assisted tunneling in heterostructures with thin barriers. The opposite is true in structures with thicker barriers. For the parameters used in Fig. 6, the impurity-assisted tunneling current becomes larger than the one-step elastic current when the AlAs barrier is thicker than about 80 Å.

V. IMPLICATIONS FOR RESONANT TUNNELING STRUCTURES

In this section, we briefly discuss implications of some of the previous results for resonant tunneling in GaAs/AlAs double barrier heterostructures. Resonant tunneling structures made of two $Al_xGa_{1-x}As$ quantum barriers separated by a GaAs quantum well display negative differential resistances in their I–V characteristics. This effect is commonly attributed to the tunneling of electrons via quasi-stationary states in the well. Furthermore, it is usually assumed that the effective barrier height for tunneling is determined by the Γ-point conduction band in the barriers, even when the $Al_xGa_{1-x}As$ is indirect. Detailed calculations of band bending, energy level positions, and voltage drops are required to determine without ambiguity, the correlation between the resonances in the well and the voltages at which negative differential resistances are observed. Simple theoretical models yield current densities in disagreement with experimental data. In structures for which the best peak-to-valley current ratios realized to date are 10:1 at 77 K,[22] calculations predict values as large as several orders of magnitude.[3] This indicates that the transport properties of these stuctures are more complex than simple models assess. In particular, the obtainable values of peak-to-valley current ratios are limited by other current transport mechanisms competing with Γ-point resonant tunneling.[23] Derivative spectra are important tools for identifying and investigating the nature of such processes. Figure 7 illustrates second derivative curves (d^2I/dV^2) (V), obtained at 4.2 K for a resonant tunneling heterostructure. The GaAs electrodes in the sample are doped n-type with Se at 2×10^{18} cm^{-3}. The AlAs

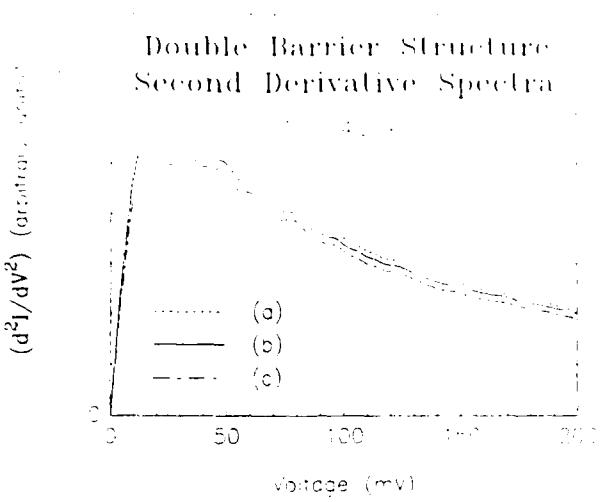

FIG. 7. Second derivative spectra $(d^2I/dV^2)(V)$, at 4.2 K for a GaAs/AlAs resonant tunneling double barrier heterostructure. The GaAs electrodes are doped n-type at 2×10^{18} cm^{-3}. The AlAs quantum barriers, approximately 50 Å thick, are doped p-type. The nominally undoped GaAs well is about 50 Å wide. The curves (a), (b), and (c) correspond to three different devices, having diameters of 145, 115, and 75 μm.

barriers, about 50 Å thick, are doped p-type with Mg. The nominally undoped GaAs well is about 50 Å wide. Three curves are shown in Fig. 7, corresponding to different size devices. They display reproducible features which have a nearly periodic spacing of 15–16 mV. Similar spectra are obtained from other samples. A definitive explanation of the observed features has not yet been found, but a possible interpretation may be proposed. The periodic structure could arise from the discrete nature of fluctuations in the quantum well width. Such fluctuations in barrier and well thicknesses would contribute in reducing and broadening the negative differential resistances observed in the I–V characteristics.

In the light of the results obtained for single barrier structures, it is possible to propose other qualitative explanations for the small peak-to-valley current ratios observed in several of our samples.[2] Whenever electrons can scatter to X-point states and tunnel through the AlAs barriers at the X point, a large background current can be expected, even for relatively thick barriers and wells. Depending upon the relative amplitudes of the resonant Γ-point current and the X-point current, the negative differential resistances may be partially or totally suppressed. Determining whether or not this will happen is, in fact, a nontrivial problem which depends upon the structure parameters and scattering mechanisms. In single barrier samples, electrons may tunnel through the AlAs band gap at the X point either inelastically by scattering near each interface, or elastically through the coupling of AlAs X-point states and GaAs Γ-point states. In double barrier structures, the problem is different due to the presence of the GaAs well between the two AlAs barriers. At voltages which are low enough that the X-point conduction band edge in the GaAs well is higher in energy than the Fermi level in the left electrode, X-point tunneling may occur through several mechanisms. First, electrons may scatter once near each of the four GaAs/AlAs interfaces, thus tunneling through the AlAs barriers at the X point, but occupying states of Γ symmetry in the GaAs electrodes and well. Secondly, electrons may scatter only near the first and last GaAs/AlAs interfaces, thus tunneling in both barriers and the well through the X-point gaps of AlAs and GaAs. Finally, electrons may tunnel elastically due to the coupling of wave functions having different symmetries. Simple estimates have shown that the relative importance of these mechanisms depends on the well width, barrier thicknesses, and applied voltage. These processes either involve higher order mechanisms than those taking place in single barrier structures, or tunneling through thick X-point barriers consisting of the two AlAs barriers and the GaAs well. Therefore, their contribution can certainly be minimized by carefully optimizing the structure parameters, improving the quality of the interfaces, and lowering the background doping in nominally undoped layers.

VI. SUMMARY

The objective of this study was to investigate elastic and inelastic tunneling processes in GaAs–AlAs–GaAs double heterojunctions grown by MOCVD in the [100] direction. The AlAs quantum barriers in the heterostructures studied were doped p-type with Mg. Measurements of current–voltage characteristics (I–V), as well as first (dI/dV) and second (d^2I/dV^2) derivatives of the I–V curves, were performed at temperatures ranging from 300 to 4.2 K. Experimental and theoretical results indicated that low temperature electron transport in structures with thin barriers is achieved through two mechanisms: (i) elastic electron tunneling through the AlAs Γ-point barrier; and (ii) inelastic and/or elastic tunneling through the AlAs X-point barrier. Inelastic X-point tunneling may occur via virtual states beneath the four X-point valleys lying parallel to the plane of the layers, and requires the scattering of electrons near each interface. Elastic X-point tunneling, due to the coupling of AlAs X-point states and GaAs Γ-point states, can take place via virtual states below the two AlAs X-point valleys lying in the direction perpendicular to the plane of the layers. A theoretical model, which treats trap levels in the AlAs barrier as intermediate states for two-step tunneling processes, was developed. Calculations indicated that this impurity-assisted tunneling mechanism can become important when the AlAs barrier is thick enough. Implications of some of these results for resonant tunneling heterostructures consisting of two AlAs quantum barriers separated by a GaAs quantum well were discussed. In particular, carefully choosing the parameters of these structures to maximize the contribution of the Γ-point resonant tunneling current is critical for increasing the peak-to-valley current ratios of the negative differential resistances. For these double barrier structures, we also presented experimental second derivative spectra (d^2I/dV^2), in which periodic features may be indicative of discrete fluctuations in well thickness.

ACKNOWLEDGMENTS

The authors wish to acknowledge R. S. Bauer, C. Mailhiot, R. H. Hauenstein, R. H. Miles, T. K. Woodward, and

G. Y. Wu for valuable discussions, and are grateful to H. F. Chung, F. Endicott, D. M. Taylor, T. T. Tjoe, T. Anderson, J. Tramontana, W. Mosby, D. W. Treat, and F. E. Nelson for technical assistance. This work was supported in part by the Defense Advanced Research Agency under Contract No. N000014-84-C-0083 and the Office of Naval Research under Contract No. N00014-82-K-0556.

[1]R. T. Collins, J. Lambe, T. C. McGill, and R. D. Burnham, Appl. Phys. Lett. **44**, 532 (1984).
[2]A. R. Bonnefoi, R. T. Collins, T. C. McGill, R. D. Burnham, and F. A. Ponce, Appl. Phys. Lett. **46**, 285 (1985).
[3]I. Hase, H. Kawai, K. Kaneko, and N. Watanabe, Electron. Lett. **20**, 491 (1984).
[4]L. L. Chang, L. Esaki, and R. Tsu, Appl. Phys. Lett. **24**, 593 (1974).
[5]D. Delagebeaudeuf, P. Delescluse, P. Etienne, J. Massies, M. Laviron, J. Chaplart, and N. T. Linh, Electron. Lett. **18**, 85 (1982).
[6]P. Guéret and U. Kaufmann, Electron. Lett. **21**, 344 (1985).
[7]T. C. L. G. Sollner, W. D. Goodhue, P. E. Tannenwald, C. D. Parker, and D. D. Peck, Appl. Phys. Lett. **43**, 588 (1983).
[8]M. A. Reed, Superlattices and Microstructures (1986).
[9]R. Tsu and L. Esaki, Appl. Phys. Lett. **22**, 562 (1973).
[10]B. Jogai and K. L. Wang, Appl. Phys. Lett. **46**, 167 (1985).
[11]H. M. Manasevit, Appl. Phys. Lett. **12**, 156 (1968).
[12]R. D. Dupuis and P. D. Dapkus, Appl. Phys. Lett. **31**, 466 (1977).
[13]C. R. Lewis, W. T. Dietze, and M. J. Ludowise, Electron. Lett. **18**, 569 (1982).
[14]R. D. Burnham, W. Streifer, D. R. Scifres, C. Lindstrom, T. L. Paoli, and N. Holonyak, Electron. Lett. **18**, 1095 (1982).
[15]G. C. Osbourn, J. Vac. Sci. Technol. **17**, 1104 (1980).
[16]C. Mailhiot and T. C. McGill, J. Vac. Sci. Technol. B **1**, 637 (1983).
[17]E. O. Kane, *Physics of III–V Compounds* (Academic, New York, 1966), Vol. 1, Chap. 3, pp. 75–100.
[18]J. Batey and S. L. Wright, J. Appl. Phys. **59**, 200 (1986).
[19]T. K. Woodward, T. E. Schlesinger, T. C. McGill, and R. D. Burnham, Appl. Phys. Lett. **47**, 631 (1985).
[20]H. P. Hjalmarson, Superlattices and Microstructures **1**, 379 (1985).
[21]G. H. Parker and C. A. Mead, Appl. Phys. Lett. **14**, 21 (1969).
[22]M. A. Reed (private communication).
[23]G. Y. Wu, A. R. Bonnefoi, and T. C. McGill (to be published).

Inverted base-collector tunnel transistors

A. R. Bonnefoi, D. H. Chow, and T. C. McGill
T. J. Watson, Sr., Laboratory of Applied Physics, California Institute of Technology, Pasadena, California 91125

(Received 1 July 1985; accepted for publication 7 August 1985)

Two novel three-terminal devices based on tunneling in quantum well and quantum barrier heterostructures are proposed and analyzed theoretically. In both devices, the relative positions of the base and collector are interchanged from conventional emitter-base-collector sequence. This provides a means for obtaining negligible base currents and large current transfer ratios. In both cases, a base voltage controls the emitter-collector tunneling current by shifting the resonances in a quantum well. Calculations indicate that significant variations in the emitter-collector current-voltage characteristics can be obtained for reasonable base-emitter voltages. We call the two devices a Stark effect transistor and a negative resistance Stark effect transistor, respectively.

Electronic tunnel structures are a source of increasing interest. Two-terminal devices based on tunneling in single and double barrier heterostructures have been studied.[1-9] While it is true that these two-terminal structures have a number of potential applications, three-terminal devices would be preferable in many cases.

The idea of making three-terminal devices based on tunneling was pioneered in 1960 by Mead.[10] He proposed a metal-insulator-metal-insulator-metal hot-electron transistor. A number of devices based on this concept have been proposed and investigated experimentally.[11-13] All of these structures suffer from very small emitter-collector current transfer ratios due to large base currents.

Recently, Jogai and Wang[14] calculated the tunneling current for a conceptual three-terminal, double barrier device consisting of alternating layers of GaAs and $Al_xGa_{1-x}As$, forming the emitter, base, and collector. They proposed a configuration in which the base contact would be made to the GaAs quantum well and the two barriers independently biased. A highly conductive base was required so that a potential could be applied to it, but no base current was allowed to flow. This is a somewhat unphysical and unrealistic assumption. In addition, varying the collector-base voltage did not produce very significant changes in the device current-voltage characteristics.

In this letter, we propose and analyze two three-terminal devices which we expect to have reduced base currents and improved device performances. Although other semiconductors could be used, the devices are presented here in the context of $GaAs/Al_xGa_{1-x}As$ heterojunction technology. Since tunneling is the main current transport mechanism, these devices should feature the high-speed characteristics associated with tunnel structures. They should also have large emitter-collector current transfer ratios. The key step in achieving this goal is to interchange the relative positions of the base and collector, thus locating the latter in the region where current is most likely to flow. Figure 1 shows schematically the first proposed structure, together with its energy-band diagram at equilibrium. The emitter is an *n*-type GaAs layer. Doping concentrations on the order of 5×10^{16}–5×10^{17} cm^{-3} should provide sufficient tunneling currents and, at the same time, allow resonant tunneling effects to be observed at room temperature.[9] The emitter is followed by a thin undoped $Al_{x_1}Ga_{1-x_1}As$ tunneling barrier and a lightly doped *n*-type quantum well. The collector contact is made to the well. Alloys which give shallow and abrupt ohmic contacts, such as Au/Ge-Ag-Au or Au/Ge-Au-WSi for example, should be used. The next layer is lightly doped $Al_{x_2}Ga_{1-x_2}As$ barrier, sufficiently thick to prevent electrons from tunneling through it. In addition, an alloy with large Al composition is desirable to minimize thermionic emission over the barrier. Finally, a heavily doped *n*-type GaAs substrate serves as the base electrode.

The principle of operation of the proposed device is described below. First, let us consider the case in which no base voltage is applied. When the collector is biased positively with respect to the emitter, electrons near the Fermi level in the emitter tunnel through the thin $Al_{x_1}Ga_{1-x_1}As$ barrier into the collector. As long as the emitter Fermi level remains below the first subband in the well, a negligible tunneling current is expected. When the bias voltage is such that the emitter Fermi level reaches the first subband, the current is significantly increased. The current-voltage (I-V) characteristics should thus feature enhancements corresponding to the alignment of the emitter Fermi level with each resonance in the well. If a potential difference is now applied between

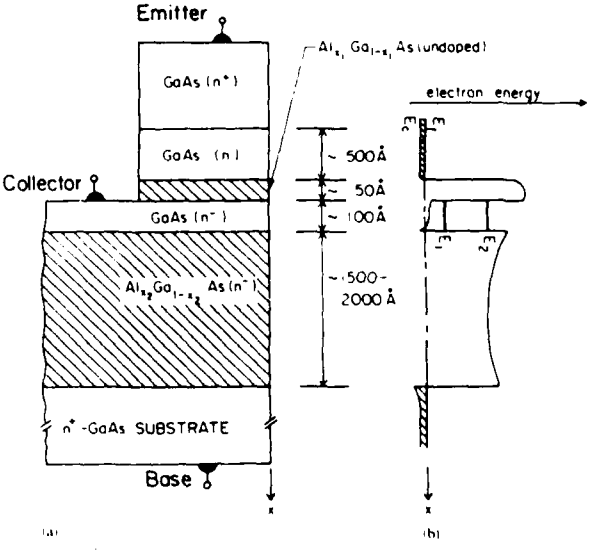

FIG. 1. Schematic diagrams (not to scale) of (a) a cross section of the proposed Stark effect transistor (SET); (b) the conduction-band edge at equilibrium as a function of position in the x direction (perpendicular to the layers).

 0003-6951/85/200888-03$01.00

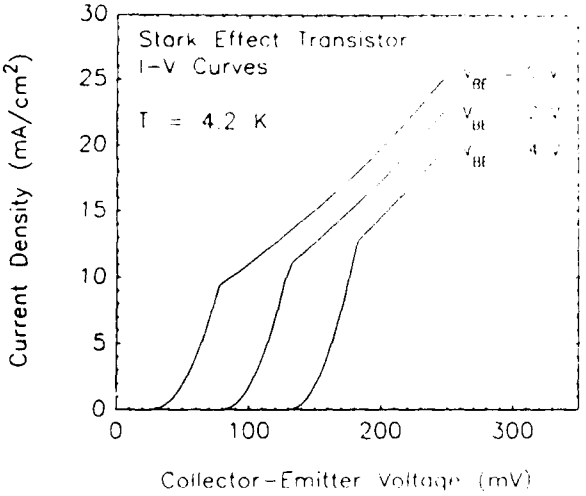

FIG. 2. Calculated current-voltage characteristics for the Stark effect transistor (SET). The barriers are pure AlAs, 50 and 1000 Å thick, respectively. The well is a 50-Å-thick GaAs layer. The conduction-band offset is taken to be 0.96 eV.

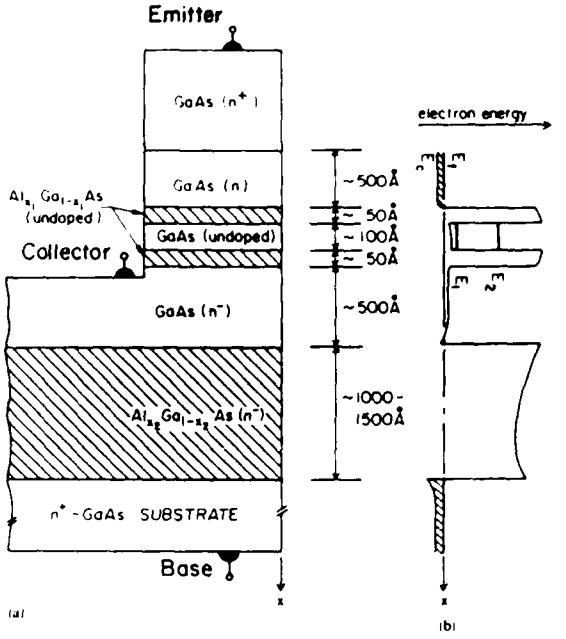

FIG. 3. Schematic diagrams (not to scale) of (a) a cross section of the proposed negative resistance Stark effect transistor (NERSET); (b) the conduction-band edge at equilibrium as a function of position in the x direction (perpendicular to the layers).

the base and emitter, an electric field perpendicular to the layers is created. The field will modify the positions of the subbands in the well with respect to the emitter Fermi level and thus modulate the tunneling current. The field will penetrate into the quantum well region for the following reasons: (i) the barriers and well are lightly doped; (ii) the $Al_{x_2}Ga_{1-x_2}As$ barrier is not thick enough to drop all of the base-emitter voltage; (iii) the device geometry is such that the collector contact does not completely shield the emitter from the base.

Theoretical I-V characteristics for the device are shown in Fig. 2. These curves were calculated using Bardeen's many-particle tunneling formalism.[15] In this approach, which starts from Fermi's Golden Rule, the density of finals states, ρ_f, appears explicitly in the calculation. In the present case, ρ_f is simply a sum of step functions since each resonance in the well is the bottom of a two-dimensional energy band. The matrix element was calculated by using WKB wave functions in the barrier region. A two-band model, $\mathbf{k}\cdot\mathbf{p}$ theory calculation was used to obtain the complex band structure in the barrier. Because the barriers and well are lightly doped, the base-emitter voltage V_{BE} was assumed to drop linearly in those regions. The calculated curves display the substantial variations of the emitter-collector I-V characteristics which may be obtained by modulating V_{BE}. Base-emitter voltages much higher than those needed to produce significant transistor action can be applied without producing avalanche breakdowns. If V_{BE} is negative, the levels in the well are shifted upwards and a small negative current might flow to the emitter when V_{CE} is small. This is an additional incentive to make the well and the $Al_{x_1}Ga_{1-x_1}As$ barrier lightly doped.

The main advantage of this configuration is a negligible base current and thus a large current transfer ratio. Because the quasistationary states in the well are modulated by an electric field to produce transistor I-V characteristics, the proposed device could be called a Stark effect transistor (SET).

The transistor I-V characteristics described above can be modified and enhanced by adding a potential step in the GaAs well constituting the collector. The step can be a thin $Al_xGa_{1-x}As$ layer with an Al composition smaller than that of the barriers. Its main effect is to modify the relative positions of the resonant states in the well. The structure can now be designed to obtain a certain energy spectrum or to produce given shifts of some of the subbands. This makes it possible to optimize device performance according to the requirements or applications.

To further illustrate the concept of subband modulation by means of an electric field applied from a controlling electrode, another device configuration is proposed. It is characterized by a resonant tunneling double barrier heterostructure. Such a device structure is shown schematically in Fig. 3, together with its energy-band diagram at equilibrium. This device operates on the same principle as the Stark effect transistor. The values of the fields and the shifts of the levels resulting from the base-emitter modulating voltage were estimated to be of the same order of magnitude as before. In this case, however, no contact needs to be made to the quantum well. The essential feature of this device configuration is the presence, in the emitter-collector I-V characteristics, of negative differential resistances controlled by the base-emitter voltage.

Theoretical I-V characteristics for the device are shown in Fig. 4. The approach of Vassell *et al.*[16] was used to calculate the tunneling current through the double barrier heterostructure separating the collector from the emitter. The base-emitter modulating voltage was once again assumed to drop linearly in each region. This device, which could be called a negative resistance Stark effect transistor (NERSET), offers several advantages over any double barrier configuration in which the base is located in the quantum well: (i) easier fabrication; (ii) no base current, and thus larger cur-

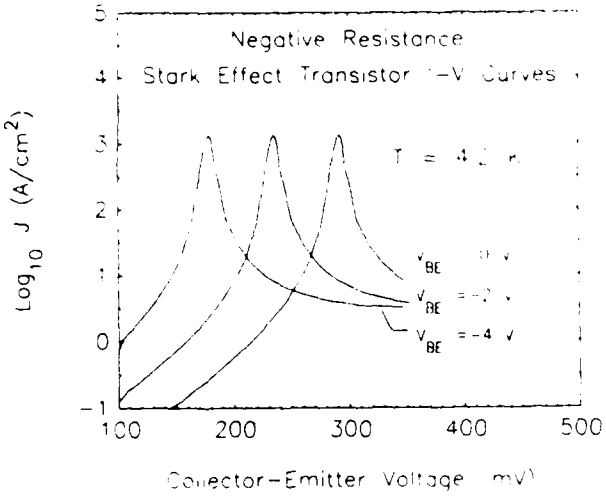

FIG. 4. Calculated current-voltage characteristics for the negative resistance Stark effect transistor (NERSET). The tunnel barriers are 20-Å-thick $Al_{0.6}Ga_{0.4}As$ layers and the well a 50-Å-thick GaAs layer. The conduction-band offset is taken to be 0.5 eV.

rent transfer ratios; (iii) undoped well; (iv) no transverse electric fields in the well which destroy the coherence of wave functions across the entire double barrier structure. These last two conditions are essential for optimum resonant tunneling.

In summary, we have proposed and analyzed two novel three-terminal devices based on tunneling in quantum well and quantum barrier heterostructures. Their main characteristic is that the relative positions of the collector and base electrodes have been interchanged with respect to the conventional emitter-base-collector sequence. This makes it possible to obtain negligible base currents and large current transfer ratios. Electric fields produced by applying a voltage to the base modulate the positions of the subband levels in the quantum well and thus control the emitter-collector tunneling current. Calculations showed that significant variations in the emitter-collector I-V characteristics can be obtained by modulating the base-emitter voltage. Although these devices were analyzed in the context of GaAs/$Al_xGa_{1-x}As$ heterojunction technology, other semiconductors could be used. Experiments are under way to measure the properties of these structures and to explore their applications in high-frequency analog and digital circuits.

John Lambe played a key role in calling our attention to the possible use of electric fields in changing the positions of subbands. A. Zur developed the computer programs used to calculate the I-V characteristics of the NERSET. M. B Johnson, T. E. Schlesinger, T. K. Woodward, and G. Y. Wu have all helped us in the clarification of our thinking on these device concepts. This work was supported in part by the Defense Advanced Research Projects Agency under contract No. N00014-84-C-0083 and the Office of Naval Research under contract No. N00014-82-K-0556.

[1] D. Delagebeaudeuf, P. Delescluse, P. Etienne, J. Massies, M. Laviron, J. Chaplart, and N. T. Linh, Electron. Lett. **18**, 85 (1982).
[2] R. T. Collins, J. Lambe, T. C. McGill, and R. D. Burnham, Appl. Phys. Lett. **44**, 532 (1984).
[3] I. Hase, H. Kawai, K. Kaneko, and N. Watanabe, Electron. Lett. **20**, 491 (1984).
[4] R. Tsu and L. Esaki, Appl. Phys. Lett. **22**, 562 (1973).
[5] T. C. L. G. Sollner, W. D. Goodhue, P. E. Tannenwald, C. D. Parker, and D. D. Peck, Appl. Phys. Lett. **43**, 588 (1983).
[6] R. T. Collins, A. R. Bonnefoi, J. Lambe, T. C. McGill, and R. D. Burnham, *Proceedings of the 17th International Conference on the Physics of Semiconductors*, San Francisco, 1984 (Springer, New York, 1984), p. 437.
[7] T. C. L. G. Sollner, P. E. Tannenwald, D. D. Peck, and W. D. Goodhue, Appl. Phys. Lett. **45**, 1319 (1984).
[8] A. R. Bonnefoi, R. T. Collins, T. C. McGill, R. D. Burnham, and F. A. Ponce, Appl. Phys. Lett. **46**, 285 (1985).
[9] T. J. Shewchuk, P. C. Chapin, P. D. Coleman, W. Kopp, R. Fischer, and H. Morkoç, Appl. Phys. Lett. **46**, 508 (1985).
[10] C. A. Mead, Proc. IRE **48**, 359 (1960).
[11] D. V. Geppert, Proc. *IRE* **50**, 1527 (1962).
[12] M. Heiblum, Solid State Electron. **24**, 343 (1981).
[13] N. Yokoyama, K. Imamura, T. Ohshima, H. Nishi, S. Muto, K. Kondo, and S. Hiyamizu, Jpn. J. Appl. Phys. **23**, L311 (1984).
[14] B. Jogai and K. L. Wang, Appl. Phys. Lett. **46**, 167 (1985).
[15] J. Bardeen, Phys. Rev. Lett. **6**, 57 (1961).
[16] M. O. Vassell, Johnson Lee, and H. F. Lockwood, J. Appl. Phys. **54**, 5206 (1983).

Photovoltaic investigations of GaAs/AlAs heterostructures

T. E. Schlesinger, R. T. Collins, and T. C. McGill
California Institute of Technology, Pasadena, California 91125

R. D. Burnham
Xerox Corporation, Palo Alto, California 94304

(Received 21 May 1984; accepted for publication 3 July 1984)

We present the results of the application of photoresponse techniques to the study of the transport of electrons past an energy barrier. In this study, the barrier was provided by a thin layer of AlAs sandwiched between GaAs layers. The experiment measured the voltage resulting from the migration of optically excited electrons from one side of the barrier to the other. The voltage is measured as a function of the wavelength of the incident light. We also present the results of calculations which explain the nature of the observed spectra and how they change when the thickness of the top layer (the illuminated side) of GaAs is changed.

In this letter we discuss experimental results of the application of photoresponse techniques to the study of GaAs/AlAs heterostructures. We have applied this technique to the study of the transport of electrons past an energy barrier. In particular, we have investigated these electronic transport properties in structures consisting of a thin layer of AlAs sandwiched between layers of GaAs. The experimental procedure consisted of illuminating samples with light in order to excite electrons in the conduction band of the GaAs which could then migrate through the AlAs barrier. We then measured the resulting open circuit voltage produced across the AlAs barrier as a function of the wavelength of the incident light.

The basic results presented in this letter can be summarized as follows. The sign of the voltage that we measured was consistent with electrons migrating from the illuminated side of the AlAs barrier to the back side of the AlAs barrier. The magnitude of the voltage was proportional to the intensity of the illuminating light. The voltage spectrum, that is, the voltage as a function of the wavelength of the incident light, had two basic shapes which were common to all the AlAs barrier samples so far studied. The two shapes seemed mainly to depend on the thickness of the top layer of GaAs. When the top layer was on the order of a few microns thick, the resulting spectrum was a broad peak whose exact position depended on doping and temperature. When the top layer was thinner (less than one micron thick) the voltage spectrum rose slowly from shorter wavelengths to longer wavelengths followed by a sharp turnoff at some particular wavelength, depending on the sample doping and the temperature.

The samples used in this study were grown by a metal-organic chemical vapor depostion technique.[1] The AlAs layer thicknesses varied from about 150 to about 250 Å, and these layers were doped p type with Mg at about 1×10^{18} cm^{-3}. The GaAs top layer (the illuminated side) varied from about 0.5 to 4.4 μm thick, depending on the sample, while the bottom layer was substantially thicker. The GaAs was degenerately doped n type with Se from 1 to 5×10^{18} cm^{-3}. For these doping levels the AlAs barrier is fully depleted. Ohmic contacts were made to the samples by evaporation of Au/Ge followed by a 20 s anneal at 420 °C. Photolithographic techniques were employed to make ring-shaped contacts to the top surface in order to allow light to penetrate into the GaAs through the center of the rings. The individual contacts were then mesa isolated from each other. The samples were mounted on transistor headers, and wire bonds were made to the Au/Ge contacts. The light source used to illuminate the samples was a tungsten filament lamp. The light was directed through a spectrometer (SPEX model 1269) and then focused onto a particular device to be studied. The measurement of the voltage resulting from the illumination was made directly, using a voltmeter when it was desired to know the sign of the voltage. In general, however, the light was chopped at about 270 Hz and the resulting voltage was measured using a lock-in amplifier. The signal was then digitized, and the spectrum stored on a signal averager (*NIC 1170*). In this letter, we discuss the results obtained for only one particular sample at room temperature (300 K). Further results describing the variations in the spectra from sample to sample as a function of doping and temperature will be discussed in a forthcoming publication.

To model the absorption of the light in these structures, we carried out the following calculations. We consider a model where we have a layer of GaAs, a layer of AlAs, and a semi-infinite layer of GaAs. Light impinges on the first layer of GaAs from a vacuum at normal incidence. We assume that no attenuation of the light takes place in the AlAs. In the GaAs, however, we model the attenuation of the light, using a coefficient of absorption, α, which we obtained by fitting and extrapolating the curves publised by Casey *et al.*[2] for heavily doped, n-type GaAs at room temperature. We used, however, constant values for the index of refraction of GaAs and AlAs of 3.4 and 3.1, respectively.[3] The light intensity was then calculated throughout the model structure and was then integrated in the region of GaAs in front of the AlAs barrier and in an equal region behind the AlAs barrier to obtain the total light intensity in each of the two regions. The total light intensity behind the AlAs barrier was then subtracted from the total in front of the AlAs, and this difference was plotted as a function of wavelength. When there is more light intensity in front of the AlAs than behind, there are correspondingly more electrons excited there. It is this difference in the concentration of electrons in the conduction band which drives the flow of electrons from the front side of the AlAs barrier to the back side. As will be discussed

 0003-6951/84/180686-03$01.00

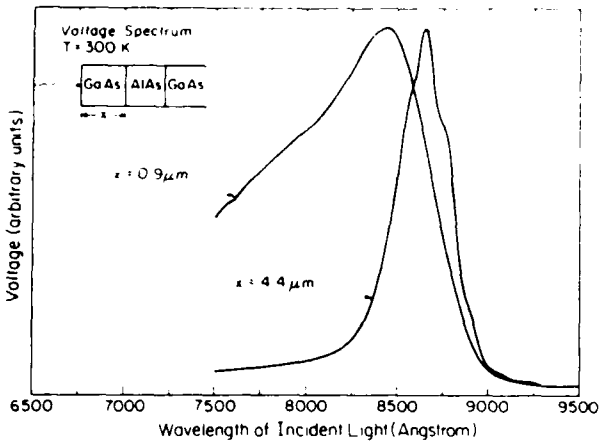

FIG. 1. Voltage spectrum taken at room temperature for a sample with a 240-Å AlAs barrier. The GaAs layers were doped n-type at about 3×10^{18} cm^{-3}. The thicknesses of the top layer of GaAs were 4.4 μm and 0.9 μm as indicated in the figure.

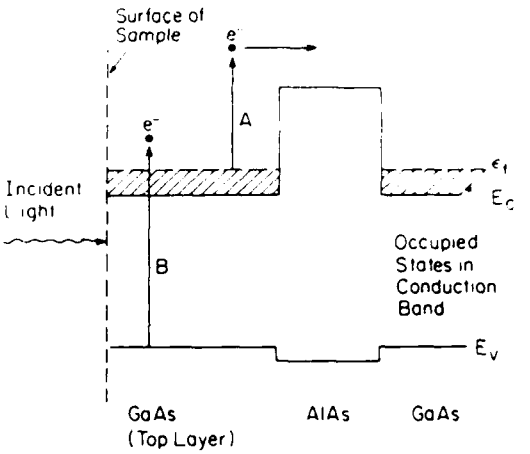

FIG. 2. Schematic diagram of the conduction band (E_c) and valence band (E_v) edges of the GaAs/AlAs heterostructure showing the Fermi level (E_f) in the conduction band. Indicated in the figure are free carrier (A) and band to band (B) absorption of light by electrons.

below, it is those electrons which are excited in the conduction band of the GaAs by free-carrier absorption which have enough energy to go over the AlAs barrier. The number of electrons excited in the conduction band due to free-carrier absorption is proportional to the light intensity. Thus, we would expect the measured voltage spectrum to have the same shape as the calculated difference in the light intensity in front of and behind the AlAs barrier. Recent calculations by Mailhot *et al.*[4] have shown that it is the Γ point of the AlAs which determines the energy barrier presented to an electron in the GaAs, and our observations so far have been consistent with this conclusion.

In Fig. 1 we present a voltage spectrum for a particular sample at room temperature. This sample had a 240-Å-thick layer of AlAs and a top layer of GaAs which was 4.4 μm thick in one case and which had been etched down to a thickness of 0.9 μm in the other case. The doping in the GaAs top layer dropped from 3×10^{18} cm^{-3} near the surface to 2×10^{18} cm^{-3} near the AlAs barrier. In the bottom layer, the doping was 3×10^{18} cm^{-3}. We note, first, that in both cases we have a substantial amount of signal at energies below the GaAs band gap (1.424 eV or 8700 Å at room temperature) and that there are marked undulations on the spectrum from the sample with the 4.4-μm-thick top layer. At wavelengths below the GaAs band gap no holes are created in the structure and hence the photovoltage is not a result of hole movement in the GaAs. At wavelengths above the GaAs band gap where we do create electron hole pairs the movement of electrons and holes in the GaAs due to the electric fields at the GaAs-AlAs interface would result in a voltage opposite in sign to the one that we measure. These observations strongly suggest that it is electrons promoted in the GaAs by free-carrier absorption which produce our observed voltages. To explain the general shape of these spectra, we refer to Fig. 2 which schematically shows the band structure and absorption processes in the sample. At a doping level of 3×10^{18} cm^{-3}, the Fermi level can be as much as 110 meV above the conduction-band minimum. The two absorption processes are free-carrier absorption (A) for which the coefficient of absorption is α_A and band to band absorption (B) for which the coefficient of absorption is α_B. Since free-carrier absorption involves a phonon and band to band absorption does not $\alpha_A \ll \alpha_B$. At long wavelengths where the energy of a photon is insufficient to promote an electron from the valence band over the Fermi level the much weaker free-carrier absorption dominates and there is not a substantial difference between the light intensity in front of and behind the AlAs barrier. There is, thus, a correspondingly small difference in the number of electrons promoted in the conduction band of the GaAs, and we expect to measure a small signal. At short wavelengths where band to band absorption is very strong, the light intensity is attenuated very quickly near the surface of the sample, and the difference in light intensity in front of and behind the AlAs barrier is very small, and, again, we expect to measure a small signal. Between these two extremes, we have some wavelength at which the difference in light intensity (and, hence, the concentration of electrons promoted in the conduction band of the GaAs) is a maximum, and we expect to see a maximum signal. We, thus, have a spectrum with a peak whose position is mainly determined by the doping of the sample. To explain the difference in the spectra when we have a thick top layer (5 μm) and a thin top layer (1 μm), consider the following. For a sample with a top layer thickness of 5 μm at wavelengths where process B cannot occur (the energy of the light is insufficient to promote carriers from the valence band over the Fermi level), the light intensity is proportional to $e^{-5\alpha_A}$. At shorter wavelengths where process B can occur, the intensity of the light is proportional to $e^{-5\alpha_A}$. Consider the same sample with a thin top layer of 1 μm. The enhancement in the light intensity at wavelengths where process A dominates is proportional to

$$e^{-1\alpha_A}/e^{-5\alpha_A} = e^{4\alpha_A},$$

but at wavelengths where process B dominates (on the short wavelength tail of the spectrum), the enhancement in the intensity of light is proportional to

$$e^{-1\alpha_B}/e^{-5\alpha_B} = e^{4\alpha_B},$$

but since $\alpha_A \ll \alpha_B$ then $e^{4\alpha_B} > e^{4\alpha_A}$ and the enhancement in the

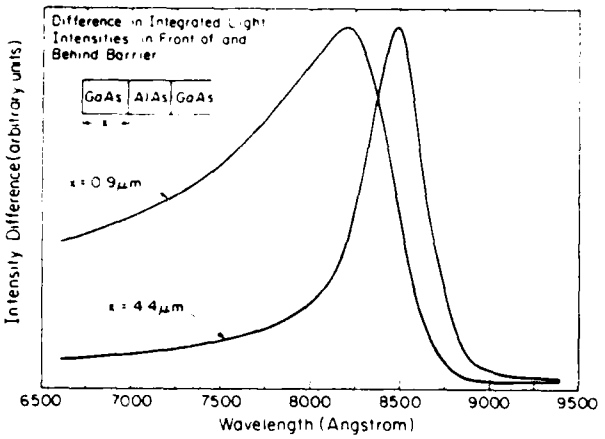

FIG. 3. Calculated difference in the integrated light intensities in front of and behind the AlAs barrier as a function of wavelength. The coefficient of absorption, α, used in calculating these curves, was for a GaAs n-type doping of 3.3×10^{18} cm^{-3} at room temperature. The results are presented for top layer thicknesses of GaAs of 4.4 μm and 0.9 μm as indicated in the figure.

intensity of the light is much greater at the shorter wavelength tail of the spectrum. Since the number of electrons promoted by process A is proportional to the light intensity, we would expect the voltage signal to be most enhanced at the short wavelength tail of the spectrum. Thus, a spectrum for a sample with a thick top layer will change qualitatively in the way it does in Fig. 1 when the top layer is made thinner. The Γ-point barrier at room temperature is at most[5] 1.35 eV[5] (9180 Å). This barrier is decreased by the fact that the Fermi level is in the conduction band but is increased by the effects of band-gap shrinkage in the GaAs due to the heavy doping[6] and is also affected by band bending in these structures. This number, however, gives us an estimate as to the longest wavelength at which we could expect to measure a voltage if there is also a difference in the light intensity in front of and behind the AlAs barrier. At wavelengths longer than 9180 Å even electrons promoted via process A may not be high enough in the conduction band to go over the barrier.

In Fig. 3 we present results of the predicted spectrum for a sample with a doping level of 3.3×10^{18} cm^{-3} in the GaAs, which has a 240-Å layer of AlAs and which has a top layer thickness of 4.4 μm or 0.9 μm as labeled. We see that since the absorption coefficient data contain in it the effects of band to band versus free-carrier absorption, they correctly predict the qualitative behavior of the spectra we measured. We note that the peak position (in the case of the thick top layer) and the turnoff wavelength (in the case of the thin top layer) are not exactly predicted by the calculations though they are in fairly good agreement. These positions depend very much on the doping of the sample used in the experiment. In the calculations these positions depend on the behavior of the coefficient of absorption, α, which in turn depends on the doping and which differs from the actual doping of the samples. In our calculations, we have assumed a constant doping profile while in the actual samples the doping in the GaAs is a function of position. The difference in peak positions for samples of different dopings is correctly predicted by the calculations and will be presented in a forthcoming publication. We also note that the undulations seen in the experimental peak are not as marked in the calculated peak. There are two possible origins for these undulations. One explanation is that they are the result of the optical properties of the structures, in particular, the detailed behavior of α. Another possible explanation is that they are a result of resonant effects in the transmission of electrons through the AlAs barrier.[4]

In summary, we have presented results of an experimental technique that we have employed to study the transport of electrons past an energy barrier. We have presented experimental results which imply that the voltage we are measuring is a result of electrons which have been promoted in the conduction band of the GaAs by free-carrier absorption to energies which allow them to migrate over the barrier presented by the AlAs. We have argued that the driving force for the migration of the electrons through the AlAs barrier is the difference in the concentration of electrons on either side of the barrier which is a result of the difference in light intensity on either side of the barrier. This difference in light intensity was calculated using a model for the structure. These calculations explain the nature of the voltage spectra as a result of the optical properties of the heterostructures, in particular, the layer thicknesses and doping levels.

The authors would like to acknowledge D. L. Smith, J. Lambe, C. Mailhiot, R. S. Bauer, T. L. Paoli, and W. Striefer for valuable discussions and are grateful to H. Chung, R. D. Yingling, Jr., F. Endicot, M. Bernstein, M. Mosby, J. Tramontana, J. Walker, A. Alimonda, G. L. Harnagel, and R. Ritter for technical assistance with this work. One of us (T.E.S.) received financial assistance from the Natural Sciences and Engineering Research Council of Canada. This work was supported in part by the Office of Naval Research under contract No. N00014-82-K-0556.

[1] R. D. Burnham, W. Streifer, D. R. Scifres, C. Lindstrom, T. L. Paoli, and N. Holonyak, Electron Lett. **18**, 1095 (1982).
[2] H. C. Casey, Jr., D. D. Sell, and K. W. Wecht, J. Appl. Phys. **46**, 250 (1975).
[3] H. C. Casey, Jr. and M. B. Panish, *Heterostructure Lasers* (Academic, New York 1978), Part A, Chap. 2.
[4] C. Mailhot, D. L. Smith, and T. C. McGill, J. Vac. Sci. Technol. B 1 637 (1983).
[5] H. C. Casey, Jr. and M. B. Panish, *Heterostructure Lasers* (Academic, New York, 1978), Part A, Chap. 4.
[6] H. C. Casey, Jr. and Frank Stern, J. Appl. Phys. **47**, 631 (1976).

Superlattices and Microstructures, Vol. 1, No. 5, 1985

PHOTOVOLTAIC INVESTIGATIONS OF GaAs/AlAs HETEROSTRUCTURES

T.E. Schlesinger, R.T. Collins, and T. C. McGill
California Institute of Technology, Pasadena, California 91125

R. D. Burnham
Xerox Corporation, Palo Alto, California 94304

(Received 13 August 1984 by J. Dow)

We present the results of the application of photoresponse techniques to the study of the transport of electrons past an energy barrier. In this study, the barrier was provided by a thin layer of AlAs sandwiched between GaAs layers. The experiment measures the voltage resulting from the flow of optically excited electrons from one side of the barrier to the other. The voltage is measured as a function of the wavelength of the incident light. We also present the results of calculations which explain the nature of the observed spectra and how they change when the thickness of the top layer (the illuminated side) of GaAs is changed and when the doping in the GaAs is varied.

1. Introduction

In this paper we discuss experimental results of the application of photoresponse techniques to the study of GaAs/AlAs heterostructures. We have applied this technique to the study of the transport of electrons past an energy barrier. In particular, we have investigated these electronic transport properties in structures consisting of a thin layer of AlAs sandwiched between layers of GaAs. The experimental procedure consisted of illuminating samples with light in order to excite electrons in the conduction band of the GaAs which could then flow past the AlAs barrier. We then measured the resulting open circuit voltage produced across the AlAs barrier as a function of the wavelength of the incident light.

The basic results presented in this paper can be summarized as follows. The sign of the voltage that we measured was consistent with electrons flowing from the illuminated side of the AlAs barrier to the back side of the AlAs barrier. The magnitude of the voltage was proportional to the intensity of the illuminating light. The voltage spectrum, that is, the voltage as a function of the wavelength of the incident light, had two basic shapes which were common to all the AlAs barrier samples so far studied. The two shapes seemed mainly to depend on the thickness of the top layer of GaAs. When the top layer was on the order of a few microns thick, the resulting spectrum was a broad peak whose exact position depended on temperature. When the top layer was thinner (less than one micron thick) the voltage spectrum rose slowly from shorter wavelengths to longer wavelengths followed by a sharp turnoff at some particular wavelength, depending on the temperature. The peak position also depended on the doping level in the GaAs layers. For samples with a higher doping level, the peak was shifted to shorter wavelengths. The nature of the spectra is explained by our calculations as will be shown below.

2. Samples and Experimental Methods

The samples used in this study were grown by a metalorganic chemical vapor deposition technique[1,2] with all the AlAs barriers doped p-type with Mg[3,4] while the GaAs was doped n-type with Se. The GaAs substrates on which these structures were grown were doped n-type at about 3×10^{18} cm^{-3} with Si. We will discuss results obtained from four different samples whose characteristics are summarized in table 1. The thicknesses of the top layer (illuminated side) of GaAs varied from about 0.5 μm thick to 4.4 μm thick. Ohmic contacts were made to the samples by evaporation of a

TABLE 1 Sample Characteristics

Sample	Barrier Thickness	GaAs Doping (cm^{-3})	Barrier Doping (cm^{-3})
1	110 Å	Se – 5×10^{18}	Mg – 1×10^{18}
2	160 Å	Se – 5×10^{18}	Mg – 1×10^{18}
3[a]	160 Å	Se – 3×10^{18}	Mg – 1×10^{18}
4[b]	240 Å	Se – 3×10^{18}	Mg – 1×10^{18}

[a] GaAs doping 1.2×10^{18} 1 μm either side of the AlAs barrier.

[b] GaAs doping gradually dropped to 2×10^{18} in front of the AlAs barrier.

0749-6036/85/050417+05 $02.00/0

Au/Ge alloy followed by a 20 second anneal at 420 °C.[5] Photolithographic techniques were employed to make ring shaped contacts to the top surface to allow light to penetrate into the GaAs through the center of the rings. The individual contacts were then mesa isolated from each other. The mesas were created by etching with a GaAs etch (4:1:1, H_2SO_4:H_2O_2 :H_2O) to a depth of about 10 μm. The samples were mounted on transistor headers, and wire bonds were made to the Au/Ge contacts. The headers could then be mounted in a Janis variable temperature dewar (Janis model DT 11), and thus could be cooled to any temperature desired from room temperature to 4.2K. The light source used to illuminate the samples was a tungsten filament lamp. The light was directed through a spectrometer (SPEX model 1269) and then focussed onto a particular device to be studied. The measurement of the voltage resulting from the illumination was made directly, using a voltmeter, when it was desired to know the sign of the voltage. In general, however, the light was chopped at about 270 Hz, and the resulting voltage was measured, using a lock-in amplifier. The signal was then digitized, and the spectrum stored on a signal averager (NIC 1170).

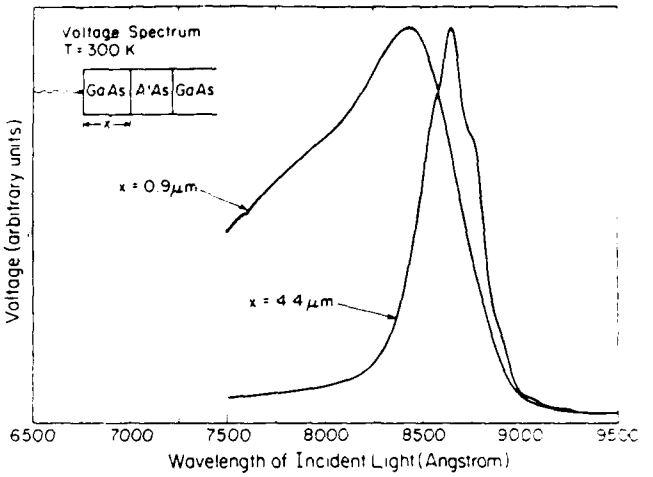

Fig. 1. Voltage spectrum taken at room temperature for a sample with a 240 Å AlAs barrier. The GaAs layers were doped n-type at about 3×10^{18} cm^{-3}. The thickness of the top layer of GaAs was 4.4 μm and 0.9 μm, as indicated in the figure.

3. Theoretical Model

To model the absorption of the light in these structures, we carry out the following calculations. We consider a model where we have a layer of GaAs, a layer of AlAs, and a semi-infinite layer of GaAs. Light impinges on the first layer of GaAs from a vacuum at normal incidence. We assume that no attenuation of the light takes place in the AlAs. In the GaAs, however, we model the attenuation of the light, using a coefficient of absorption, α, which we obtained by fitting and extrapolating the curves published by H.C. Casey et al.[6] for heavily doped n-type GaAs at room temperature. We used constant values for the index of refraction of GaAs and AlAs of 3.4 and 3.1, respectively[7]. The light intensity was then calculated throughout the model structure and was integrated in the region of GaAs in front of the AlAs barrier and in an equal region behind the AlAs barrier to obtain the total light intensity in each of the two regions. The total light intensity behind the AlAs barrier was then subtracted from the total in front of the AlAs, and this difference was plotted as a function of wavelength. When there is more light intensity in front of the AlAs than behind, there are correspondingly more electrons excited there. It is this difference in the concentration of electrons in the conduction band which drives the flow of electrons from the front side of the AlAs barrier to the back side. As will be discussed below, it is those electrons which are excited in the conduction band of the GaAs by free carrier absorption which have enough energy to go over the AlAs barrier. The number of electrons excited in the conduction band due to free carrier absorption is proportional to the light intensity. Thus, we would expect the measured voltage spectrum to have the same shape as the calculated difference in the light intensity in front of and behind the AlAs barrier. Recent calculations by C. Mailhot et al.[8] have shown that it is the Γ-point of the AlAs which determines the energy barrier presented to an electron in the GaAs, and our observations so far have been consistent with this conclusion in that we have not observed a voltage at wavelengths corresponding to energies substantially below this value.

4. Results

In Fig. 1, we present a voltage spectrum for sample 4 at room temperature. This sample had a top layer of GaAs which was 4.4 μm thick in one case and which had been etched down to a thickness of 0.9 μm in the other case. We note, first, that in both cases we have a substantial amount of signal at energies below the GaAs band gap (1.424 eV or 8700 Å at room temperature) At wavelengths below the GaAs band gap, no holes are created in the structure and, hence, the photo-voltage is not a result of hole movement in the GaAs. At wavelengths above the GaAs band gap where we do create electron hole pairs, the movement of electrons and holes in the GaAs due to the electric fields at the GaAs-AlAs interface would result in a voltage opposite in sign to the one that we measure. These observations strongly suggest that it is electrons promoted in the GaAs by free carrier absorption to energies greater than the GaAs-AlAs offset which can flow past this barrier and produce our observed voltages. To explain the general shape of these spectra, we refer to Fig. 2 which schematically shows the band structure and absorption processes in the sample. At a doping level of 3×10^{18} cm^{-3}, the fermi level can be as much as 110 meV above the conduction band minimum. The two absorption processes are free carrier absorption (A) for which the coefficient of absorption is α_A and band-to-band absorption (B) for which the coefficient of absorption is α_B. Since free carrier absorption involves a phonon and band-to-band

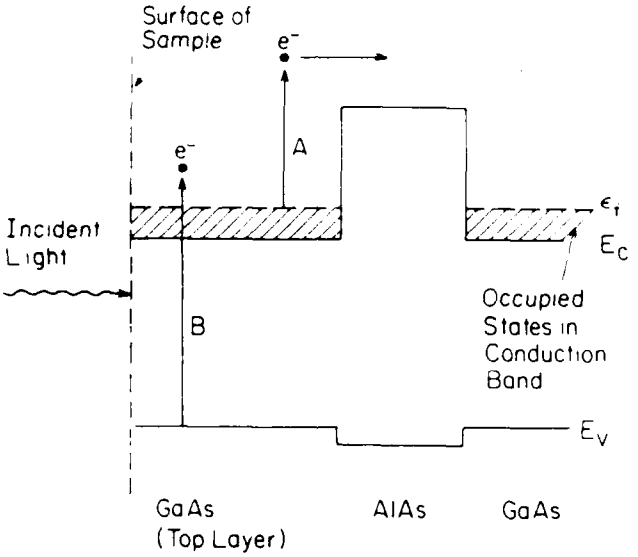

Fig. 2. Schematic diagram of the conduction band (E_c) and valence band (E_v) edges of the GaAs/AlAs heterostructure showing the fermi level (ϵ_f) in the conduction band. Indicated in the figure are free carrier (A) and band-to-band (B) absorption of light by electrons.

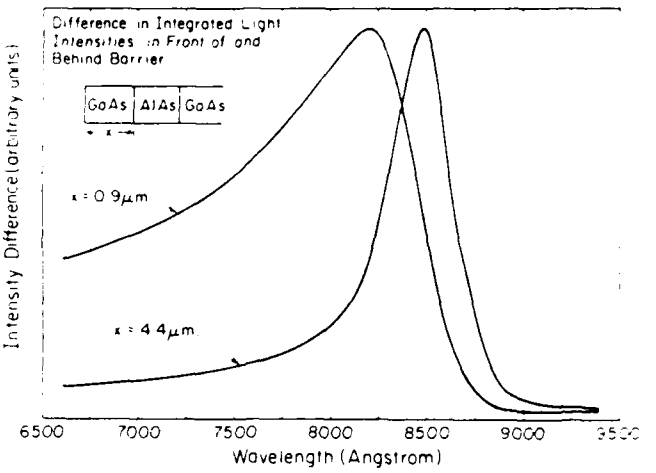

Fig. 3. Calculated difference in the integrated light intensities in front of and behind the AlAs barrier as a function of wavelength. The coefficient of absorption, α, used in calculating these curves was for a GaAs n-type doping of 3.3×10^{18} cm^{-3} at room temperature. The results are presented for a top layer thickness of GaAs of 4.4 μm and 0.9 μm, as indicated in the figure.

absorption does not $\alpha_A \ll \alpha_B$. At long wavelengths where the energy of a photon is insufficient to promote an electron from the valence band over the fermi level, the much weaker free carrier absorption dominates, and there is not a substantial difference between the light intensity in front of and behind the AlAs barrier. There is, thus, a correspondingly small difference in the number of electrons promoted in the conduction band of the GaAs, and we expect to measure a small signal. At short wavelengths where band-to-band absorption is very strong, the light intensity is attenuated very quickly near the surface of the sample, and the difference in light intensity in front of and behind the AlAs barrier is very small, and, again, we expect to measure a small signal. Between these two extremes, we have some wavelength at which the difference in light intensity (and, hence, the concentration of electrons promoted in the conduction band of the GaAs) is a maximum, and we expect to see a maximum signal. We, thus, have a spectrum with a peak whose position is mainly determined by the doping of the sample. To explain the difference in the spectra when we have a thick top layer (5 μm) and a thin top layer (1 μm), consider the following. For a sample with a top layer thickness of 5 μm at wavelengths where process B cannot occur (the energy of the light is insufficient to promote carriers from the valence band over the fermi level), the light intensity is proportional to $e^{-5\alpha_A}$. At shorter wavelengths where process B can occur, the intensity of the light is proportional to $e^{-5\alpha_B}$. Consider the same sample with a thin top layer of 1 μm. The enhancement in the light intensity at wavelengths where process A dominates is proportional to

$$e^{-1\alpha_A}/e^{-5\alpha_A} = e^{4\alpha_A},$$

but at wavelengths where process B dominates (on the short wavelength tail of the spectrum), the enhancement in the intensity of light is proportional to

$$e^{-1\alpha_B}/e^{-5\alpha_B} = e^{4\alpha_B},$$

but since $\alpha_A \ll \alpha_B$ then $e^{4\alpha_B} \gg e^{4\alpha_A}$ and the enhancement in the intensity of the light is much greater at the shorter wavelength tail of the spectrum. Since the number of electrons promoted by process A is proportional to the light intensity, we would expect the voltage signal to be most enhanced at the short wavelength tail of the spectrum. Thus, a spectrum for a sample with a thick top layer will change qualitatively in the way it does in Fig. 1 when the top layer is made thinner. The Γ-point barrier at room temperature is at most 1.35 eV[9] (9180 Å). This barrier is decreased by the fact that the fermi level is in the conduction band but is increased by the effects of band gap shrinkage in the GaAs due to the heavy doping[10] and is also affected by band bending in these structures. This number, however, gives us an estimate as to the longest wavelength at which we could expect to measure a voltage if there is also a difference in the light intensity in front of and behind the AlAs barrier. At wavelengths longer than 9180 Å, even electrons promoted via process A may not be energetic enough to go over the barrier.

In Fig. 3, we present results of the predicted spectrum for a sample with a doping level of 3.3×10^{18} cm^{-3} in the GaAs, which has a 240 Å layer of AlAs and which has a top layer thickness of 4.4 μm or 0.9 μm as labeled. We see that since the absorption coefficient data contains in it the effects of band-to-band versus free carrier absorption, it correctly predicts the qualitative behaviour of the spectra we measured. We note that the peak position (in the case of the thick top layer) and the

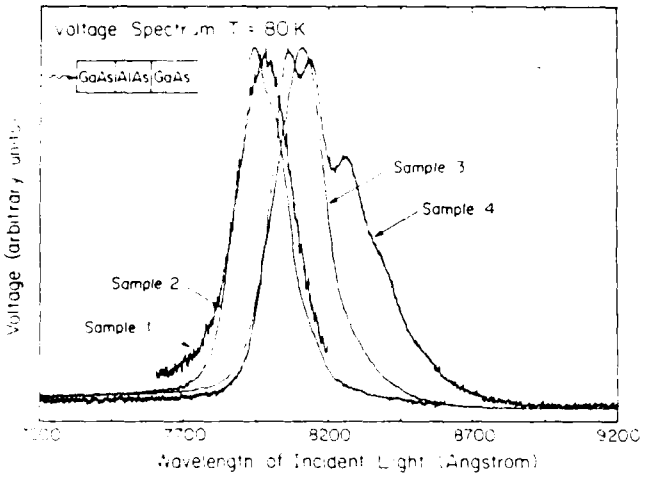

Fig. 4. Voltage spectrum for samples 1 through 4 at 80 K illustrating the relative peak positions. The band gap of GaAs at 80 K is about 1.51 eV (corresponding to about 8230 Å); samples 3 and 4 show signal at wavelengths corresponding to energies below this value.

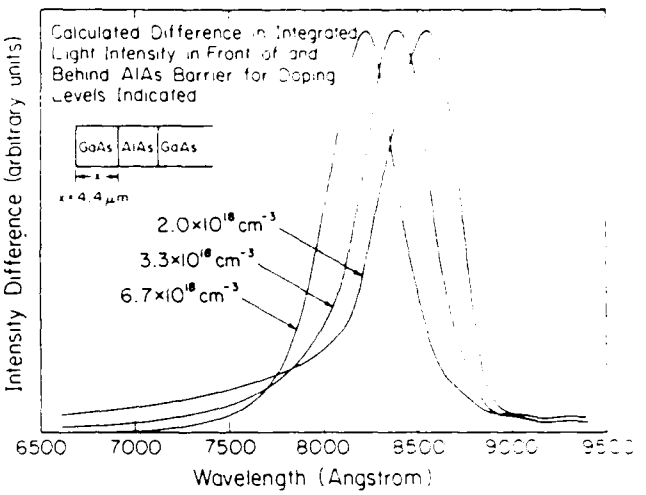

Fig. 5. Calculated difference in the integrated light intensities in front of and behind the AlAs barrier as a function of wavelength. The model in all three cases was for a top layer of GaAs which was 4.4 μm thick and for an AlAs layer thickness of 240 Å. The coefficient of absorption, α, used in calculating these curves was for a GaAs n-type doping of 2.0×10^{18} cm^{-3}, 3.3×10^{18} cm^{-3}, and 6.7×10^{18} cm^{-3}, as indicated in the figure.

turnoff wavelength (in the case of the thin top layer) are not exactly predicted by the calculations though they are in fairly good agreement. These positions depend very much on the doping of the sample used in the experiment. In the calculations, these positions depend on the behaviour of the coefficient of absorption α, which, in turn, depends on the doping and which differs from the actual doping of the samples. In our calculations, we have assumed a constant doping profile, while in the actual samples, the doping in the GaAs is a function of position.

In Fig. 4, we present the voltage spectrum for four different samples at 80 K. We note that there are differences in the spectrum from sample to sample, we can nonetheless identify and explain the relative peak positions. We see that in Fig. 4 the peak positions for samples 1 and 2 are the same and that the peak positions for samples 3 and 4 are the same though shifted to longer wavelengths than for 1 and 2. In Fig. 5, we present the results of the calculations for the light intensity difference in front of and behind the AlAs layer for various dopings in the GaAs regions as indicated. These curves would correspond to spectra obtained at room temperature since the behaviour of α was taken from data obtained at room temperature. In the calculations we have kept the AlAs layer thickness and the GaAs top layer thickness constant. This is done in order to isolate the effects of the doping level. We note that the peak positions shift to shorter wavelengths as the doping in the GaAs is increased. The difference in the peak position is about 200 Å when the doping level is changed from 3.3×10^{18} cm^{-3} to 6.7×10^{18} cm^{-3} in the GaAs. Since these calculations are performed at room temperature and the experiment at 80 K, we would expect the absolute peak positions in the experiment to be at shorter wavelengths than in the calculations, but we would expect the relative peak positions for similar differences in doping levels to be the same. The absolute peak position is a function of temperature, since for lower temperatures, the band gap of the GaAs increases. This, in turn, means that at lower temperatures the absorption edge of the GaAs shifts to shorter wavelengths. We see that the experimental peaks are at shorter wavelengths than the calculated peaks due to the temperature difference as expected. We note that the peaks in the spectra for samples 1 and 2 which are both doped at 5×10^{18} cm^{-3} are at the same position and are at shorter wavelengths than the peaks in the voltage spectrum for samples 3 and 4. This is consistent with the fact that 1 and 2 are more heavily doped in the GaAs region than samples 3 and 4. The peaks for samples 3 and 4, are also at the same position and this too is consistent with the fact that they have similar doping levels in the GaAs regions. The difference in the peak positions is about 150 Å, and this is consisitent with the predicted difference in peak positions when one considers the fact that the difference in doping levels used in the calculations is larger than the difference in doping levels in the actual samples. Changing the AlAs layer thickness over the range found in these samples while maintaining a constant doping level does not result in such a shift in the peak position. In the experimental spectra presented, we see that there are undulations which are not as marked but nonetheless visible in the calculated spectra. There are two possible origins for these undulations in the experimental data. One explantion is that they are the result of the optical properties of the structures, in particular, the detailed behaviour of α. In our calculations, for example, we have assumed a constant doping profile, while in the actual samples, the doping in the GaAs is a function

of position. Another possible explanation is that they are the result of resonant effects in the transmission of electrons over the AlAs barrier.[9]

5. Summary

In summary, we have presented results of an experimental technique that we have employed to study the transport of electrons past an energy barrier. We have presented experimental results which imply that the voltage we are measuring is a result of electrons which have been promoted in the conduction band of GaAs by free carrier absorption to energies which allow them to flow over the barrier presented by the AlAs. We have argued that the driving force for the flow of the electrons through the AlAs barrier is the difference in the concentration of excited electrons on either side of the barrier which is a result of the difference in light intensity on either side of the barrier. Thus, two conditions must be satisfied in order for there to be a measured voltage. The wavelength of the incident light must correspond to an energy larger than the barrier provided by the AlAs, and there must be a difference in the light intensity in front of and behind the AlAs layer. The difference in light intensity was calculated using a model for the structure. We have also presented data showing the change in the spectra as a function of doping level in the GaAs layers. We presented the results of calculations which explain the difference in peak positions for the spectra resulting from samples with different doping levels in the GaAs and different AlAs layer thicknesses as being a result of the change in the optical absorption properties of the structures which result from the different doping levels.

Acknowledgement—The authors would like to acknowledge D.L. Smith, J. Lambe, C. Mailhiot, R.S. Bauer, T.L. Paoli, and W. Streifer for valuable discussions and are grateful to H. Chung, R.D. Yingling, Jr., F. Endicott, M. Bernstein, M. Mosby, J. Tramontana, J. Walker, A. Ammonda, G.L. Harnagel, and R. Ritter for technical assistance with this work. One of us (T.E.S.) received financial assistance from the Natural Sciences and Engineering Research Council of Canada. This work was supported in part by the Office of Naval Research under Contract No. N00014-82-K-0556.

References

1. H.M. Manasevit, *Appl. Phys. Lett.* **12**, 156 (1968).
2. R.D. Dupuis and P.D. Dapkus, *Appl. Phys. Lett.* **31**, 466 (1977).
3. C.R. Lewis, W.T. Dietze, and M.J. Ludowise, *Electron. Lett.* **18**, 569 (1982)
4. R.D. Burnham, W. Streifer, D.R. Scifres, C. Lindstrom, T.L. Paoli, and N. Holonyak, *Electron. Lett.* **18**, 1095 (1982).
5. G.Y. Robinson, *Solid-St. Electron.* **18**, 331 (1975).
6. H.C. Casey, Jr., D.D. Sell, and K.W. Wecht, *J. Appl. Phys.* **46**, 250 (1975).
7. H.C. Casey, Jr. and M.B. Panish, *Heterostructure Lasers* (Academic Press, New York,1978), Part A, Chap. 2.
8. C. Mailhot, D.L. Smith, and T.C. McGill, *J. Vac. Sci. Technol.* B 1 (3), 637 (1983).
9. H.C. Casey, Jr. and M.B. Panish, *Heterostructure Lasers* (Academic Press, New York,1978), Part A, Chap. 4.
10. H.C. Casey, Jr. and Frank Stern, *J. Appl. Phys.* **47**, 631 (1976).

Optical investigations of electron transport through GaAs/AlAs heterostructures

T. E. Schlesinger, R. T. Collins, and T. C. McGill
California Institute of Technology, Pasadena, California 91125

R. D. Burnham
Xerox Corporation, Palo Alto, California 94304

(Received 20 September 1984; accepted for publication 6 March 1985)

We present the results of the application of photoresponse techniques to the study of the transport of electrons past an energy barrier. In this study, the barrier was provided by a thin layer of AlAs sandwiched between GaAs layers. The experiment measures the voltage resulting from the flow of optically excited electrons from one side of the barrier to the other. The voltage is measured as a function of the wavelength of the incident light. We present results obtained for samples with different doping levels, AlAs layer widths, and at various temperatures. We find that for increasing temperatures the voltage spectrum shifts to longer wavelengths, and that for higher doping levels in the GaAs the voltage spectrum shifts to shorter wavelengths. We also present the results of calculations which explain why the observed spectra change as a function of temperature and as the doping level in the GaAs is varied.

INTRODUCTION

The transport properties of small structures is currently an area of very active research[1-3]. The precise character of the barrier and its influence on the transport is a key aspect to understanding the phenomena governing the applications discussed in Refs. 1–3. In this paper we discuss basic results obtained by photoresponse techniques applied to study GaAs/AlAs single barrier heterostructures. Photoresponse was employed to study the transport of electrons past an energy barrier which was provided by a thin layer of AlAs sandwiched between layers of GaAs. The experimental procedure consisted of illuminating samples with light to excite electrons in the conduction band of the GaAs which could then flow past the AlAs barrier. We then measured the resulting open-circuit voltage produced across the AlAs barrier as a function of the wavelength of the incident light. We present results, both of experiment and calculation, which describe the voltage spectrum obtained as a function of temperature and for samples with different doping levels in the GaAs.

The basic results presented in this paper can be summarized as follows. The sign of the voltage that we measured was consistent with electrons flowing from the illuminated side of the AlAs barrier to the back side of the AlAs barrier. The magnitude of the voltage was proportional to the intensity of the illuminating light and was generally greater in the samples with larger zero-bias impedances. The voltage spectra, that is, the voltage as a function of the wavelength of the incident light, for the samples discussed in this paper are broad peaks. The reasons for this have been discussed previously.[4] In this paper we show that the position of the peak depends on the sample temperature and on the doping in the GaAs cladding layers. It was found that for lower temperatures or higher doping levels the spectrum shifted to shorter wavelengths. Based on our calculations we show that the shifts in the spectra are explained as resulting from the change in the optical absorption properties of these structures which, in turn, depend on the temperature and doping, and that these shifts are consistent with the mechanism that we have proposed produces the observed voltages.

SAMPLES AND EXPERIMENTAL METHODS

The samples used in this study were grown by a metalorganic chemical vapor deposition technique,[5,6] with all the AlAs barriers doped p type with Mg[7,8] while the GaAs was doped n type with Se. The substrates on which these structures were grown were (100)-oriented GaAs wafers doped at about 3×10^{18} cm^{-3} with Si. In this paper we will discuss the results obtained from four different samples whose characteristics are summarized in Table I. For these doping levels, the AlAs barrier is fully depleted.

In Fig. 1 we present a schematic cross-sectional view of the sample geometry which is discussed below. The thicknesses of the top layer (illuminated side) of GaAs varied from about 3.3 μm thick to 4.4 μm, depending on the sample, while the bottom layer was substantially thicker. Ohmic contacts were made to the samples by evaporation of a Au/Ge alloy followed by a 20-sec anneal at 420 °C.[9] Photolithographic techniques were employed to make ring-shaped contacts to the top surface to allow light to penetrate into the GaAs through the center of the rings. The individual contacts were then mesa isolated from each other. The rings had an outer diameter of about 300 μm and an inner diameter of about 120 μm while the mesas were about 350 μm in diameter. The mesas were created by etching with a GaAs etch (4:1:1, H_2SO_4:H_2O_2:H_2O) to a depth of about 10 μm. The samples were mounted on transistor headers, and wire bonds were made to the Au/Ge contacts. The headers could then

TABLE I. Sample characteristics.

Sample	Barrier thickness (Å)	GaAs doping Se ($\times10^{18}$ cm^{-3})	Barrier doping Mg ($\times10^{18}$ cm^{-3})
1	110	5	1
2	160	5	1
3[a]	160	3	1
4[b]	240	3	1

[a] GaAs doping 1.2×10^{18} cm^{-3} 1 μm either side of the AlAs barrier
[b] GaAs doping gradually dropped to 2×10^{18} cm^{-3} in front of the AlAs barrier

 0021-8979/85/140852-05$02.40

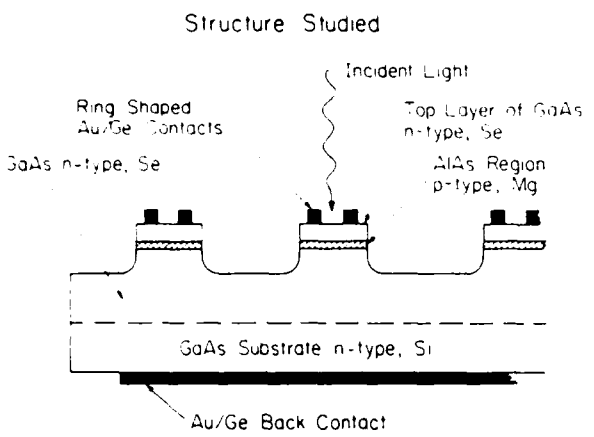

FIG. 1. Schematic diagram of the structure studied. The mesas are approximately 350 μm in diameter and about 10 μm high. The ring-shaped top contacts have an inner diameter of about 120 μm. The experiment consists of measuring the voltage between the top and bottom contacts as a function of the wavelength of the incident light.

be mounted in a Janis variable temperature dewar (Janis model DT 11), and, thus, the samples could be cooled to any temperature desired from room temperature to 4.2 K. The light source used to illuminate the samples was a tungsten filament lamp. The light was directed through a spectrometer (SPEX model 1269) and then focused onto a particular device to be studied. The measurement of the voltage resulting from the illumination was made directly, using a volt meter, when it was desired to know the sign of the voltage. In general, however, the light was chopped at about 270 Hz, and the resulting voltage was measured using a lock-in amplifier. The signal was then digitized, and the spectrum stored on a signal averager (NIC 1170). In either case, the measurement was an open circuit measurement of the voltage across the sample.

THEORETICAL MODEL

To model the absorption of the light in these structures, we carried out the following calculations. We consider a one dimensional model where we have a layer of GaAs, a layer of AlAs, and a semi-infinite layer of GaAs. Light impinges on the first layer of GaAs from a vacuum at normal incidence. We assume that no attenuation of the light takes place in the AlAs. In the GaAs, however, we model the attenuation of the light, using a coefficient of absorption α, which we obtained by fitting and extrapolating the curves published by H.C. Casey *et al.*[10] for heavily doped n-type GaAs at room temperature. We used, however, constant values for the index of refraction of GaAs and AlAs of 3.4 and 3.1, respectively.[11] For an electromagnetic wave incident onto the interface between two dielectric media the boundary conditions at the interface are the continuity of the tangential components of the electric and magnetic fields **E** and **H**, respectively If we have a wave propogating in the $\hat{z}$ direction normal to the interface then the electric field is given by,

$$\mathbf{E} = E_0 \exp[i(\omega t - kz)]\hat{x} ,$$

where

$$k = \frac{\omega n}{c} - \frac{i\alpha}{2} ,$$

and where n is the real part of the index of refraction and α is the absorption coefficient. From Maxwell's equation

$$\nabla \times \mathbf{E} + \mu \frac{\partial \mathbf{H}}{\partial t} = 0$$

we obtain that for nonmagnetic materials the continuity of the tangential component of **H** is equivalent to the continuity of $\partial E/\partial z$. In matching these boundary conditions at the interface we take into account the total electric field due to the incident, reflected, and transmitted waves in any region. The computer programs employed a transfer matrix technique to solve for the electric field throughout the model structure. This allows us, in principle, to extend the calculation to more layers. The light intensity was then calculated as the square of the electric field throughout the model structure and was then integrated in the region of GaAs in front of the AlAs barrier and in an equal region behind the AlAs barrier to obtain the total light intensity in each of the two regions. The quantitative results obtained from these calculations (i.e., exact peak positions and symmetries) depend somewhat on the size of the regions on either side of the AlAs barrier one chooses to integrate over, however, this does not affect the qualitative nature of the results. The integration also included an integration over the phase of the electric field in order to account for the incoherence of the light. The total light intensity behind the AlAs barrier was then subtracted from the total in front of the AlAs and this difference was plotted as a function of wavelength. At present the calculations assume that the absorption properties of the GaAs are those of bulk GaAs at the same doping levels. This is not completely true at the GaAs/AlAs interface where the band bending can drastically alter the free-carrier concentration, and thus, the absorption properties of the GaAs layers.

RESULTS

In Fig. 2, we present the voltage spectrum for sample 2 with a 4.0-μm thick top layer of GaAs for various temperatures. We note that there is measurable signal at energies

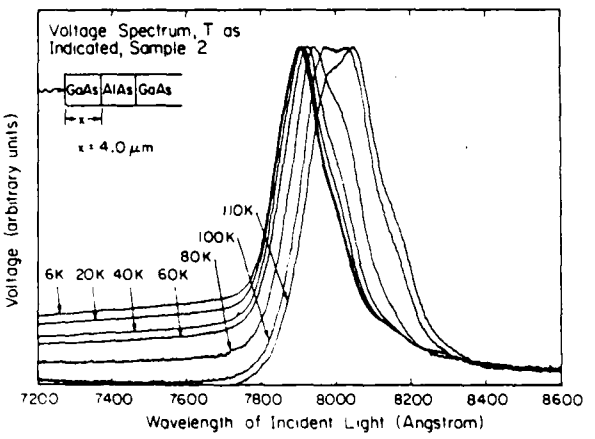

FIG. 2. Voltage spectrum for sample 2 at the temperatures indicated. The GaAs layers were doped n-type at 5×10^{18} cm^{-3} with the top layer of GaAs 4.0 μm thick. The AlAs layer was doped p type at 1×10^{18} cm^{-3} and was about 160 Å thick.

below the GaAs band gap (1.52 eV or 8160 Å at 6 K). The heavy doping causes the band gap to shrink,[12] but it also pushes the Fermi level into the conduction band. For an n-type doping of 5×10^{18} cm^{-3} in the GaAs we estimate that the Fermi level is 160 meV above the conduction band minimum. The net effect is to increase the energy required to take an electron from the valence band into the conduction band and thus increase the energy required to produce holes in this structure. As will be presented below, samples 3 and 4 show signal at even longer wavelengths than samples 1 and 2 at a given temperature. At wavelengths below the GaAs band gap, no holes are created in the structure, and hence, the photovoltage is not the result of hole movement in the GaAs. At wavelengths which correspond to energies that could promote an electron from the valence band into the conduction band and, thus, also create a hole, band bending at the GaAs/AlAs interface would cause electron and hole movement which would create a voltage opposite in sign to the one that we measure. We also note that the sign of the voltage is consistent with electrons flowing from the illuminated side of the AlAs barrier to the back of the AlAs barrier. On the basis of these observations we conclude that electrons promoted from the occupied states in the conduction band of the GaAs by free-carrier absorption to energies greater than the GaAs/AlAs conduction band offset flow past this barrier and produce the observed voltages. The difference in light intensity in front of and behind the AlAs barrier creates a difference in the concentration of optically excited electrons on either side of the AlAs barrier. It is this difference in the concentration of optically excited electrons which drives the electron flow from the front to the back of the AlAs barrier and which, in turn, produces the voltage that we measure. Since the number of electrons excited in the conduction band due to free-carrier absorption is proportional to the light intensity, we would expect the measured voltage spectrum to have the same shape as the calculated difference in the light intensity in front of and behind the AlAs barrier. Recent calculations by C. Mailhot *et al.*[13] have shown that it is the Γ-point offset between the AlAs and the GaAs which determines the energy barrier presented to an electron in the GaAs. The energy required to take an electron over this barrier is less than the conduction band offset due to the fact that the Fermi level is above the conduction band minimum but is increased by the effects of band-gap shrinkage in the GaAs due to the heavy doping, and is also affected by band bending in these structures. The energy required to promote an electron over this barrier also depends on the relative change in the band gaps of GaAs and AlAs as the temperature is varied. There is a controversy regarding the value of the conduction-band energy-gap discontinuity between the GaAs and the AlAs.[14] At room temperature if the offset is 85% of the total energy-gap discontinuity, the barrier presented to an electron would be about 1.35 eV. For a smaller value of the offset the barrier would be substantially less than this. One may then ask why we do not measure an appreciable signal at long wavelengths that still correspond to energies greater than this barrier? We do not measure any signal when there is no difference in the number of optically excited electrons in front of and behind the AlAs barrier. Thus we measure a signal as long as there is a difference in the light intensity in front of and behind the AlAs barrier. The wavelength at which there ceases to be such a difference may correspond to an energy that is still substantially greater that the barrier presented to an electron due to the conduction band offset between the AlAs and the GaAs. Thus, the cutoff in our spectra at both long and short wavelengths is determined by the optical properties of the structure and not the conduction-band offset.

We can explain why in Fig. 2 the peak position shifts to longer wavelengths with increasing temperature. It is band-to-band and free-carrier absorption which determine the nature of the optical absorption in the GaAs and which, in turn, determine the peak position.[4] Thus, as temperature increases, the shift of the peak position to longer wavelengths is a reflection of the shift to lower energies of the band-to-band absorption edge of the GaAs for increasing temperature. The band gap of GaAs, as a function of temperature, can be approximated by[15]

$$E_g = 1.519 - 5.405\times10^{-4}T^2/(204+T)eV.$$

To see whether the shift in the peak position follows the change in band gap, we proceed as follows. We choose the half maximum position on the shorter wavelength edge of the peak as an indication of the peak position. We then plot the change in the peak position referenced to its position at 6 K versus the change in the band gap referenced to its value at 6 K. If then the shift in the peak position is indeed a reflection of the change in the band gap, we expect to have a straight line with slope of one passing through the origin of our plot. In Fig. 3, we present this plot. We see that we do have the behavior we expect though the band gap tends to initially change slightly faster than the peak position. This difference between the movement in the peak position and the change in band gap results from two sources. The first is

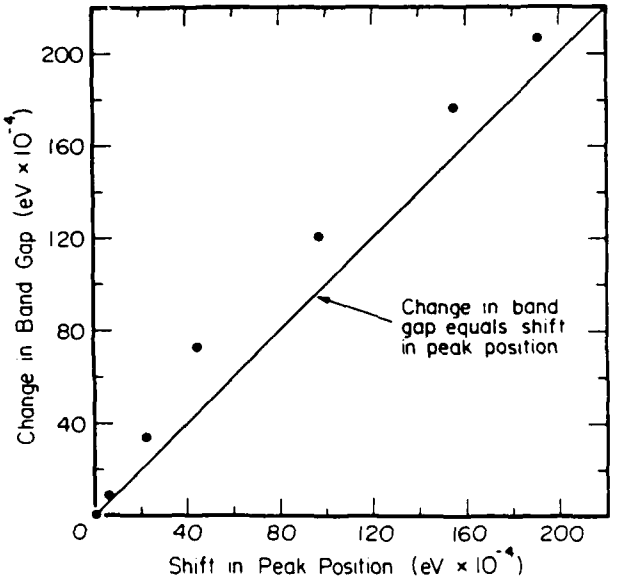

FIG. 3. Change in the band gap vs the shift in the peak position in the voltage spectrum of sample 2 as a function of temperature. The straight line indicates the values for the change in the band gap equal to the shift in the peak position.

the inaccuracy in assigning a value to the peak position at different temperatures. The second is the fact that we have not included the effect on the absorption edge produced by the change in the distribution of the electrons in the conduction band of the GaAs as a function of temperature.

In Fig. 4, we present the voltage spectrum for four different samples at 80 K. We note that while there are differences in the spectrum from sample to sample, we can nonetheless identify and explain the relative peak positions. We see that in Fig. 4 the peak positions for samples 1 and 2 are the same and that the peak positions for samples 3 and 4 are the same though shifted to longer wavelengths than for 1 and 2. In Fig. 5, we present the results of the calculations for the light intensity difference in front of and behind the AlAs layer corresponding to various dopings in the GaAs regions as indicated. These curves would correspond to spectra obtained at room temperature since the behavior of α was taken from data obtained at room temperature. We are restricted to carrying out our calculations at room temperature and for these particular doping levels in the GaAs since, to our knowledge, the only data available for the behavior of α in heavily doped GaAs is that which we obtained from Ref. 10. In the calculations, we have kept the AlAs layer thickness and the GaAs top layer thickness constant. This is done in order to isolate the effects of the doping level. We note that the peak positions shift to shorter wavelengths as the doping in the GaAs is increased. The difference in the peak position is about 180 Å when the doping level is changed from 3.3×10^{18} cm^{-3} to 6.7×10^{18} cm^{-3} in the GaAs. Since these calculations are performed at room temperature and the experiment at 80 K, we would expect the absolute peak positions in the experiment to be at shorter wavelengths than in the calculations, but we would expect the relative peak positions for similar differences in doping levels to be the same. We see that in Fig. 4 the experimental peaks are at shorter wavelengths than the calculated peaks (Fig. 5) due to the temperature difference as expected. We note that the peaks in the spectra for samples 1 and 2 which are both doped at 5×10^{18} cm^{-3} are at the same position and are at shorter wavelengths than the peaks in the voltage spectrum for samples 3 and 4. This is consistent with the fact that 1 and 2 are more heavily doped in the GaAs region than samples 3 and 4. The peaks for samples 3 and 4 are also at the same position, and this, too, is consistent with the fact that they have similar doping levels in the GaAs regions. The difference in the peak positions is about 125 Å, and this is consistent with the predicted difference in peak positions when one considers the fact that the difference in doping levels used in the calculations is larger than the difference in doping levels in the actual samples. Changing the AlAs layer thickness over the range found in these samples, while maintaining a constant doping level, does not result in such a shift in the peak position.

In the experimental spectra presented, we see that there are undulations which are not as marked but nonetheless visible in the calculated spectra. There are two possible origins for these undulations. One explanation is that they are the result of the optical properties of the structures, in particular, the detailed behavior of α. In our calculations, for example, we have assumed a constant doping profile, while in the actual samples the doping in the GaAs is a function of position. Another possible explanation is that they are a result of resonant effects in the transmission of electrons over the AlAs barrier. The peak position is constant as we move from one device to another across the surface of a given wafer. The undulations are reproduced from device to device across a given wafer in terms of their amplitudes but not necessarily in terms of their position. Either origin for the undulations would be very sensitive to small variations in the properties of the structure from one position to another on a wafer. In the case of the optical origin, any variation of the doping profile or layer thicknesses from point to point would affect the undulations, while any resonant effects would be very sensitive to the exact thickness of the AlAs barrier.

Larger voltages are generally observed for samples with larger zero-bias impedances. By zero-bias impedance we

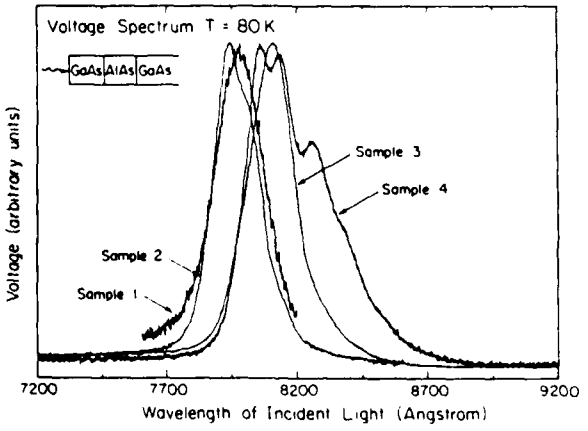

FIG. 4. Voltage spectrum for samples 1 through 4 at 80 K, illustrating the relative peak positions. The band gap of GaAs at 80 K is about 1.51 eV (corresponding to about 8230 Å), samples 3 and 4 show strong signal at wavelengths corresponding to energies below this value.

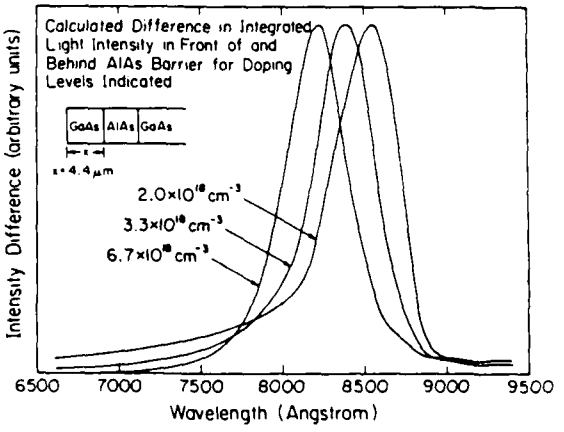

FIG. 5. Calculated difference in the integrated light intensities in front of and behind the AlAs barrier as a function of wavelength. The model in all three cases was for a top layer of GaAs which was 4.4 μm thick and for an AlAs layer thickness of 240 Å. The coefficient of absorption α used in calculating these curves was for a GaAs n-type doping of 2.0×10^{18} cm^{-3}, 3.3×10^{18} cm^{-3}, and 6.7×10^{18} cm^{-3}, as indicated in the figure.

mean the slope of the voltage versus current curve at the origin. As samples are cooled from room temperature, their zero-bias impedances increase, and we observe that in general, for a given sample, we measure a larger voltage at lower temperatures. Sample 1, for example, has a zero-bias impedance of about 37 $k\Omega$ at 4.2 K, while sample 4 has a zero-bias impedance which we can only estimate to be greater than 500 $M\Omega$ at room temperature. Samples 2 and 3 have intermediate impedances. The experiment is an open-circuit measurement of the voltage across the barrier. Hence, there is no net current through the barrier. The light, which illuminates the samples at any given wavelength and for a given intensity, produces a constant number of electrons per unit time which can flow through the AlAs barrier and produce the voltage which we measure. We assert this on the basis of the fact that the signal we measure is proportional to the intensity of the illuminating light. As these electrons move to the back side of the barrier, a voltage is set up which tends to drive electrons from the back side to the front side of the barrier. In steady state these two currents must balance each other. The measured voltage is given by the sample impedance times the fixed current due to the light and is thus larger in samples with larger zero-bias impedances. Sample 4 is an exception to this trend, in that as it is cooled its zero-bias impedance increases as with all the samples, but the voltage we measure decreases. The above explanation breaks down, but we do not have as yet a satisfactory explanation for this.

SUMMARY

In summary, we have presented results of an experimental technique that we have employed to study the transport of electrons past an energy barrier. We have presented experimental results which imply that the voltage we are measuring is a result of electrons which have been promoted in the conduction band of GaAs by free-carrier absorption to energies which allow them to flow over the barrier presented by the AlAs. We have argued that the driving force for the flow of the electrons through the AlAs barrier is the difference in the concentration of excited electrons on either side of the barrier which is a result of the difference in light intensity on either side of the barrier. Thus, two conditions must be satisfied for there to be a measured voltage. The wavelength of the incident light must correspond to an energy larger than the barrier provided by the AlAs, and there must be a difference in the light intensity in front of and behind the AlAs layer. The difference in light intensity was calculated, using a model for the structure. We have presented data showing the behavior of the voltage spectra as a function of temperature which we have explained by considering the change in the band gap of GaAs. We have also presented data showing the change in the spectra as a function of doping level in the GaAs layers. We presented the results of calculations which explain the difference in peak positions for the spectra, resulting from samples with different doping levels in the GaAs, and different AlAs layer thicknesses, as being a result of the change in the optical absorption properties of the structures which result from the different doping levels.

ACKNOWLEDGMENTS

The authors would like to acknowledge D. L. Smith, J. Lambe, C. Mailhiot, R. S. Bauer, T. L. Paoli, R. Thornton, D. I. Smith, and W. Striefer for valuable discussions and are grateful to H. Chung, R. D. Yingling, Jr., F. Endicott, M. Bernstein, M. Mosby, J. Walker, A. Alimonda, G. L. Harnagel, and R. Ritter for technical assistance with this work. One of us (T.E.S.) received financial assistance from the Natural Sciences and Engineering Research Council of Canada. This work was supported in part by the Office of Naval Research under Contract No. N00014-82-K-0556.

[1] R. Chin, N. Holonyak, G. E. Stillman, J. Y. Tang, and K. Hess, Electron. Lett. **16**, 467 (1980).
[2] F. C. Capasso, W. T. Tsang, and G. Williams, IEEE Trans. on Electron Devices **ED-30**, 381 (1983).
[3] A. R. Bonnefoi, R. T. Collins, T. C. McGill, R. D. Burnham, and F. A. Ponce, Appl. Phys. Lett. **46**, 285 (1985).
[4] T. E. Schlesinger, R. T. Collins, T. C. McGill, and R. D. Burnham, Appl. Phys. Lett. **45**, 686 (1984).
[5] H. M. Manasevit, Appl. Phys. Lett. **12**, 156 (1968).
[6] R. D. Dupuis and P. D. Dapkus, Appl. Phys. Lett. **31**, 466 (1977).
[7] C. R. Lewis, W. T. Dietze, and M. J. Ludowise, Electron. Lett. **18**, 569 (1982).
[8] R. D. Burnham, W. Streifer, D. R. Scifres, C. Lindstrom, T. L. Paoli, and N. Holonyak, Electron. Lett. **18**, 1095 (1982).
[9] G. Y. Robinson, Solid-State Electron. **18**, 331 (1975).
[10] H. C. Casey, Jr., D. D. Sell, and K. W. Wecht, J. Appl. Phys. **46**, 250 (1975).
[11] H. C. Casey, Jr. and M. B. Panish, Heterostructure Lasers (Academic, New York, 1978), Part A, Chap. 2.
[12] H. C. Casey, Jr. and Frank Stern, J. Appl. Phys. **47**, 631 (1976).
[13] C. Mailhot, D. L. Smith, and T. C. McGill, J. Vac. Sci. Technol. **B1**, 637 (1983).
[14] R. C. Miller, D. A. Kleinman, and A. C. Gossard, Phys. Rev. B **29**, 7085 (1984).
[15] H. C. Casey, Jr. and M. B. Panish, Heterostructure Lasers (Academic, New York, 1978), Part A, Chap. 4.

Ohmic contacts to *n*-type GaAs

W. J. Boudville and T. C. McGill
California Institute of Technology, Pasadena, California 91125

(Received 24 April 1985; accepted 25 April 1985)

We present a model of the metal–semiconductor junction, for heavily doped GaAs, so that tunneling dominates the current. It is assumed that the imaginary part of the wave vector in the semiconductor is given by the two-band model. Modifications in the barrier potential due to image charge, negative charge near the interface, and the degenerate doping of the semiconductor are included. The role of the *L*-point minimum in the GaAs in determining the position of the Fermi level in the semiconductor is included. The energy distribution of the conductance as a function of doping and barrier height is given. The contact resistance as a function of doping and barrier height is also presented. The results suggest that previous calculations are substantially in error due to the simple models that were used for the dependence of the imaginary part of the wave vector on energy.

I. INTRODUCTION

The development of GaAs technology has led to a continuing search for methods of making Ohmic contacts to *n*-type GaAs. One of the very interesting recent developments has been the growth of heavily doped layers using molecular beam epitaxy (MBE).[1] Furthermore, the most widely used theory of Ohmic contacts is that due to Chang, Fang, and Sze (CFS),[2] in which a metal–semiconductor contact is treated. Attempts to compare theory with experiment have been mainly based on this theory.[3,4,5]

In CFS's theory, they treat the tunneling of carriers through a Schottky barrier as a function of doping in the semiconductor. The theory includes the correction of the image potential to the barrier. It assumes that the tunneling through the barrier is characterized by an imaginary wave vector vs energy that is simple parabolic (one-band) relationship. Given the current interest in the theory, it is desirable to improve the theory so that it treats the best model available. With these improved results, one might hope for a more realistic comparison between the theory and experiment.

In this paper, we present the results of a more realistic treatment of the contact resistance for electrons tunneling through the Schottky barrier between a metal and GaAs, which is heavily doped *n* type. The theory includes the effects of image charge, negative charge at the interface, and the presence of the *L*-point minimum in the GaAs. The biggest correction is due to the improvement in the model of the imaginary wave vector vs energy relation. We assume a two-band model that uses the correct energy gap and conduction band effective mass for GaAs. We find results for the contact resistance which differ by as much as an order of magnitude in the doping ranges of interest for devices.

This paper is organized in the following way. Section II presents the theoretical model. In Sec. III we give the results for the model, and compare them with CFS. In Sec. IV, we show an example of fluctuations in the barrier potential due to the discrete nature of the doping. Finally, in Sec. V we present our conclusions.

II. THEORY

For a metal-*n*-semiconductor junction in reverse bias, with the semiconductor being degenerate, the energy diagram is shown in Fig. 1.

The corrections due to the image force,[6] negative charge at the interface,[7] and nonparabolic corrections to the potential due to the presence of conduction electrons[8] in part of the depletion region are all included. The metal is modeled as a degenerate electron gas, with the radius of the Fermi sphere (the Fermi energy) being ~7–8 eV. (This is not shown in Fig. 1, as it would be offscale.)

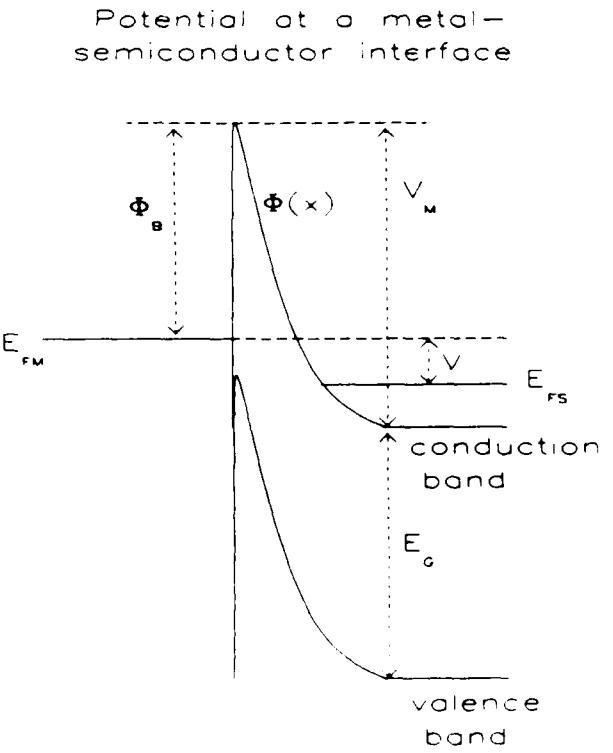

FIG. 1. Diagram of a metal-*n*-semiconductor junction for an applied bias V

 0734-211X/85/041192-05$01.00

In Fig. 1, the energy is measured upwards from the conduction band edge far from the depletion region; E_{FS}, E_{FM} are the Fermi levels in the semiconductor and metal, respectively, and V is the applied bias. Then, following Ref. 9,

$$J = \frac{m_C k_B T q}{2\pi^2 \hbar^3} \int_0^\infty dE T(E) \times \ln\left(\frac{\exp[-(E-E_{FS})/k_B T]+1}{\exp[-(E-E_{FM})/k_B T]+1}\right), \quad (1)$$

where E is the energy of electron normal to interface, m_C is the conduction band effective mass at the Γ point, and $T(E)$ is the transmission probability. Equation (1) neglects phonon-assisted processes, i.e., the transverse wave vector k is assumed to be conserved for tunneling particle. The large Fermi radius of the metal in reciprocal space, relative to the distribution of free carriers in reciprocal space for doped GaAs, or indeed most semiconductors, makes this a good approximation.[10] In the derivation of Eq. (1), a number of other approximations have been made. These approximations are detailed in Ref. 11. The approximations are very commonly made in treating a Schottky barrier and are not likely to result in large errors. One major assumption is used to guarantee that zero current will result when zero voltage is applied, by assuming that the boundary conditions on the current from the semiconductor to the metal are appropriate for the current in the other direction.

By the WKB approximation, take

$$T(E) = \begin{cases} \exp\left(-2i\int_{x_1}^{x_2} k(x)dx\right), & \text{if } 0 \leqslant E \leqslant qV_m, \\ 1, & E \geqslant qV_m. \end{cases} \quad (2)$$

where x_1 and x_2 are the turning points of the forbidden region for k. Assuming a direct-gap semiconductor, a two-band model, from $k\cdot p$ theory, gives for k everywhere within the forbidden region,[12]

$$k = -i\left\{\frac{2m_C}{\hbar^2 E_g}[\phi(x)-E][E_g+E-\phi(x)]\right\}^{1/2}, \quad (3)$$

$$\frac{1}{R_c} \equiv \frac{\partial J}{\partial V} \equiv \int_0^\infty dE G(E). \quad (4)$$

R_c is the specific contact resistance of the interface, measured in Ω cm^2, and $G(E)$ is the conductance distribution function. (Often, in the literature, R_c is defined at $V=0$, but there is no need to confine ourselves to this.) Then,

$$\frac{1}{R_c} = \frac{m_C q^2}{2\pi^2\hbar^3}\int_0^\infty dE \frac{T(E)}{\exp[(E-E_{FM})/k_B T]+1} + \frac{m_C^2 q^2 k_B T}{\pi^2 \hbar^5 E_g} \times \int_0^{qV_m} dE T(E) \ln\left(\frac{\exp[-(E-E_{FM})/k_B T]+1}{\exp[-(E-E_{FS})/k_B T]+1}\right) \times \int_{x_1}^{x_2} dx \frac{[-E_g - 2E + 2\phi(x)]}{k(x)}. \quad (5)$$

R_c and $G(E)$ are found from Eq. (5) by numerical methods. [Note that at zero bias the second term in Eq. (5) is 0.] To obtain E_{FS} in Eq. (5), n, the free carrier concentration, is compared with N_C, the effective density of states in the conduction band. We assume that T is sufficiently large to neglect carrier freezeout. Then

$$E_{FS} = \begin{cases} k_B T \ln(n/N_C), & n \leqslant N_C, \\ \frac{\hbar^2}{2m_C}(3\pi^2 n)^{2/3}, & n > N_C. \end{cases} \quad (6)$$

For carrier concentrations in the GaAs sufficiently large such that the L-point states are occupied, the semiconductor Fermi level is given by

$$n = \frac{1}{3\pi^2}\left[\left(\frac{2m_C}{\hbar^2}\right)^{3/2} E_{FS}^{3/2} + 4\left(\frac{2m_L}{\hbar^2}\right)^{3/2}(E_{FS}-E_{\Gamma L})^{3/2}\right], \quad (7)$$

where m_L is the effective mass at the L point, and $E_{\Gamma L}$ is the energy separation between the L point and the Γ point. The factor of 4 in the second term on right-hand side of Eq. (7) arises because each Brillouin zone has a net of four L points.

The potential energy of the electron is given by

$$\phi(x) = -\frac{q^2}{16\pi\epsilon x} + \phi_1(x), \quad (8)$$

where, for degenerate doping, ϕ_1 satisfies the implicit relationships

$$\frac{d^2\phi_1}{dx^2} = \frac{q^2}{\epsilon}[n - n_e(x)] \quad (9)$$

$$n_e(x) = \begin{cases} \frac{1}{3\pi^2}\left\{\left[\left(\frac{2m_C}{\hbar^2}\right)(E_{FS}-\phi_1)\right]^{3/2} + 4\left[\left(\frac{2m_L}{\hbar^2}\right)(E_{FS}-\phi_1-E_{\Gamma L})\right]^{3/2}\right\}, & E_{FS}-\phi_1 > E_{\Gamma L}, \\ \frac{1}{3\pi^2}\left[\left(\frac{2m_C}{\hbar^2}\right)(E_{FS}-\phi_1)\right]^{3/2}, & E_{FS}-\phi_1 < E_{\Gamma L}. \end{cases} \quad (10)$$

For nondegenerate doping, where $E_{FS} < 0$, let $n_e \equiv 0$. Equations (9) and (10) are solved for ϕ_1 by the method of successive integration.[13] In doing this, the boundary condition of $\phi_1(x) = 0$ at $x = 1.2\times$ the depletion length is chosen to ensure convergence. The complete solution for ϕ_1 would tend to 0 asymptotically as $x \to \infty$. Thus the boundary condition lowers ϕ_1 near the edge of the depletion region. However, this occurs at large tunneling distances, relative to the tunneling distances at higher energies, and so will have little effect on the results.

The effect of negatively charged surface states can be included by adding the following term to the right-hand side of Eq. (8):

$$\phi_{surf}(x) = -\frac{dq^2 N}{\epsilon}\exp(-x/d), \quad (11)$$

where N is the area density of surface states and d is the penetration length of the states.

III. RESULTS AND DISCUSSION

We have used the following values for the parameters in the theory: $T = 300$ K, $E_G = 1.42$ eV, $E_{\Gamma L} = 0.284$ eV,

$m_C = 0.063$, $m_L = 0.55$, $\epsilon = 12.85$, and $N_C = 4.21 \times 10^{17}$ cm^{-3}. The value of E_G is taken from Ref. 14, while the other values are taken from Ref. 15.

To illustrate the contributions to the conductance per unit area per unit energy, for various doping concentrations, we have plotted in Fig. 2 the barrier shapes and values of $G(E)$ for four different dopings: 10^{17}, 10^{18}, 10^{19}, and 10^{20} cm^{-3}. These are at $\phi_{B0} = 0.8$ eV, $T = 300$ K, and $V = 0$ V. Negative surface charges are included, with the choice of $N = 5 \times 10^{14}$ cm^{-2}, $d = 5$ Å. $G(E)$ is plotted on a log scale due to its large variation when the energy is varied from 0 to 1 eV. For example, at a doping of 10^{19} cm^{-3}, $G(E)$ ranges over 10 orders of magnitude. Notice that $G(E)$ has a discontinuity in its slope at $E = qV_m$. This is due to Eq. (2), where the transmission below the barrier is given by the WKB approximation, while the transmission above the barrier was taken to be 1.

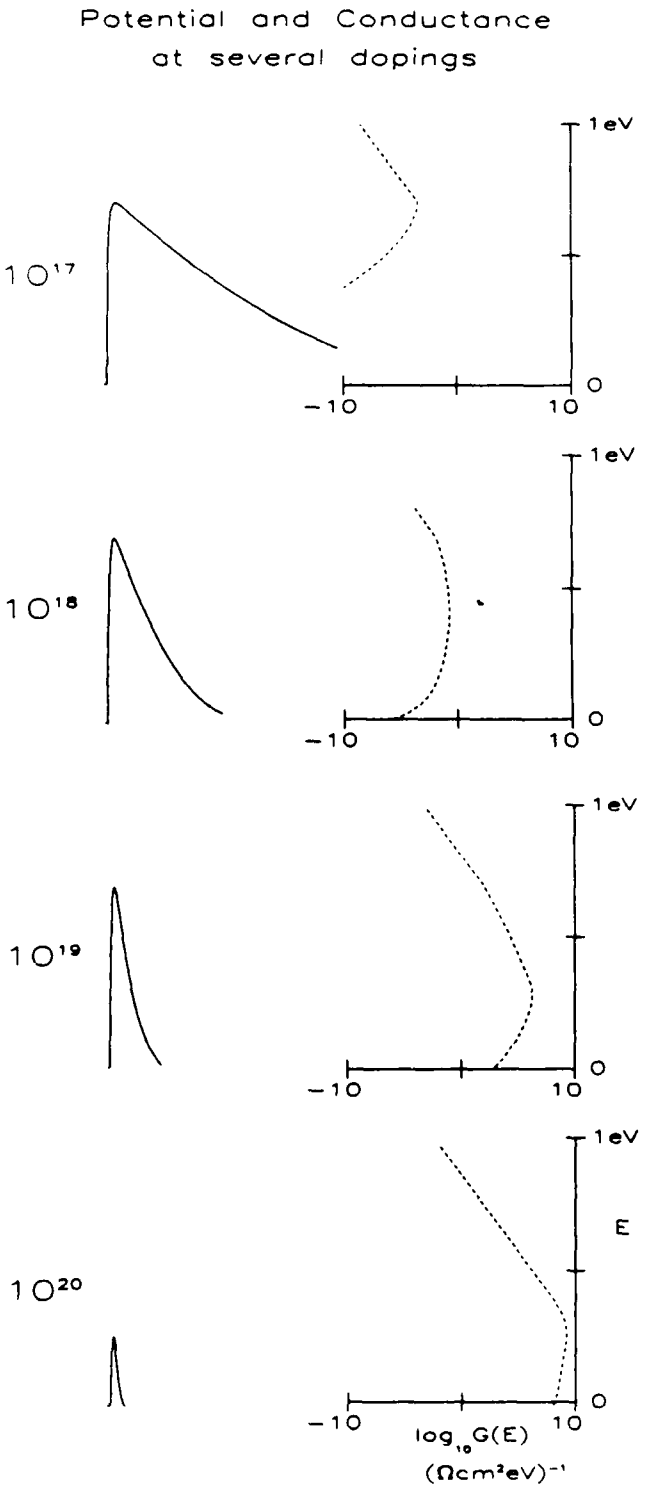

FIG. 2. Distributions of the specific contact conductance as a function of energy. To illustrate the energy position on the barrier, the barrier shape is plotted using the same energy scale. The log of the conductance is shown, with the conductance being measured in Ω^{-1} m^{-2} J^{-1}.

For a doping of 10^{17} cm^{-3}, the maximum in $G(E)$ occurs at qV_m, and the total conductance has roughly equal contributions from carriers going over the barrier in thermionic emission and Fowler–Nordheim tunneling.[16] Observe that the tunneling contribution is significant only for energies down to ~ 0.2 eV below qV_m, since the tunneling length increases strongly for decreasing energy. There is no direct tunneling, since $E_{FM} = E_{FS} < 0$. At a doping of 10^{18} cm^{-3} the maximum in $G(E)$ increases and it occurs at $E = 0.42$ eV, which is below qV_m. Due to the narrowing of the barrier, we get significant conductance over most of the tunneling energies. Fowler–Nordheim tunneling dominates the conductance, while some direct tunneling occurs, for $E < E_{FS} = 0.06$ eV. When the doping is raised to 10^{19} cm^{-3}, $G(E)$ increases strongly, with its maximum occurring at $E = 0.27$ eV $\simeq E_{FS}$. Now direct tunneling is comparable to Fowler–Nordheim tunneling. Finally, for a doping of 10^{20} cm^{-3}, V_m falls con-

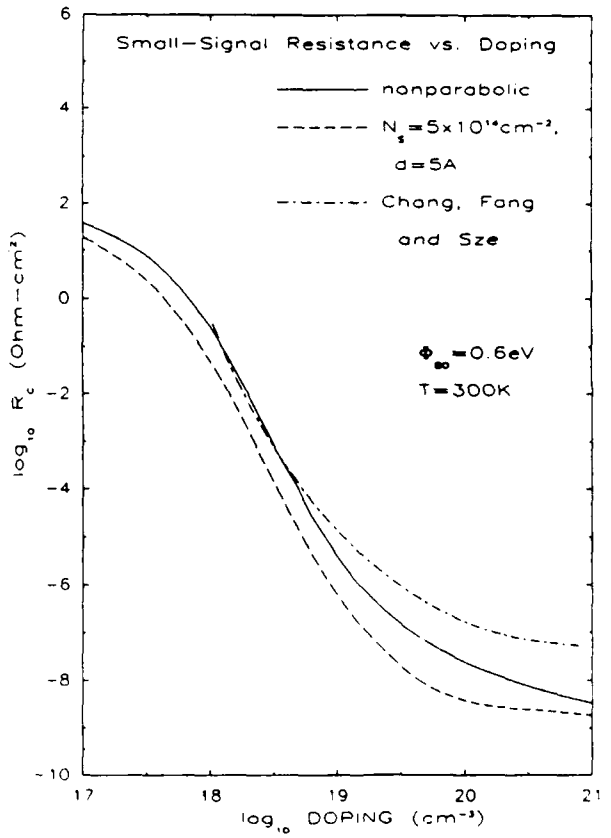

FIG. 3. Specific contact resistance vs doping, for $\phi_B = 0.6$ eV and $V = 0$ V, with and without negative surface charge, with the results from CFS.

siderably after being approximately constant at lower dopings. This is due to the negative surface states "annulling" most of the thin barrier. Here $E_{FS} = 0.33$ eV, and so, direct tunneling is seen to dominate the conductance.

The specific contact resistance as a function of doping is presented for three different intrinsic barrier heights: 0.6, 0.8, and 1.0 eV in Figs. 3–5, respectively. Our results include all of the effects described above. For comparison we have plotted the results assuming no negative surface charge, and also those from CFS. In Fig. 4, where $\phi_{B0} = 0.8$ eV, we also show the parabolic result. This occurs if in Eq. (10) we set $n_e \equiv 0$, regardless of whether or not the semiconductor is degenerately doped.

Comparison of the results in these figures allows us to draw a number of conclusions. First, let us describe those which are common to both CFS's and our models. The contact resistance is seen to increase as the barrier height increases, at fixed doping. For example, at a doping of 10^{19} cm^{-3}, in going from $\phi_{B0} = 0.6$ to 1.0 eV, the contact resistance increases by about two orders of magnitude in both models. For dopings between 10^{18} and 10^{19} cm^{-3}, the contact resistance falls steeply by about seven orders of magnitude. Recall from Fig. 2 and the discussion above, that over this doping range for $\phi_{B0} = 0.8$ eV, tunneling increased to dominate the total conductance, and $G(E)$ increased strongly over all the tunneling energies. Similar results are seen in our model for $\phi_{B0} = 0.6$ and 1.0 eV. Thus we may consider the doping range from 10^{18} to 10^{19} cm^{-3} as a transition from a Schottky barrier to an Ohmic contact. As a final point of similarity, note that CFS's results and our nonparabolic curves (with no surface charge) tend to merge for dopings near 10^{18} cm^{-3}. This is to be expected, since the two models differ in their expressions for the tunneling transmission, and hence should yield the same results when the tunneling contribution is small.

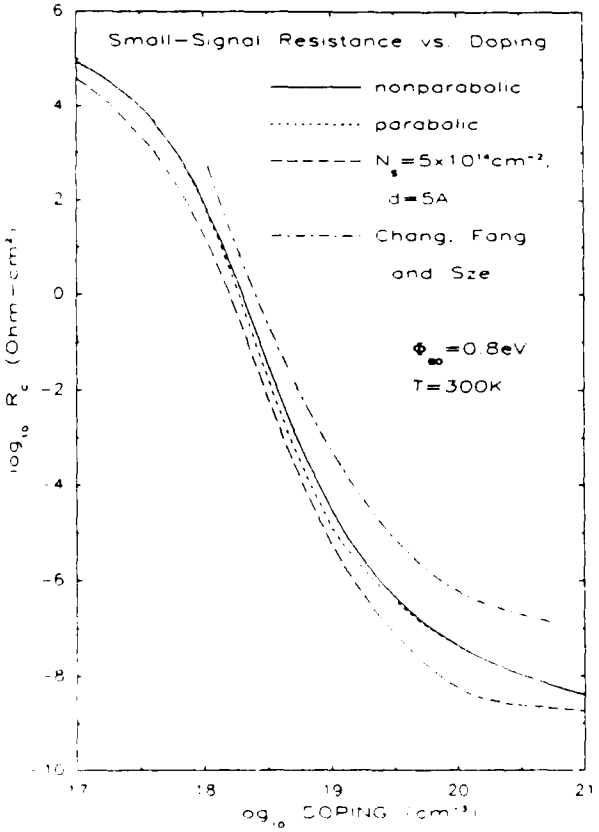

FIG. 4. Specific contact resistance vs doping, for $\phi_B = 0.8$ eV and $V = 0$ V, with and without negative surface charge, with the results from CFS. For comparison, the results assuming a parabolic conduction band in the depletion region are shown.

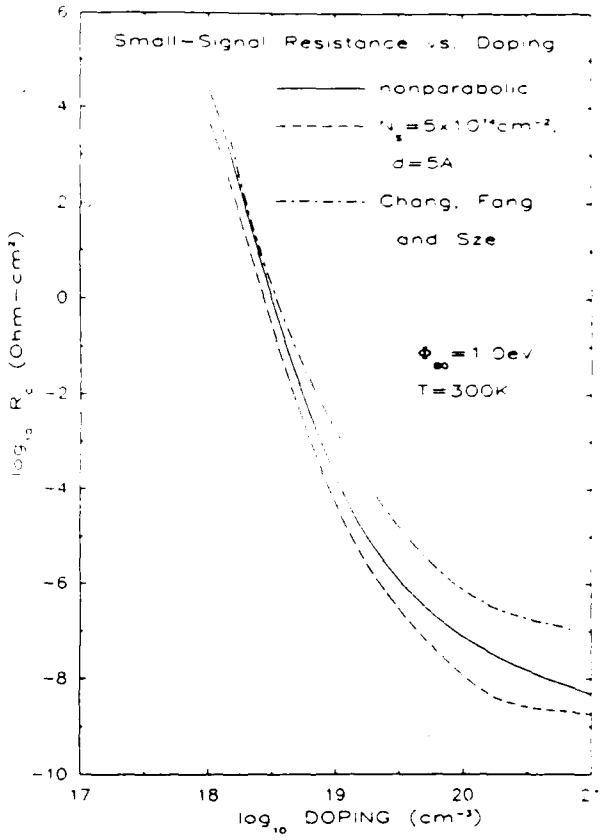

FIG. 5. Specific contact resistance vs doping, for $\phi_B = 1.0$ eV and $V = 0$ with and without negative surface charge, with the results from CFS.

Next, consider the difference between the results of the two models. The nonparabolic curves tend to lie below CFS's curves for dopings greater than 10^{18} cm^{-3}. Between dopings of 10^{18} and 10^{19} cm^{-3}, our nonparabolic curves fall with steeper slope, and continue doing so up to 10^{21} cm^{-3}, whereas by 10^{20} cm^{-3} the slopes on CFS's curves are much reduced. Thus the gap between the nonparabolic and CFS's curves increases with increasing doping. That the differences between the curves increases with doping is expected, since the tunneling contribution dominates the conductance, and the change in the function relating the imaginary part of the wavevector to the energy plays an important role, and accounts for most of the changes. Thus, at high dopings ($> 10^{19}$ cm^{-3}) it may be possible to obtain metal–semiconductor junctions with substantially lower contact resistance than previously thought feasible.

To illustrate the relative importance of the various factors in our theory, consider Fig. 4. For dopings below 10^{18} cm^{-3} or greater than 10^{20} cm^{-3}, there is negligible difference

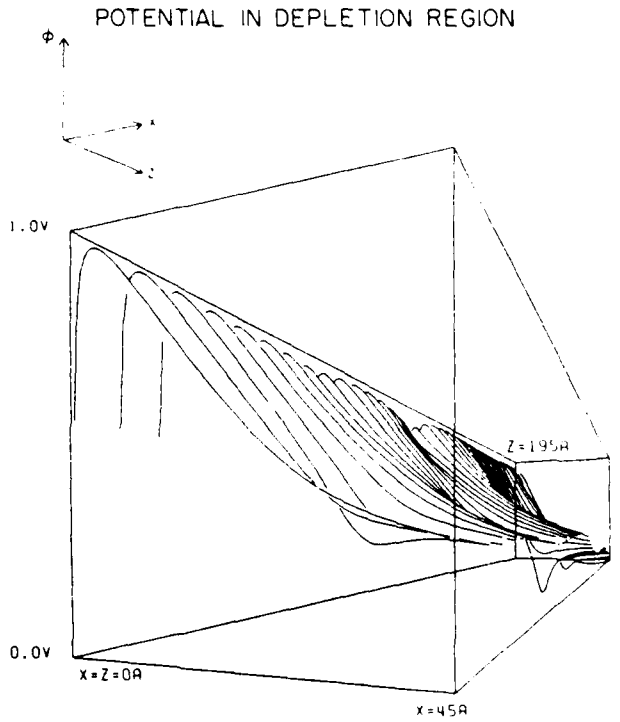

FIG. 6. Potential in the depletion region, for doping = 8×10^{19} cm^{-3}, ϕ_B = 0.8 eV, and V = 0 V. The x direction is normal to the interface and the z direction is along the interface, with resolutions of 0.5 and 1.0 Å, respectively. Also, the direction is in the ⟨100⟩ direction of the lattice.

between the parabolic and nonparabolic results. Indeed, between these doping limits, the difference is less than 0.2 on the log scale. [That the parabolic curve falls below the nonparabolic curve is obvious from Eq. (9).] By our choice of parameters for the surface charges, greater difference is seen between this curve and the nonparabolic curve than between that and the parabolic curve. Qualitatively, including surface charges causes little difference, except at dopings greater than 10^{20} cm^{-3}, where the curve flattens. The reason for this can be seen from Fig. 2. At 10^{20} cm^{-3}, the negative surface charges have greatly reduced the barrier. Effectively, there is no barrier, so further increases in doping will have little effect. Quantitatively, we may say that the presence of any negative surface charge will accentuate the difference between our results and CFS's results. The effect of neglecting image-force lowering is slight; it causes the curves to shift upwards slightly by $\sim$0.2.

IV. FLUCTUATIONS

One significant effect that has not been included in this theory is fluctuations in the potential due to the discreteness in the doping. A simple Monte Carlo model has been used to calculate the fluctuations, wherein dopants have been randomly placed as substitutional impurities within a GaAs lattice, in the depletion region. One such result is illustrated in Fig. 6, for a doping of 8×10^{19} cm^{-3} and ϕ_{B0} = 0.8 eV. The potential is shown in a 45 Å $\times$ 195 Å rectangle in an xz plane, where x is normal to the interface and z is parallel to the interface. The potential is seen to exhibit significant variations. In a future paper,[17] we shall describe our model, and calculate the effects of such fluctuations on the conductance as a function of doping, and compare these to the results presented here.

V. CONCLUSION

We have presented a model for the calculation of contact resistance and conductance as a function of energy of the tunneling electron, for a metal-*n*-GaAs junction, where the GaAs is heavily doped, so that tunneling is significant. This model uses the WKB approximation and the two-band model to obtain a nonanalytic expression for the transmission probability. The contact resitance at zero bias is compared with that from CFS's model. We suggest that our model determines the transmission probability more accurately than CFS's model, which assumes constant transmission for all tunneling energies.

ACKNOWLEDGMENTS

We would like to gratefully acknowledge the support of the Office of Naval Research under Contract No. N00014-82-K-0556. We would also like to thank A. Zur and G. Y. Wu for their advice. One of us (WJB) is the recipient of a Hackett Studentship from the University of Western Australia.

[1] P. A. Barnes and A. Y. Cho, Appl. Phys. Lett. **33**, 651 (1978).
[2] C. Y. Chang, Y. K. Fang, and S. M. Sze, Solid State Electron. **14**, 541 (1971).
[3] J. G. Werthen and D. R. Scifres, J. Appl. Phys. **52**, 1127 (1981).
[4] R. L. Mozzi, W. Fabian, and I. J. Piekarski, Appl. Phys. Lett. **35**, 337 (1979).
[5] N. Braslau, J. Vac. Sci. Technol. **19**, 803 (1981).
[6] S. M. Sze, *Physics of Semiconductor Devices* (Wiley, New York, 1981), Chap. 5.
[7] G. H. Parker, T. C. McGill, C. A. Mead, and D. Hoffman, Solid State Electron. **11**, 201 (1968).
[8] J. W. Conley and G. D. Mahan, Phys. Rev. **161**, 681 (1967).
[9] D. R. Fredkin and G. H. Wannier, Phys. Rev. **128**, 2054 (1962).
[10] J. W. Conley, C. B. Duke, G. D. Mahan, and J. J. Tiemann, Phys. Rev **150**, 466 (1966).
[11] D. J. BenDaniel and C. B. Duke, Phys. Rev. **152**, 683 (1966) (see also Ref. 9).
[12] E. O. Kane, *Physics of III–V Compounds* (Academic, New York, 1966), Vol. 1, Chap. 3.
[13] K. S. Kunz, *Numerical Analysis* (McGraw-Hill, New York, 1957).
[14] C. D. Thurmond, J. Electrochem. Soc. **122**, 1133 (1975).
[15] J. S. Blakemore, J. Appl. Phys. **53**, R123 (1982).
[16] R. H. Fowler and L. W. Nordheim, Proc. R. Soc. London Ser. A **119**, 173 (1928).
[17] W. J. Boudville and T. C. McGill (unpublished).

Resistance fluctuations in ohmic contacts due to discreteness of dopants

W. J. Boudville and T. C. McGill
California Institute of Technology, Pasadena, California 91125

(Received 30 September 1985; accepted for publication 28 January 1986)

The role of fluctuations in the potential due to randomly distributed dopants in the depletion layer of a metal-semiconductor junction is explored. To be specific, the case of *n*-GaAs is considered. Monte Carlo simulation techniques are used to calculate the potential in the junction. By using the WKB approximation and the two-band model, the small-signal resistance at zero bias is found to be lowered by up to half an order of magnitude from the result assuming a continuum distribution of dopant charge. The resistance is found to vary by an order of magnitude in the plane of the interface resulting in a very nonuniform distribution of the current.

One of the standard models of ohmic contacts is a metal-semiconductor junction in which the semiconductor is sufficiently heavily doped that tunneling is the major transport mechanism through the Schottky barrier.[1] This ideal model of the ohmic contact has been realized in recent years. Ohmic contacts to *n*-GaAs have been made by molecular beam epitaxy, where the layers of GaAs have been heavily doped with Sn (Ref. 2) or Si,[3] with dopings in the range of 10^{19}–10^{20} cm^{-3}. At these dopings, the current through a metal-*n*-GaAs junction thus formed is dominated by tunneling. The model of ohmic contacts by Chang, Fang, and Sze (CFS)[1] has been most commonly used to analyze results such as those in Refs. 2 and 3.

In a previous paper[4] we have presented an improved theory. Here we extend that theory to include the effects of fluctuations in the potential due to the randomness of the doping within the depletion region. These fluctuations could be important in the range of doping where ohmic contacts are formed. For example, at dopings around 10^{19} cm^{-3}, where the average interdopant separation is ~ 30 Å, the depletion length is ~ 120 Å. Thus an electron traversing through the depletion region would be likely to encounter, not a potential due to a continuum of ionized dopants, but a potential influenced strongly by a few dopants, and hence varying considerably.

The WKB approximation is used to give the transmission,

$$T(E) = \begin{cases} \exp\left(-2i \int_{x_1}^{x_2} k(x)\,dx \right) & \text{if } 0 < E < qV_m \\ 1 & \text{if } E > qV_m \end{cases}, \quad (1)$$

where V_m is the height of the potential barrier, with respect to the conduction band outside the depletion region, and x_1, x_2 are the turning points of the forbidden region for k, where the x direction is normal to the interface. Within the forbidden region, from the two-band model,[5]

$$k = -i\left(\frac{2m_C}{\hbar^2 E_g} [U(x) - E][E_g + E - U(x)] \right)^{1/2}, \quad (2)$$

where E_g is the band gap energy and $U(x)$ is the potential energy in the depletion region. At zero bias, the small-signal resistance is given by

$$\frac{1}{R_s} = G_s = \frac{m_c q^2}{2\pi^2 \hbar^3} \int_0^\infty dE \, \frac{T(E)}{\exp[(E - E_{FM})/k_B T] + 1}. \quad (3)$$

Previously,[4] U was found by including nonparabolic corrections and the L point states. The depletion region was assumed to consist of a uniform continuum of ionized dopants.

To include the effects of fluctuations in the potential, we have taken a different approach. In principle, one could put down the dopants in a random fashion, solve for the electrostatic potential, and then solve for the transport through the potential barrier. However, this problem is much too difficult and we were forced to make some approximations.

Consider a rectangle with one side in the plane of the interface and the other side normal to the interface, and of length x_d. For the purpose of calculation, the length of the rectangle in the plane of the interface is taken to be 200 Å. To compute the potential in this rectangle, we have made a number of simplifying approximations. First, we assume that the width of the depletion region does not vary in the plane of the interface. We take the depletion width to be given by the standard continuum approximation,

$$x_d = \left(\frac{2\epsilon}{nq} (\phi_{b0} + E_{FS}) \right)^{1/2}, \quad (4)$$

where ϕ_{b0} is the intrinsic barrier height, n is the density of donors, and E_{FS} is the fermi level in the semiconductor. E_{FS} is found from Eqs. (6) and (7) in Ref. 4.

Second, we divide the contributions to the potential seen by the electron into three parts,

$$U = \frac{-q^2}{16\pi\epsilon x} + U_1 + U_2. \quad (5)$$

The first term on the right-hand side is the image term of the electron. The term U_1 is due to dopants far from the electron, and, hence, should cause small fluctuations in the potential. The term U_2 is the potential due to ionized dopants near the electron, and is responsible for most of the fluctuations in the potential.

To be specific, the regions contributing to the potential seen by an electron are illustrated in Fig. 1. We divide the depletion region into two parts: a cylinder of radius R and depth x_d, and the region outside the cylinder. The radius of the cylinder is taken to be three times the thickness of the depletion layer. [$R = 3x_d$ in Eq. (6) below.] The contribution to the potential from the ionized donors outside the cylinder is calculated by assuming that the charge density is continuous. The image in the metal is included; however, the image potential due to the undepleted GaAs is not included because of the small electron density when compared to a metal.[6] This yields

 0003-6951/86/120791-03$01.00

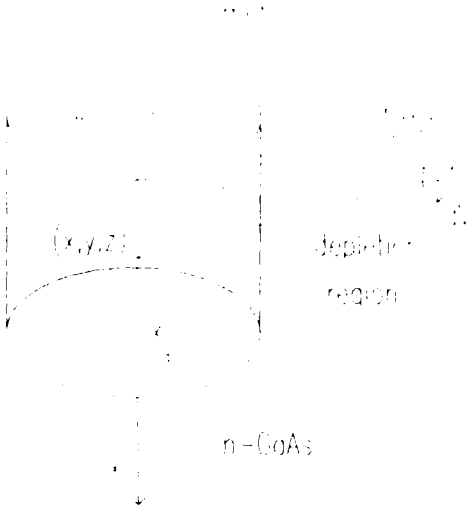

FIG. 1. Contribution to the potential at (x, y, z) in the depletion region, from a differential charge at (x_0, y_0, z_0) outside the cylinder, is shown. Also illustrated is the contribution from the differential image at $(-x_0, y_0, z_0)$.

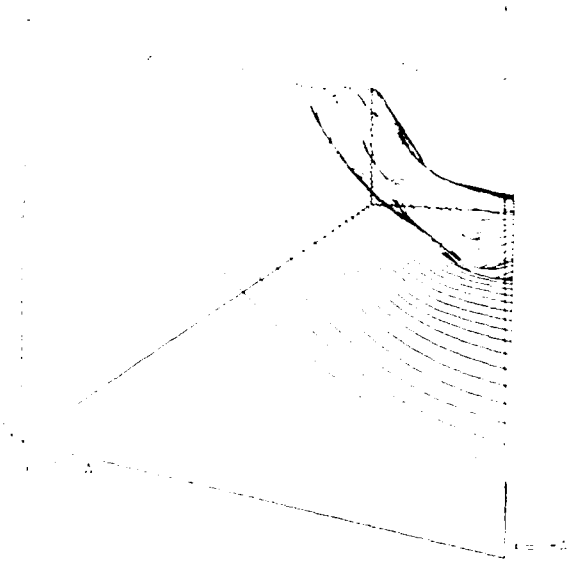

FIG. 2. Random potential for one configuration of ionized donors in a rectangle in the depletion region. The average doping is 2.5×10^{19} cm^{-3}. The Schottky barrier height is 0.8 eV. The applied bias is zero. The x direction is normal to the interface, and the z direction is along the interface. The x direction is the $\langle 100\rangle$ direction of the GaAs lattice.

$$U_1 = \phi_{m0} + \frac{nq^2R^2}{4\epsilon}\left[\frac{2x}{R}\left[1+\left(\frac{x}{R}\right)^2\right]^{1/2} - \frac{x+x_d}{R}\left[1+\left(\frac{x+x_d}{R}\right)^2\right]^{1/2} + \frac{x_d-x}{R}\left[1+\left(\frac{x_d-x}{R}\right)^2\right]^{1/2}\right.$$
$$\left. - 2\ln\left\{\left[1+\left(\frac{x}{R}\right)^2\right]^{1/2} - \frac{x}{R}\right\} - \ln\left(\left\{\left[1+\left(\frac{x_d-x}{R}\right)^2\right]^{1/2} - \frac{x_d-x}{R}\right\}\Big/\left\{\left[1+\left(\frac{x+x_d}{R}\right)^2\right]^{1/2} - \frac{x+x_d}{R}\right\}\right)\right], \quad (6)$$

where $\phi_{m0} = U(0)$ in the absence of image force lowering.

The charged donors inside the cylinder are taken to be discrete, and their contribution to the potential is calculated in detail including their image in the metal. (The image contribution from the undepleted GaAs is neglected again.) Of course, this contribution to the potential will depend in detail on the spatial arrangement of the ionized donors found in the depletion region. The spatial configuration of the ionized donors is given by using a random number generator to distribute the ionized dopants on one of the two atomic sites in a zincblende lattice. The density is set by the doping. The atoms are inside a rectangular slab of GaAs whose thickness equals x_d. The dimensions of the rectangular slab are chosen to be large enough to include the rectangle within which we are finding U and cylinders centered on any point within the rectangle.

The contribution to conductance per unit area for a given cross-sectional area is calculated using Eqs. (1)–(3). The transport is calculated as if the potential depended only on the x direction. The formulas are evaluated on an equally spaced grid with a grid spacing of 5 Å.

To examine the variations in potential and transport that would be obtained for other configurations, we have used the random number generator to generate a number of different spatial arrangements of atoms. The entire transport calculation was carried out for each case.

Figure 2 shows an example of a potential found by this method at a doping of 2.5×10^{19} cm^{-3} and $\phi_{b0} = 0.8$ eV. The contour lines are lines of constant z, spaced 5 Å apart, where z is in the plane of the interface. It is seen that the potential fluctuates significantly. Thus, at a given tunneling energy, the length of the forbidden region can vary widely, especially if a dopant is nearby, causing the potential to fall. From Eqs. (1), (2), and (3), it is seen that this variation in length can cause a large variation in R_c.

In Figs. 3 and 4 we show the results of our calculations for barrier energies of 0.8 and 1.0 eV along with the results for various models. The x direction has been chosen to be the $\langle 100\rangle$ direction of the lattice. The results are presented as specific contact resistance (the reciprocal of the conductance per unit area) as a function of doping. Each dot in the figures is obtained from a different random configuration of dopants and represents G_c, averaged over 200 Å in the plane of the interface, where individual G_c's are found at 40 z coordinates spaced 5 Å apart. Between four and six simulations are done at each doping value. Having obtained an averaged G_c for each dopant configuration, these averaged results are in turn averaged at each doping value. (These are not displayed in Figs. 3 and 4.) A least-squares polynomial is then fitted to the resultant $[(\log_{10} n,\ \log_{10} r_c)]$ at each barrier height. The curves are shown in the figures under the label "Monte Carlo $\langle 100\rangle$." For comparison, the results from CFS[1] and Ref. 4 (labeled "nonparabolic") are also displayed. The results from Ref. 4 are obtained by assuming a continuum distribution of charged dopants within the depletion region, rather than the discrete case considered here. The results in Figs. 3 and 4 took ~30 days CPU time on a VAX 11/785.

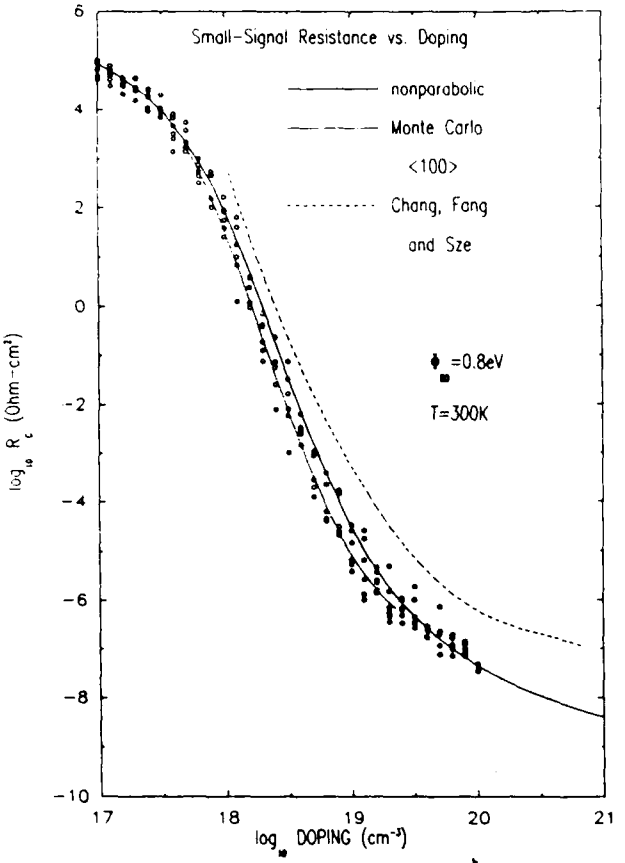

FIG. 3. Specific contact resistance vs doping. The value of the Schottky barrier is 0.8 eV. The calculations are carried out at zero bias. The points are the results of the Monte Carlo simulations. The dashed line is produced from the Monte Carlo results by the procedure described in the text. The solid line is produced using the theory described in Ref. 4. The dash-dotted line is the result obtained from the original theory by Chang, Fang, and Sze (see Ref. 1).

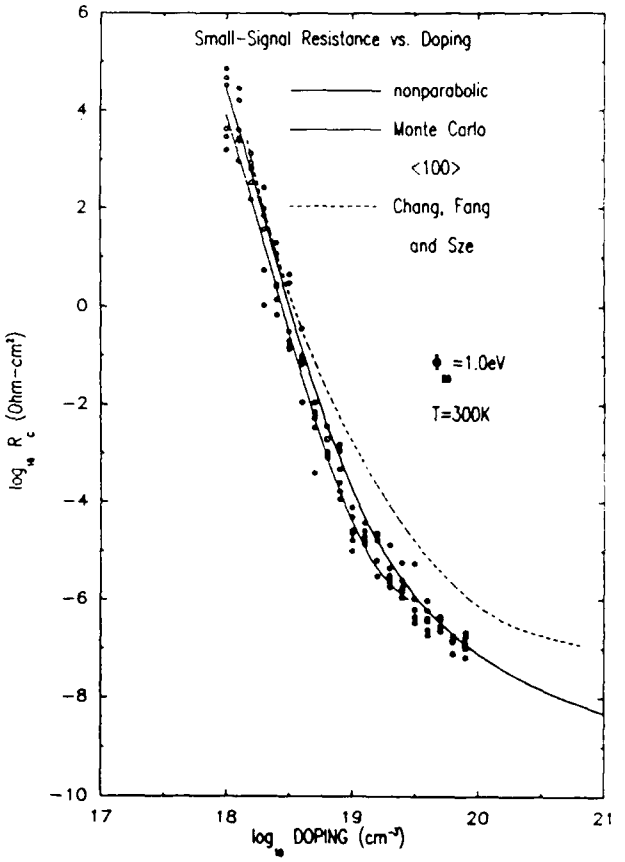

FIG. 4. Specific contact resistance vs doping. The value of the Schottky barrier is 1.0 eV. The calculations are carried out at zero bias. The points are the results of the Monte Carlo simulations. The dashed line is produced from the Monte Carlo results by the procedure described in the text. The solid line is produced using the theory described in Ref. 4. The dash-dotted line is the result obtained from the original theory by Chang, Fang, and Sze (see Ref. 1).

A number of important points can be obtained by studying the results presented in these figures. From the figures, it is seen that for dopings $< 10^{18}$ cm^{-3}, the Monte Carlo results exhibit small fluctuations about the continuum curve. However, as the doping is increased, the average resistance falls about half an order of magnitude below the continuum curve. Furthermore, the fluctuations increase to as much as one and a half orders of magnitude between results from different dopant configurations at the same doping and barrier height. Thus current through the junction may flow preferentially through "hot spots"—regions of high conductance.

In summary, we have found that the discreteness of the ionized dopants, within the depletion region of a metal-*n*-GaAs junction, causes a significant lowering in the small-signal resistance at zero bias, as a function of doping. The small-signal resistance can be up to half an order of magnitude less than those resulting from assuming a continuous charge distribution, and up to an order and a half less than the results obtained by CFS.[1] More importantly, large fluctuations in the conductance are found. These fluctuations may have serious implications for the transport properties of metal-semiconductor junctions. The results indicate that for a semiconductor which is uniformly doped on a macroscopic scale, the conductance, and hence the current, can differ by over an order of magnitude in different spatial regions of the interface. This large spatial variation in the current may be a significant contribution to the noise of a metal-semiconductor junction, and hence may adversely affect the performance of micron or submicron size devices employing such junctions.

We expect similar phenomena to occur in other doped barrier structures. Studies are under way to explore the role of potential fluctuations in other device structures with small characteristic dimensions.

We would like to gratefully acknowledge the support of the Office of Naval Research under contract No. N00014-82-K-0556. One of us (WJB) is the recipient of a Hackett studentship from the University of Western Australia.

[1] C. Y. Chang, Y. K. Fang, and S. M. Sze, Solid State Electron. **14**, 541 (1971).
[2] P. A. Barnes and A. Y. Cho, Appl. Phys. Lett. **33**, 651 (1978).
[3] P. D. Kirchner, T. N. Jackson, G. D. Pettit, and J. M. Woodall, Appl. Phys. Lett. **47**, 26 (1985).
[4] W. J. Boudville and T. C. McGill, J. Vac. Sci. Technol. B **3**, 1192 (1985).
[5] E. O. Kane, *Physics of III-V Compounds* 1 (Academic, New York, 1966), Chap. 3.
[6] N. W. Ashcroft and N. D. Mermin, *Solid State Physics* (Holt, Rinehart and Winston, New York, 1976).

Band offsets, defects, and dipole layers in semiconductor heterojunctions

A. Zur and T. C. McGill[a)]

T. J. Watson, Sr., Laboratory of Applied Physics, California Institute of Technology, Pasadena, California 91125

(Received 13 March 1984; accepted 17 April 1984)

The role of defects in heterojunctions was investigated. The density of such defects required to pin the Fermi level or to affect the band offset was estimated using simple electrostatic considerations. We conclude that it is very unlikely that defects play any role in determining the band offsets, but they might affect the Fermi-level position at the interface.

PACS numbers: 73.40.Lq, 71.25.Tn, 61.70. – r

I. INTRODUCTION

Experiments performed on clean, cleaved surfaces of III–V semiconductors have demonstrated that the Fermi level at the surface is pinned by deposition of very thin coverages (submonolayer to several atomic layers) of either metal,[1–9] semiconductor,[10–12] or oxygen[1,2,4,8,13–17] atoms. The fact that the Fermi-level position at the surface was almost the same for very different adatoms, as well as the fact that clean, cleaved III–V semiconductors do not have surface states in the gap,[2,18–21] led Spicer *et al.*[4,22–24] to propose the unified defect model. According to that model, chargeable native defects are formed upon deposition of minute quantities of adatoms (being either metal, semiconductor or oxygen atoms), and these defects may determine the position of the Fermi level at III–V semiconductor interfaces.

The unified defect model of Spicer *et al.*, which explains the position of the Fermi level at semiconductor interfaces in the limit of very thin coverages and is successful in predicting some interfacial properties, is currently used in the literature to predict the behavior of semiconductor interfaces when the coverage, either metallic of semiconducting, is thick. For example, it was predicted that in a metal–semiconductor interface, the Fermi level would be pinned at the various defect levels,[3,9,25] and that this pinning position would depend on the semiconductor type[26] but not on the metal work function. Other researchers have applied the unified defect model to semiconductor heterojunctions and have predicted that the defect levels might pin the Fermi level at the interface.[26]

In this paper we examine the role defects might play in determining band offsets and the position of the Fermi level at semiconductor heterojunctions. In a recent paper,[27] we have argued that the Fermi-level-pinning mechanism for very thin metallic coverages of semiconductor surfaces is different from the mechanism of Fermi-level pinning at the interface between two bulk materials, the main difference between the two cases being the source of charge that balances the charge captured on the surface defects. In the case of very thin coverage, this source must be the depletion charge in the bulk semiconductor. Therefore, only surface acceptors can be charged on bulk n-type semiconductors, and only surface donors can be charged on bulk p-type semiconductors, even if both surface acceptors and surface donors are present in both cases. This will result in pinning of the Fermi level at the surface-acceptor level on n-type and at the surface-donor level on p-type semiconductors. The density of defects required to pin the Fermi level is comparable to the total depletion charge, which is of the order of 10^{12} cm^{-2} for a doping concentration of 10^{17} cm^{-3} in most wide-band-gap semiconductors. Such a low defect density can be formed by a submonolayer coverage of the semiconductor. It was also argued that if the defect density will be further increased, the two "pinned" Fermi-level positions would move and eventually merge.[28] The "pinning" at submonolayer coverage is, therefore, not complete.

In contrast to the case of very thin coverages, a defect concentration of 10^{12} cm^{-2} was shown[28] to be approximately two orders of magnitude too low to pin the Fermi level at a macroscopic metal–semiconductor junction. In this paper we shall investigate the effect of defects on semiconductor heterojunctions for both thin and thick coverages and contrast it with our previous papers concerning a metal–semiconductor interface.[27,28] We shall show that the effect of defects in a bulk heterojunction is, qualitatively, very similar to the case of a submonolayer coverage. (This was implictly assumed by Kroemer[29] in his treatment of interface charges in heterojunctions.) Quantitatively, we shall show that a defect concentration of 10^{12} cm^{-2} is also too low to *pin* the Fermi-level at the interface between two semiconductors, although it does have an effect on the Fermi-level position, which is more pronounced at semiconductor heterojunctions than at metal–semiconductor interfaces. A defect density of at least an order of magnitude more will be shown to be required to pin the Fermi level in a heterojunction.

We would like at this point to clarify the meaning of "Fermi-level pinning". This term means that the position of the Fermi level at the interface, relative to the band edges, is independent of some external conditions. The degree of this independence however, is important to our discussion. The experiments leading to the unified defect model show that the Fermi level at the surfaces of III–IV semiconductors is "pinned" by submonolayer coverages. The word pinned is used in this context to mean that the curve of Fermi-level position versus coverage, flattens out and reaches some "final" position at submonolayer coverages. There are, however, differences of about 0.1 eV between these "final" Fermi-level positions as measured on surfaces covered with different adatoms, as well as differences of about 0.2 eV

between the final Fermi-level positions measured on n- and p-type semiconductors covered with the same adatom.[26] Moreover, more recent experiments using a thicker coverage of metallic atoms[30,31] demonstrate that this final Fermi-level position is not final and can still move about when the coverage becomes thicker. It appears, therefore, that enough defects are created at the surface to affect significantly the Fermi level but not quite to pin it. In our paper we shall reserve the term "pinning" to the case in which the Fermi-level position at the interface is determined by the defects but not by the bulk doping.

In our calculations, we assume that interface defects have no effect on the band offsets. To justify this assumption, we note that the interface defects would have to form a dipole layer in order to affect the band offsets; a single layer of trapped charge cannot abruptly change the potential, only its slope. Therefore, three conditions have to be satisfied if the defects form a dipole layer which affects the band offsets. First, both donor- and acceptor-type defects should be present at the interface. Second, the layer of donors should be separated from the layer of acceptors by some distance. This requirement is different from the case of a metal–semiconductor interface, in which the metal is guaranteed to supply charges of the opposite sign by screening. A reasonable value for this separation is several angstroms. It cannot be smaller than one atomic layer separation, and, on the other hand, it cannot be larger than a few tens of angstroms, since the band offset is abrupt. The third condition that has to be satisfied is that the defect density would be high enough. We can estimate the charge density required to affect the band offset by 0.1 V using the parallel-plate-capacitor formula:

$$\Delta\phi = \frac{\sigma \cdot d}{\epsilon\epsilon_0}.$$

For a separation of $d = 5$ Å between the defect donors and acceptors, and assuming a dielectric constant on the order of 10, one obtains a defect density of approximately $\sigma = 10^{13}$ cm^{-2}. This defect density seems to be very high, especially when one considers the fact that this density of $\sigma = 10^{13}$ cm^{-2} counts only those defects which participate in this narrow dipole layer, that is, only those defects which are separated by several angstroms from a layer of defects charged with the opposite sign. We must conclude, therefore, that it is very unlikely that interface defects determine the band offsets or have a significant influence on them. Some experimental evidence supports this assumption.[32,33]

This paper is organized in the following way. In Sec. II, we discuss the theoretical methods. In Sec. III, we present the results based on our calculations. The conclusions of this paper are given in Sec. IV.

II. THEORETICAL METHODS

The schematic of our model is given in Fig. 1. Our model consists of two bulk semiconductors (infinitely thick) extending from $x = 0$ to either side. The interface at $x = 0$ is assumed to be abrupt. The band discontinuities at the interface

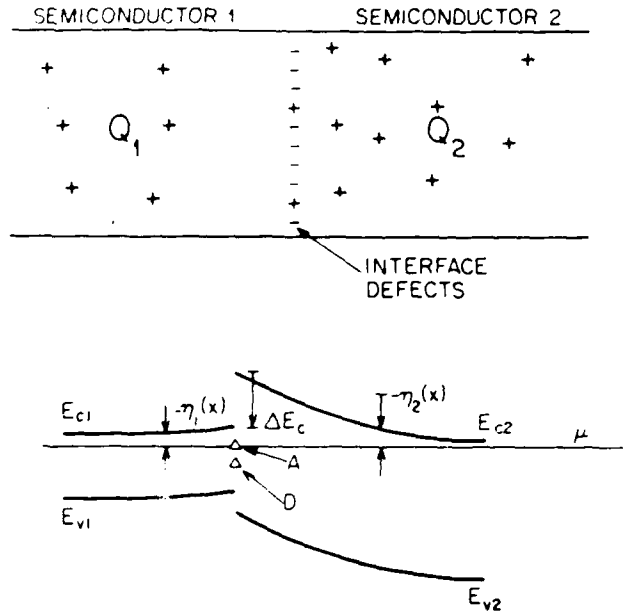

FIG. 1. The geometry and energy levels of our heterojunction model. We assume a very thin defect layer between the two bulk semiconductors, containing both defect donors and defect acceptors. The ionization energies of these defects relative to the band edges of the two semiconductors are denoted by "D" and "A", respectively. We assume that the band offset (denoted by ΔE_c) is independent of the defects.

are prescribed, and the interface contains a layer of defects (both donors and acceptors) with prescribed densities and ionization energies.

The calculation of the Fermi level at the interface is based on conservation of charge. It uses a property of semi-infinite semiconductors, namely, that the Fermi-level position at the surface ($x = 0$) determines the total charge per unit area in the semi-infinite semiconductor. Thus, if $\eta(x)$ denotes the position of the Fermi level relative to the conduction band edge,

$$\eta(x) = \mu - E_c(x), \tag{2.1}$$

and $Q(x)$ denotes the total number of charges per unit area between x and ∞,

$$Q(x) = \int_x^\infty (p - n + N_d^+ - N_a^-)dx, \tag{2.2}$$

then Poisson's equation relates $\eta(x)$ to $Q(x)$:

$$\frac{d\eta}{dx} = \frac{q^2}{\epsilon\epsilon_0} Q(x),$$
$$\frac{dQ}{dx} = n(\eta) - p(\eta) + N_a^-(\eta) - N_d^+(\eta). \tag{2.3}$$

Here, q is the electron charge (taken positive), ϵ is the dielectric constant of the semiconductor, n and p are the densities of the electrons in the conduction band and holes in the valence band, and N_d^+ and N_a^- are the densities of ionized donors and acceptors, respectively. Expressions for n, p, N_d^+, and N_a^- can be found in textbooks on the physics of semiconductors[34] and are not repeated here.

Dividing the two equations in Eq. (2.3) by each other, integrating from $\eta(\infty)$ to η and taking the square root, we obtain:

$$Q(\eta) = \pm \sqrt{\frac{2\epsilon\epsilon_0}{q^2} \int_{\eta(\infty)}^{\eta} [n(\eta') - p(\eta') - N_d^+(\eta') + N_a^-(\eta')] d\eta'}. \quad (2.4)$$

Equation (2.4) relates the Fermi-level position at the interface (η) to the total number of charges per unit area $Q(\eta)$. The sign in front of the square root in Eq. (2.4) is positive if $\eta(0) < \eta(\infty)$, negative otherwise. $\eta(\infty)$, the bulk Fermi-level position, is calculated from the local-charge-neutrality condition:

$$n(\eta) - p(\eta) + N_a^-(\eta) - N_d^+(\eta) = 0. \quad (2.5)$$

Now, we can put the interface together. Given $\eta_1(0)$, the Fermi-level position at the interface, relative to the conduction-band edge of semiconductor 1, we obtain $\eta_2(0)$, the Fermi-level position at the interface relative to the conduction-band edge of semiconductor 2, from the band discontinuity (which is an input to this model)

$$\eta_2(0) - \eta_1(0) = -\Delta E_c. \quad (2.6)$$

From $\eta_1(0)$ and $\eta_2(0)$, we obtain the total number of charges per unit area in the two bulk semiconductors, Q_1 and Q_2 using Eq. (2.4). Finally, the Fermi-level position at the interface determines the fraction of ionized interface defects. This fraction multiplied by the density of these defects gives the number of ionized defects per unit area Q_{sa}^- and Q_{sa}^+.

$$Q_{sa}^+ = \frac{\sigma_d}{1 + g_d \exp\left(\frac{\mu - E_{sd}}{kT}\right)},$$

$$Q_{sa}^- = \frac{\sigma_a}{1 + g_a \exp\left(\frac{E_{sa} - \mu}{kT}\right)}. \quad (2.7)$$

Here, σ_d and σ_a are the densities, g_d and g_a are the degeneracy factors, and E_{sd} and E_{sa} are the ionization energies of interface donors and acceptors, respectively.

The Fermi-level position at the interface is now determined by an overall charge-neutrality condition:

$$Q_1 + Q_2 + Q_{sd}^+ - Q_{sa}^- = 0. \quad (2.8)$$

In the case shown in Fig. 1, both semiconductors are n type. Therefore, the depletion regions on both sides of the interface (Q_1 and Q_2) are positively charged. The Fermi level (μ) at the interface approximately equals the defect acceptor level ("A"), and, therefore, approximately half the defect acceptors will be negatively charged and balance the depletion charge. Since the Fermi level at the interface is above the defect-donor level ("D"), most of the defect donors will remain neutral.

III. RESULTS

A. Submonolayer coverage

The case of submonolayer coverage was treated before.[26,27] The model for treating this case assumes that the adatoms cannot contribute any significant amount of charge, and their only role is the creation of defects. Therefore, one might assume $Q_2 = 0$ in Eq. (2.8), and that the charge due to the surface states balances the substrate depletion charge. Figure 2 shows the resulting Fermi-level position at the interface as a function of surface-defect density for both n- and p-type semiconductors. We assume that both defect donors and defect acceptors are present at the interface at the same concentration. The shape of both curves is in good qualitative agreement with experimental results (compare to Figs. 3 and 8 in Mönch[26]).

We should observe here that our assumption about the relative abundance of defect acceptors and defect donors is not restrictive in any way. If we assume any other fixed ratio of defect acceptors to defect donors, there will be a corresponding change in the horizontal scale of the two curves in Fig. 2. By comparing the curves of Fig. 2 with experimental results (for example, the point of maximum curvature), we may conclude that both defect donors and defect acceptors are present, and their concentration is of the same order of magnitude though not necessarily equal.

The curves in Fig. 2 seem to stabilize at a defect density on the order of 10^{12} cm^{-2}. (In fact, these two curves have some small but nonzero slope at that density, and they slowly approach each other). This defect density corresponds to a doping concentration of 10^{17} cm^{-3} and scales like the square root of the doping. Moreover, the pinning positions for n- and p-type semiconductors are substantially different and determined essentially by the defect-donor level for a p-type semiconductor and by the defect-acceptor level for an n-type semiconductor. One should be aware of the fact that this behavior is typical for the case of very thin coverage. A thick coverage of either a metal or a semiconductor can contribute a significant amount of charge to the system. In other words, Q_2 in Eq. (2.8) cannot be neglected, and as a result, the behavior of the Fermi-level position at the interface might be different. This difference in behavior between thin and thick

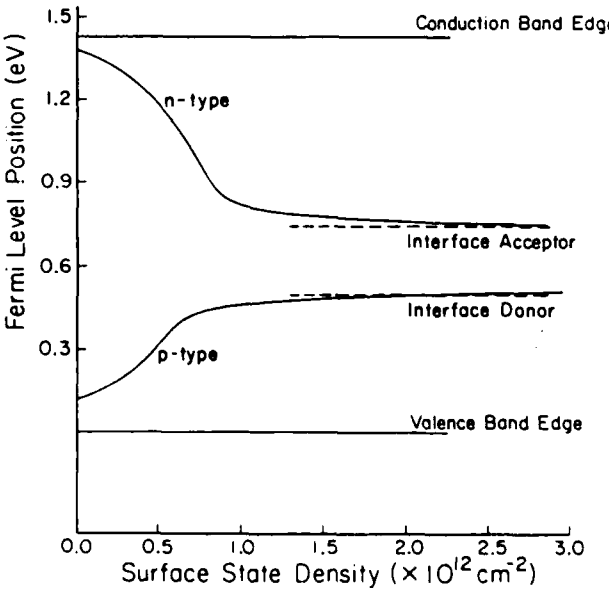

FIG. 2. The position of the Fermi level at the surface as a function of defect concentration for GaAs. The positions of the defect levels (either acceptors or donors) are shown by arrows. The density axis refers to either the defect donors or the defect acceptors.

coverage was treated in another paper for the case of a metal–semiconductor interface.[28] In the case of a metal-semiconductor interface, the charge contributed by the metal can be substantially higher than that contributed by the semiconductor ($Q_2 \gg Q_1$). As a result, the behavior of thick coverages was shown to be qualitatively different than that of a thin coverage. We now treat the case of a thick semiconductor coverage, i.e., a bulk heterojunction. Here, the charge contributed by both bulk materials is of the same order of magnitude. Therefore, one expects a similar behavior between thin and thick coverages, with some quantitative changes due to the presence of another bulk material.

B. Thick coverage

In our calculations, we have used the Ge/GaAs junction as a typical heterostructure. The band offset was chosen to be[35,36]

$$\Delta E_c = 0.54 \text{ eV}.$$

This band offset is not the only one appearing in the literature. Other possible values for ΔE_c are 0.4[11,12] and 0.13–0.28[32]. The interface-defect levels in this model correspond to the GaAs defect levels.[22] Their energies are given by

$$E_c(\text{GaAs}) - E_{sd} = 0.93 \text{ eV},$$

$$E_{sa} - E_v(\text{GaAs}) = 0.68 \text{ eV}.$$

Our choice of band offsets and defect levels, though somewhat arbitrary, is reasonable, but more importantly, our conclusions based on these calculations do not depend on this particular choice.

In Fig. 3, we show the band bending in the ideal Ge–GaAs heterostructure (ideal meaning that there are no interface defects or that the defect density is smaller than 10^{11} cm^{-2}). We show four different cases corresponding to either *n*- or *p*-type GaAs on either *n*- or *p*-type germanium. The doping concentration (either donors or acceptors) is 10^{17} cm^{-2} in all four cases. The important feature of the ideal heterojunction is that the Fermi-level position can be moved all the way across the germanium band gap by changing the doping. In fact, with the right doping concentration, the Fermi level can be anywhere in the gap without any band bending in either the germanium or the GaAs.

In Fig. 4, we show the result of introducing interface defects. The defect density in this figure is 10^{13} cm^{-2}, *half of them* donors and the other half acceptors. One can see that the possible range of the Fermi-level position at the interface decreases substantially as a result of this high defect density. The Fermi-level position at the interface as a function of defect density is shown in Fig. 5. The four curves correspond to the four combinations of either *n*- or *p*-type germanium on either *n*- or *p*-type GaAs. The doping in all four cases is 10^{17} cm^{-3}. One can divide Fig. 5 into three regions. For a defect density below 10^{12} cm^{-2}, the Fermi-level position at the interface is determined by the doping of the bulk semiconductors; the defect density is too small to have any effect. For a defect density of 10^{14} cm^{-2} or more, the Fermi-level position is determined by the interface defects. Between these two regions, that is, for a defect density in the range 10^{12}–10^{14} cm^{-2}, the Fermi-level position is determined both by the bulk doping and by the defects.

It is interesting to compare the case of a thick coverage, described above, to either the thin coverage, described in the previous subsection, or to the case of a thick metallic coverage.[27,28] The behavior of the Fermi-level position at the interface in Fig. 5 (representing a thick semiconductor coverage) is similar to the one shown in Fig. 2 (thin coverage). In both cases, the Fermi-level position shifts from being determined by the bulk to being determined by the interface defects at a defect density of 10^{12}–10^{13} cm^{-2} (in the case of a bulk heterojunction, approximately twice as many defects are required to have the same effect). At that defect density, the bulk

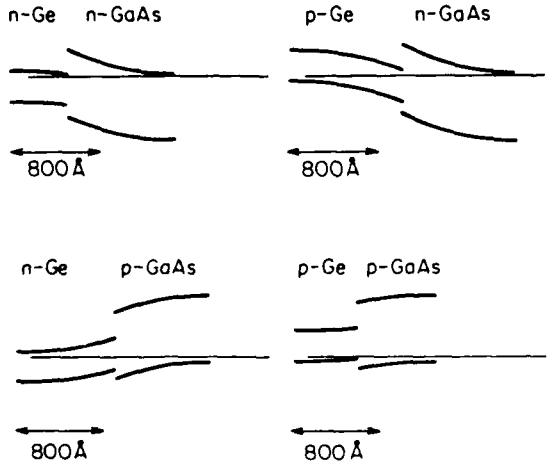

FIG. 3. The energy levels near the interface of a Ge–GaAs heterojunction with very few interface defects (less than 10^{11} cm^{-2}). The four band structures shown are the four combinations of either *n*- or *p*- type GaAs on either *n*- or *p*-type germanium. The doping concentration is 10^{17} cm^{-3} on both sides of the interface. The band offsets correspond to Ref. 36. The Fermi-level position can be moved throughout the germanium gap by changing the doping.

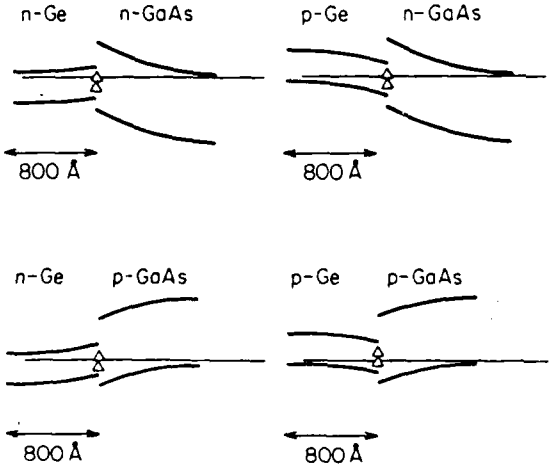

FIG. 4. The energy levels near the interface of a Ge–GaAs heterojunction with a high concentration of interface defects (10^{13} cm^{-2}, half of them donors and half acceptors). All the semiconductor parameters are the same as in Fig. 3. The interface-defect levels were taken from Ref. 22. The Fermi level is not quite pinned at the interface, i.e., it can be slightly moved, depending on the doping, but the range of this movement is very limited due to the high concentration of interface defects.

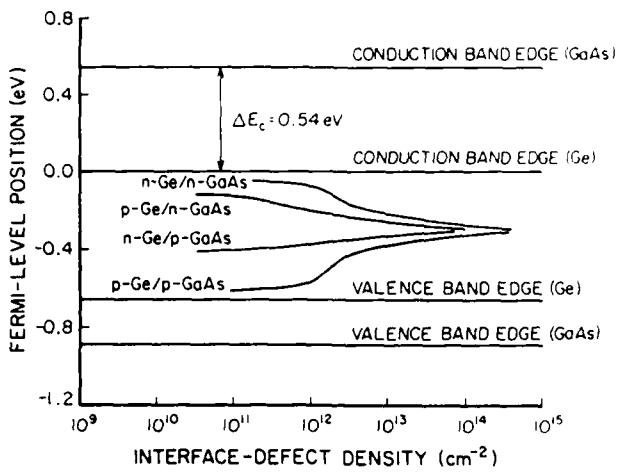

FIG. 5. The Fermi-level position at the interface of a Ge–GaAs heterojunction as a function of interface-defect density (50% acceptors and 50% donors). The semiconductor parameters (doping, bands offset, and defect levels) are the same as in Figs. 3 and 4.

doping still has some influence on the position of the Fermi level, namely, it determines on which defect level it will be pinned. Only when the defect density becomes substantially higher, does the influence of the bulk doping on the Fermi-level position vanish. This behavior should be contrasted with that of a bulk metal–semiconductor interface, in which the effect of the defects is very small below 10^{14} cm^{-2}, and the Fermi-level position is independent of the semiconductor doping.

IV. SUMMARY AND CONCLUSIONS

The effect of interface defects on semiconductor heterojunctions was investigated. It was shown that a defect density of approximately 10^{12} cm^{-2} (which is formed at submonolayer coverages) can affect the Fermi-level position at the interface of bulk heterojunctions. This defect density is comparable to the depletion charge in the bulk semiconductors. It was also shown that a much higher density 10^{13}–10^{14} cm^{-2} is required to pin the Fermi level in a bulk semiconductor heterojunction (compared to approximately 10^{14} cm^{-2} in the case of a metal–semiconductor interface[28]). When such a high density of defects is present, the defect charge is much higher than the bulk depletion charge. The experimental evidence supporting the unified defect model does not show the existence of such a high defect density.

An even stronger statement can be made regarding the effect (or lack thereof) of interface defects on band offsets. We have argued that if the defects affect the band offsets, then they have to satisfy three conditions. Firstly, there should be both defect donors and defect acceptors near the interface. Secondly, the layer of defect donors should be physically separated from the layer of defect acceptors by several angstroms. Thirdly, it requires a large density of such defects (so large, in fact, that it will affect the Fermi-level position even more, thus making the interface undesirable from a device point of view). In view of these requirements, we can say that it is unlikely that interface defects determine the band offsets, or have a significant effect on them.

[a]Work supported in part by the Office of Naval Research under Naval Contract No. N-00014-82-K-0556.

[1]W. E. Spicer, I. Lindau, P. E. Gregory, C. M. Garner, P. Pianetta, and P. W. Chye, J. Vac. Sci. Technol. **13**, 780 (1976).
[2]W. Gudat and D. E. Eastman, J. Vac. Sci. Technol. **13**, 831 (1976).
[3]I. Lindau, P. W. Chye, C. M. Garner, P. Pianetta, C. Y. Su, and W. E. Spicer, J. Vac. Sci. Technol. **15**, 1332 (1978).
[4]W. E. Spicer, P.W. Chye, P. R. Skeath, C. Y. Su, and I. Lindau, J. Vac. Sci. Technol. **16**, 1422 (1979).
[5]P. Skeath, I. Lindau, P. W. Chye, C. Y. Su, and W. E. Spicer, J. Vac. Sci. Technol. **16**, 1143 (1979).
[6]P. Skeath, C. Y. Su, I. Hino, I. Lindau, and W. E. Spicer, Appl. Phys. Lett. **39**, 349 (1981).
[7]T. Zhao, R. R. Daniels, A. D. Katnani, and G. Margaritondo, J. Vac. Sci. Technol. B **1**, 610 (1983).
[8]J. R. Waldrop, S. P. Kowalczyk, and R. W. Grant, J. Vac. Sci. Technol. B **1**, 628 (1983).
[9]T. Kendelewicz, W. G. Petro, S. H. Pan, M. D. Williams, I. Lindau, and W. E. Spicer, Appl. Phys. Lett. **44**, 113 (1984).
[10]A. D. Katnani, N. G. Stoffel, R. R. Daniels, Te-Xiu Zhao, and G. Margaritondo, J. Vac. Sci. Technol. A **1**, 692 (1983).
[11]W. Mönch and H. Gant, J. Vac. Sci. Technol. **17**, 1094 (1980), Phys. Rev. Lett. **48**, 512 (1982).
[12]W. Mönch, R. S. Bauer, H. Gant, and R. Murschall, J. Vac. Sci. Technol. **21**, 498 (1982).
[13]W. E. Spicer and P. E. Gregory, CRC Crit. Rev. Solid State Sci. **5**, 231 (1975).
[14]P. E. Gregory and W. E. Spicer, Phys. Rev. B **13**, 725 (1976).
[15]P. Pianetta, I. Lindau, P. E. Gregory, C. M. Garner, and W. E. Spicer, Surf. Sci. **72**, 278 (1978).
[16]R. A. Street, R. H. Williams, and R. S. Bauer, J. Vac. Sci. Technol. **17**, 1001 (1980).
[17]R. W. Grant, J. R. Waldrop, S. P. Kowalczyk, and E. A. Kraut, J. Vac. Sci. Technol. **19**, 477 (1981).
[18]J. van Laar and J. J. Scheer, Surf. Sci. **8**, 343 (1967).
[19]A. Huijser and J. van Laar, Surf. Sci. **52**, 202 (1975).
[20]W. Gudat, D. E. Eastman, and J. L. Freeouf, J. Vac. Sci. Technol. **13**, 250 (1976).
[21]J. van Laar and A. Huijser, J. Vac. Sci. Technol. **13**, 769 (1976).
[22]W. E. Spicer, I. Lindau, P. Skeath, and C. Y. Su, J. Vac. Sci. Technol. **17**, 1019 (1980).
[23]W. E. Spicer, I. Lindau, P. Skeath, C. Y. Su, and P. Chye, Phys. Rev. Lett. **44**, 420 (1980).
[24]W. E. Spicer, S. Eglash, I. Lindau, C. Y. Su, and P. Skeath, Thin Solid Films **89**, 447 (1982).
[25]J. D. Daw and R. E. Allen, J. Vac. Sci. Technol. **20**, 659 (1982).
[26]W. Mönch, Surf. Sci. **132**, 92 (1983).
[27]A. Zur, T. C. McGill, and D. L. Smith, Surf. Sci. **132**, 456 (1983).
[28]A. Zur, T. C. McGill, and D. L. Smith, Phys. Rev. B **28**, 2060 (1983).
[29]H. Kroemer, Surf. Sci. **132**, 543 (1983).
[30]R. Ludeke, T.-C. Chiang, and T. Miller, J. Vac. Sci. Technol. B **1**, 581 (1983).
[31]S. H. Pan, D. Mo, W. G. Petro, I. Lindau, and W. E. Spicer, J. Vac. Sci. Technol. B **1**, 593 (1983).
[32]S. P. Kowalczyk, R. W. Grant, J. R. Waldrop, and E. A. Kraut, J. Vac. Sci. Technol. B **1**, 684 (1983).
[33]P. Chiaradia, A. D. Katnani, H. W. Sang, Jr., and R. S. Bauer, J. Vac. Sci. Technol. B (to be published).
[34]S. M. Sze, *Physics of Semiconductor Devices*, 2nd ed. (Wiley, New York, 1981), p. 25.
[35]R. S. Bauer, P. Zurcher, and H. W. Sang, Jr., Appl. Phys. Lett. **43**, 663 (1983).
[36]P. Zurcher and R. S. Bauer, J. Vac. Sci. Technol. A **1**, 695 (1983).

Transition-metal silicides lattice-matched to silicon

A. Zur, T. C. McGill, and M-A. Nicolet
California Institute of Technology, Pasadena, California 91125

(Received 29 May 1984; accepted for publication 8 August 1984)

We have used a systematic search to determine all the possible transition-metal silicides that are geometrically lattice-matched to either the (100), (110), or the (111) face of silicon. A short table with the best possible matches is presented here, and a more comprehensive table including slightly worse matches is deposited with the editor.

Recently, there has been a considerable interest in thin films of transition-metal silicides grown epitaxially on silicon.[1-5] The traditional application of transition-metal silicides is as contacts and interconnects; this application uses their metallic character and their ability to be oxidized or to withstand high temperatures. Transition-metal silicides also have possible applications in novel devices.[6-9]

The problem of epitaxial growth is complicated. One of the factors that can be of relevance to epitaxial growth is the lattice mismatch. In a previous paper[10] we have described a general method that enables one to find systematically all the possible matching faces of any pair of crystalline materials. In this paper we apply this method to the interfaces of transition-metal silicides on silicon, and thereby obtain the most comprehensive tabulation of such lattice matches for this system. Partial lists were published before.[2,11] The silicides that were considered are those of the three transition periods in the periodic table (columns IIIA through IB) including lanthanum, but not the other lanthanides.

The precise definition of lattice match, as well as a systematic procedure to find them, was given in a previous publication[10]; we shall repeat here only the essential definitions and concepts. By "lattice match" we mean a periodic translational symmetry of the interface that is compatible with the crystal structures on both sides of that interface. To understand this definition, refer to Fig. 1, in which we show a hypothetical lattice match between $V_3Si(111)$ and Si(111). To see the positions of the atoms relative to the cubic axes, the atoms are shown within a cube of 20 Å on a side, from which one corner was cut; this cut corner reveals a (111) face. The lattice translations in the (111) face of silicon (face-centered cubic, $a = 5.431$ Å) form a two-dimensional lattice. This lattice is shown in Fig. 1 as a fine-line grid. It is shown both at the bottom of the figure to demonstrate the translations and the atoms, and at the top of the figure for clarity. The sides of each of the little rhombes (the "unit cells" of that grid) are $5.431\ \text{Å}/\sqrt{2} = 3.840$ Å, and they are oriented parallel to the $[1\bar{1}0]$, $[01\bar{1}]$, or the $[\bar{1}01]$ directions. Similarly, the lattice

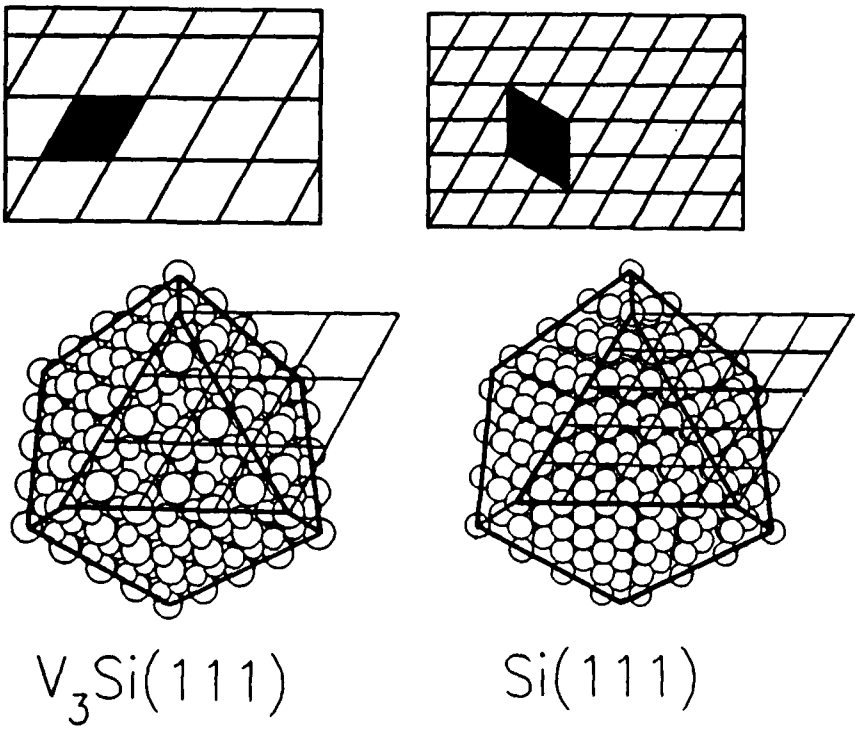

FIG. 1. Lattice match of $V_3Si(111)$ on Si(111). The atomic positions for both materials are shown in the lower part of the figure (V_3Si on the left, silicon on the right). The atoms are shown as spheres packed in a $20 \times 20 \times 20$-Å cube oriented parallel to the cubic axes. One corner of each cube is cut in a (111) plane, and the viewer is looking down the (111) direction. The translational symmetry parallel to the (111) face is shown as a grid of 60° rhombes. Larger unit cells can be formed on those grids to obtain a good match; in this case a larger unit cell containing three silicon unit cells, as shown in the upper right corner, matches almost precisely (0.4%) the V_3Si original unit cell.

 0021-8979/85/020600-04$02.40

translations perpendicular to the (111) face of V_3Si (simple cubic, β–W structure, $a = 4.722$ Å) form a similar rhombic grid whose unit cell dimensions are $4.722\ \text{Å} \times \sqrt{2} = 6.678$ Å. One can, therefore, form a superlattice on the silicon surface, whose unit cell is composed to three silicon unit cells as shown in Fig. 1. This larger unit cell is oriented such that its sides are parallel to the $[1\bar{2}1]$, $[11\bar{2}]$, or $[\bar{2}11]$ directions, and their lengths are $5.431 \times \sqrt{3/2} = 6.652$ Å, or less than 0.4% off the V_3Si unit cell. These two unit cells are shaded in the upper part of Fig. 1.

One can see that the lattice match, as defined here, is characterized by two parameters: the mismatch and the common-unit-cell dimensions. In the example given in Fig. 1, the mismatch is 0.4% and the common unit-cell area is approximately 38 Å^2 (38.32 for the silicon, 38.62 for the V_3Si). In the most general case, the common unit cell is not necessarily a rhombus, like in Fig. 1, but rather a parallelogram, whose sides are a and b, with an acute angle α between them. These three parameters, namely, a_1, b_1 and α_1 for the substrate, may be slightly different for the corresponding a_2, b_2, and α_2 of the film. This difference determines the *mismatch* (ϵ) of the match:

$$\epsilon = \max\left(\left|\frac{a_1 - a_2}{a_1}\right|, \left|\frac{b_1 - b_2}{b_1}\right|, \left|\frac{\alpha_1 - \alpha_2}{\alpha_1}\right|\right).$$

The area of the common parallelogram, i.e.,

$$A = ab \sin\alpha$$

is the other parameter relevant to lattice match (there are actually two areas, A_1 and A_2, corresponding to the substrate and the film, but they are very close to each other). For every choice of maximal area and mismatch, the number of possible matches is finite, and all of them can be found in a way that was described in our previous paper.[10] We would like to emphasize that the procedure described above does not ensure that the silicon atoms in the substrate are aligned with the silicon atoms in the silicide. It does ensure, however, that any alignment of the silicide atoms with respect to the silicon atoms can repeat itself periodically along the interface.

A sample of our results is given in Table I. In this table we list only the few best matches, i.e., those with mismatch of 0.5% or less in all three parameters a, b, and α of the common unit cell, and unit-cell area of 50 Å^2 or less. Under these conditions, we have scanned every known transition-metal silicide and tried to match it to the (100), (110), or (111) faces of silicon. Since the restrictions on the match were very tight (0.5% mismatch and 50-Å^2 cell area), only five silicides were found to match. These are the V_3Si [simple cubic, $a = 4.722$ (Ref. 12)], Ni_3Si_2 [trigonal, $a = 5.617$, $\alpha = 72°50'$ (Ref. 13)], $NiSi_2$ [face-centered cubic, $a = 5.407$ (Ref. 14)], γ-Y_5Si_3 [hexagonal, $a = 3.842$, $c = 4.144$ (Ref. 15)], and RuSi [simple cubic, $a = 4.703$ (Ref. 16)].

Much more extensive tables, similarly structured but with less tight matches (up to 3% mismatch and 150-Å^2 unit-cell area) are deposited at the Physics Auxiliary Publication Service (PAPS),[17] and can be requested from the editor of this journal. Matches of up to 2% mismatch and 80-Å^2 unit-cell area are shown graphically in Fig. 2. These matches are shown on the mismatch versus unit-cell area plane, and they cluster (as expected) near the upper right corner, corresponding to poor match (both large mismatch and large unit-cell area). For every pair of matching faces only one point

TABLE I. The best lattice matches of transition-metal silicides on silicon. The primitive common unit cells in this table do not exceed 50 Å^2, and the mismatch is less than 0.5%. Under these conditions, all the possible matches of the silicides on Si (100), (110), and (111) are given in this table. For each possible match, we give here the epitaxial condition, as well as the common unit cell dimensions on each side of the interface. The epitaxial condition is a pair of crystal directions, one on each side of the interface, that will be parallel to each other. Many such pairs are possible, and only one of them is given here. The cells' dimensions in angstroms and degrees are given here for comparison. The mismatch percentage in all the three dimensions of the common unit cell is given in the last three columns.

Matching faces	Epitaxial condition	Cell area	Silicide			Silicon					
		(Å^2)	a	b	α	a	b	α	$\%_a$	$\%_b$	$\%_\alpha$
V_3Si(111)/Si(111)	$[10\bar{1}]\|\|[1\bar{2}1]$	39.	6.68	6.68	60.00	6.65	6.65	60.00	0.4	0.4	0.0
Ni_3Si_2 (111)/Si(111)	$[1\bar{1}0]\|\|[1\bar{2}1]$	39.	6.67	6.67	60.00	6.65	6.65	60.00	0.3	0.3	0.0
$NiSi_2$ (111)/Si(111)	$[1\bar{1}0]\|\|[1\bar{1}0]$	13.	3.82	3.82	60.00	3.84	3.84	60.00	0.4	0.4	0.0
$NiSi_2$ (511)/Si(111)	$[01\bar{1}]\|\|[01\bar{1}]$	38.	3.82	10.12	79.11	3.84	10.16	79.11	0.4	0.4	0.0
$NiSi_2$ (100)/Si(100)	$[011]\|\|[011]$	15.	3.82	3.82	90.00	3.84	3.84	90.00	0.4	0.4	0.0
$NiSi_2$ (221)/Si(100)	$[1\bar{1}0]\|\|[01\bar{1}]$	44.	3.82	11.47	90.00	3.84	11.52	90.00	0.4	0.4	0.0
$NiSi_2$ (110)/Si(110)	$[1\bar{1}0]\|\|[1\bar{1}0]$	21.	3.82	5.41	90.00	3.84	5.43	90.00	0.4	0.4	0.0
Y_5Si_3 (0001)/Si(111)	$[2\bar{1}\bar{1}0]\|\|[1\bar{1}0]$	13.	3.84	3.84	60.00	3.84	3.84	60.00	0.1	0.1	0.0
RuSi(111)/Si(111)	$[10\bar{1}]\|\|[1\bar{2}1]$	38.	6.65	6.65	60.00	6.65	6.65	60.00	0.0	0.0	0.0

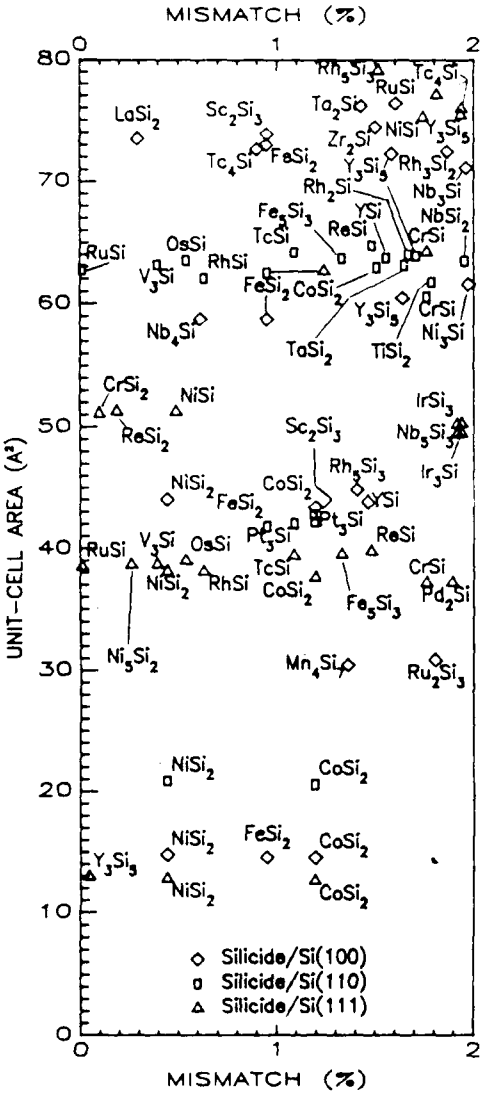

FIG. 2. Lattice matches of transition-metal silicides on silicon (100), (110), (111). All the possible matches such that the mismatch is smaller than 2%, and the common unit-cell area is smaller than 80 Å² are considered. These matches are characterized by mismatch and unit-cell area, and are shown here as diamonds for matches on silicon (100), rectangles for matches on silicon (110), and triangles for matches on silicon (111). Only the better matches are labeled. All the matches as well as the relative orientations can be found in a set of tables deposited at the PAPS.[17]

(corresponding to the smallest cell area) is shown in Fig. 2, for lack of space in that figure. Different faces of either the silicide or the silicon, however, are shown separately on Fig. 2. For example, the five $NiSi_2$ points in Fig. 2, all at 0.44%, correspond to $NiSi_2$(111)/Si(111), $NiSi_2$(100)/Si(100), $NiSi_2$(110)/Si(110), $NiSi_2$(511)/Si(111), and $NiSi_2$(221)/Si(100), respectively, from the bottom of Fig. 2. The three faces of the substrate considered, namely, (100), (110), and (111) are shown in Fig. 2 as diamonds, rectangles, and triangles. The corresponding faces of the silicides are not shown in Fig. 2, and the reader is referred to our tables[17] for that information. The best matches at the lower left corner of Fig. 2 are the same matches appearing in Table I.

It is interesting to compare the experimentally known cases of epitaxial growth with the lattice-match predictions presented here. Seven transition-metal silicides are currently known to grow epitaxially on silicon. These are $NiSi_2$,[18–25] $CoSi_2$,[9,23,27,29–32] Pd_2Si,[19,21,23,25,33–46] PtSi,[21,24,47–51] Pt_2Si,[52,53] $FeSi_2$,[55] and $CrSi_2$.[56] Out of these seven, the three that correspond to good lattice match, namely, $NiSi_2$ (0.4% mismatch), $CoSi_2$ (1.2%), and Pd_2Si (1.8%–2.3%), grow as single crystals.[57] The other two, PtSi and Pt_2Si, also grow epitaxially (in the sense that the crystallites in the film have preferred orientations with respect to the substrate) despite a large mismatch, but the resulting PtSi and Pt_2Si films are polycrystalline.[53] The mismatch between the Pt_2Si[100] and Si[110] is 2.4%, and that between PtSi[001] and Si[110] is 3.0%. Ben Ghozlene *et al.*[53] list several other preferred orientations of the platinum silicides with respect to the silicon substrate; the mismatch in all of them is at least 3%. No information is yet available for the crystalline quality of epitaxial $FeSi_2$ and $CrSi_2$, but they would correspond to good lattice match (0.1% for $CrSi_2$, 1.0% for $FeSi_2$, see Fig. 2). On the other hand, epitaxial γ-Y_3Si_5 or RuSi, for example, have not been reported, despite a very good lattice match. In view of these experimental results, one can conclude that lattice-match considerations alone are insufficient to determine all silicide films that grow epitaxially. A correlation between lattice match and epitaxy does seem to exist, though. Some other systems, however, most notably silicon (100) on sapphire ($1\bar{1}02$), demonstrate that good lattice match is not always necessary for a single-crystalline film[58]; the mismatch in this case is 12.5%. One can see, therefore, that no definitive statements regarding heteroepitaxy can be made based on the criterion of lattice match alone.[58] The reason is that this criterion takes into account only the geometry of the substrate and the film, but not the chemistry between them. Hence, only a combination of chemical and geometrical considerations may yield accurate predictions regarding heteroepitaxial growth. Despite this fact, a comprehensive listing of good matches is useful to designate some silicide films as better candidates than others for epitaxial growth. Moreover, the lattice-match criterion is straightforward to apply, and one can scan all the possible phases of transition-metal silicides (well over one hundred such phases) and compare systmatically all the possible crystal faces and relative orientations, as was done in this work.

This work was supported in part by the Office of Naval Research under naval contract No. N-00014-82-K-0556.

[1] M-A. Nicolet and S. S. Lau, in *VLSI Electronics: Microstructure Science*, edited by N. Einspruch (Academic, New York, 1983), Vol. 6, Chap. 6
[2] S. P. Murarka, *Silicides for VLSI Applications* (Academic, New York, 1983), p. 172.
[3] K. N. Tu and J. W. Mayer, in *Thin Films—Interdiffusion and Reactions*, edited by J. M. Poate, K. N. Tu, and J. W. Mayer (Wiley, New York, 1978), p. 359.
[4] R. T. Tung, J. M. Poate, J. C. Bean, J. M. Gibson, and D. C. Jacobson, Thin Solid Films **93**, 77 (1982).
[5] G. Ottaviani, J. Vac. Sci. Technol. **16**, 1112 (1979).
[6] G. Oya, H. Inabe, and Y. Sawada, J. Vac. Soc. Jpn. **24**, 613 (1981).
[7] S. R. Herd, K. N. Tu, K. Y. Ahn, T. H. Di Stefano, and N. J. Mazzeo, J. Appl. Phys. **53**, 3777; 4372 (1982).
[8] W. F. Kosonocky, H. G. Erhardt, G. Meray, F. V. Shallcross, H. Elabd, M. J. Cantella, J. Klein, L. H. Skolnik, B. R. Capone, R. W. Taylor, W. Ewing, F. D. Shepherd, and S. A. Roosild, Soc. Photo-Opt. Instrum. Eng. **225**, 69 (1980).

[9]S. Saitoh, H. Ishiwara, and S. Furukawa, Appl. Phys. Lett. **37**, 203 (1980).
[10]A. Zur and T. C. McGill, J. Appl. Phys. **55**, 378 (1984).
[11]H. Ishiwara, S. Saitoh, and K. Hikosaka, Jpn. J. Appl. Phys. **20**, 843 (1981).
[12]Wallbaum, Z. Metallkd. **31**, 362 (1939).
[13]G. Pilström, Acta Chem. Scand. **15**, 893 (1961).
[14]P. K. Panday and K. Schubert, J. Less-Common Met. **18**, 175 (1969).
[15]J. E. E. Baglin, F. M. d'Heurle, and C. S. Petersson, J. Appl. Phys. **52**, 2841 (1981).
[16]L. N. Finnie, J. Less-Common Met. **4**, 24 (1962).
[17]A. Zur, T. C. McGill, and M-A. Nicolet, "Tables of Lattice Matches between Transition-Metal Silicides and Silicon"; see AIP document No. PAPS JAPIA-57-600-76 for 76 pages of tables. Order by PAPS number and journal reference from American Institute of Physics, Physics Auxiliary Publication Service, 335 E. 45 St., New York, NY 10017. The price is $1.50 for each microfiche (98 pages) or $5.00 per photocopies of up to 30 pages, and $0.15 for each additional page over 30 pages. Airmail additional. Make checks payable to the American Institute of Physics. This material appears in the monthly *Current Physics Microform* edition of all journals published by AIP, on the frames following this article.
[18]K. N. Tu, E. I. Alessandrini, W. K. Chu, H. Krautle, and J. W. Mayer, *Proceedings of the 6th International Vacuum Congress*, 1974 [Jpn. J. Appl. Phys., Suppl. 2, Pt. 1, 669 (1974)].
[19]S. S. Lau, W. K. Chu, J. W. Mayer, and K. N. Tu, Thin Solid Films **23**, 205 (1974).
[20]H. Ishiwara, M. Nagatomo, and S. Furukawa, Nucl. Instrum. Methods **149**, 417 (1978).
[21]H. Ishiwara, K. Hikosaka, M. Nagatomo, and S. Furukawa, Surf. Sci. **86**, 711 (1979).
[22]S. S. Lau and N. W. Cheung, Thin Solid Films **71**, 117 (1980).
[23]H. Ishiwara, in *Proceedings of the Symposium on Thin Film Interfaces and Interactions*, edited by J. E. E. Baglin and J. M. Poate (Electrochem. Soc. Inc., New Jersey, 1980), p. 159.
[24]K. C. R. Chiu, J. M. Poate, L. C. Feldman, and C. J. Doherty, *Proceedings of the Symposium on Thin Film Interfaces and Interactions*, edited by J. E. E. Baglin and J. M. Poate (Electrochem. Soc. Inc., New Jersey, 1980), p. 171.
[25]F. Föll, P. S. Ho, and K. N. Tu, J. Appl. Phys. **52**, 250 (1981).
[26]L. J. Chen, L. S. Hung, J. W. Mayer, J. E. E. Baglin, J. M. Neri, and D. A. Hammer, Appl. Phys. Lett. **40**, 595 (1982).
[27]L. J. Chen, J. W. Mayer and K. N. Tu, Thin Solid Films **93**, 135 (1982).
[28]R. T. Tung, J. M. Gibson, and J. M. Poate, Phys. Rev. Lett. **50**, 429 (1983).
[29]J. C. Bean and J. M. Poate, Appl. Phys. Lett. **37**, 643 (1980).
[30]R. T. Tung, J. C. Bean, J. M. Gibson, J. M. Poate, and D. C. Jacobson, Appl. Phys. Lett. **40**, 684 (1982).
[31]L. J. Chen, J. W. Mayer, K. N. Tu, and T. T. Sheng, Thin Solid Films **93**, 91 (1982).
[32]L. J. Chen and T. T. Chang, Thin Solid Films **104**, 183 (1983).
[33]W. V. T. Rusch and C. A. Burrus, Solid-State Electron. **11**, 517 (1968).
[34]C. J. Kircher, Solid-State Electron. **14**, 507 (1971).
[35]J. Drobek, R. C. Sun, and T. C. Tisone, Phys. Status Solidi A **8**, 243 (1971).
[36]W. D. Buckley and S. C. Moss, Solid-State Electron. **15**, 1331 (1972).
[37]H. Muta and D. Shinoda, J. Appl. Phys. **43**, 2913 (1972).
[38]D. H. Lee, R. R. Hart, D. A. Kiewit, and O. J. Marsh, Phys. Status Solidi A **15**, 645 (1973).
[39]R. W. Bower, D. Sigurd, and R. E. Scott, Solid-State Electron. **16**, 1461 (1973).
[40]D. Sigurd, R. W. Bower, W. F. van der Weg, and J. W. Mayer, Thin Solid Films **19**, 319 (1973).
[41]G. A. Hutchins and A. Shepela, Thin Solid Films **18**, 343 (1973).
[42]S. S. Lau and D. Sigurd, J. Electrochem. Soc. **121**, 1538 (1974).
[43]H. Ishiwara and S. Furukawa, J. Vac. Sci. Technol. **12**, 1374 (1975).
[44]H. Ishiwara and S. Furukawa, J. Appl. Phys. **47**, 1686 (1976).
[45]U. Köster, K. N. Tu, and P. S. Ho, Appl. Phys. Lett. **31**, 634 (1977).
[46]Z. Liliental, R. W. Carpenter, and R. Tuenge, Thin Solid Films, **104**, 17 (1983).
[47]T. Kawamura, D. Shinoda, and H. Muta, Appl. Phys. Lett. **11**, 101 (1967).
[48]A. K. Sinha, R. B. Marcus, T. T. Sheng, and S. E. Haszko, J. Appl. Phys. **43**, 3637 (1972).
[49]R. M. Anderson and T. M. Reith, J. Electrochem. Soc. **122**, 1337 (1975).
[50]A. K. Sinha, S. E. Haszko, and T. T. Sheng, J. Electrochem. Soc. **122**, 1714 (1975).
[51]M. Severi, E. Gabilli, S. Guerri, and G. Celotti, J. Appl. Phys. **48**, 1998 (1977).
[52]P. Joubert, P. Auvray, A. Guivarc'h, and G. Pelous, Appl. Phys. Lett. **31**, 753 (1977).
[53]H. Ben Ghozlene, P. Beaufrère, and A. Authier, J. Appl. Phys. **49**, 3998 (1978).
[54]H. Ishiwara, K. Hikosaka, and S. Furukawa, J. Appl. Phys. **50**, 5302 (1979).
[55]H. C. Cheng, L. J. Chen, and T. R. Your, Thin Solid Films (to be published).
[56]F. Y. Shiau, H. C. Cheng, and L. J. Chen, Appl. Phys. Lett. **45**, 524 (1984).
[57]S. Saitoh, H. Ishiwara, T. Asano, and S. Furukawa, Jpn. J. Appl. Phys. **20**, 1649 (1981).
[58]J. W. Cullen, in *Heteroepitaxial Semiconductors for Electronic Devices*, edited by G. W. Cullen and C. C. Wang (Springer, New York, 1978), p. 50.

END

FILMED

FEB. 1988

DTIC